MALIGNANT GLIOMAS ORIGINATE FROM NEURAL STEM/PROGENITOR CELLS AND ARE MAINTAINED BY CANCER STEM CELLS

.

Luis F. Parada, Ph.D. (Mentor)

James F. Amatruda, M.D., Ph.D (Chairman)

Jane E. Johnson, Ph.D.

Jerry W. Shay, Ph.D.

DEDICATION

For my parents and brother. For everyone that encourages me to continue research.

MALIGNANT GLIOMAS ORIGINATE FROM NEURAL STEM/PROGENITOR CELLS AND ARE MAINTAINED BY CANCER STEM CELLS

by

JIAN CHEN

DISSERTATION

Presented to the Faculty of the Graduate School of Biomedical Sciences

The University of Texas Southwestern Medical Center at Dallas

In Partial Fulfillment of the Requirements

For the Degree of

DOCTOR OF PHILOSOPHY

The University of Texas Southwestern Medical Center at Dallas

Dallas, Texas

April, 2011

MALIGNANT GLIOMAS ORIGINATE FROM NEURAL STEM/PROGENITOR CELLS AND ARE MAINTAINED BY CANCER STEM CELLS

Jian Chen Ph.D.

The University of Texas Southwestern Medical Center at Dallas, 2011

Supervising Professor: Luis F. Parada, Ph.D.

Malignant glioma is one of the most aggressive cancers. To study the biology of glioma, our lab previously developed a series of mouse models that phenocopy both tumor initiation and progression through stochastic tumor suppressor loss-of-heterozygosity (LOH). To determine whether the mouse models recapitulate human glioma at the molecular level, we have performed gene set enrichment analysis (GSEA) comparing the molecular signature of tumors that develop in our mouse glioma models to the gene expression profiles of a number of human tumors. Our mouse glioma models share high similarity with human GBM and showed a generally proneural marker gene expression

profile. We also found that tumors from the same initial genetic mutations can be further divided into several subtypes.

Previous studies suggested a neural stem/progenitor cell (NSC) origin for gliomas, however strict exprimental evidence was still lacking. To examine the role of NSCs in glioma, we developed an NSC-specific tamoxifen-inducible nestin-cre driver mouse. When crossed to the NF/p53/Pten flox mice and induced with tamoxifen at E13.5, the Nes-Cre;Nf/p53/Pten mutant mice exhibited tumor initiation and progression similar to our previous mouse model using hGFAP-cre, with complete penetrance. All analyzed mice that were induced at 4 weeks such that only adult neural stem cells were targeted, developed malignant astrocytoma 7 - 12 months after induction. These findings indicate that despite their rarity, neural stem/progenitor cells are sufficient targets for the accumulation of mutations that initiate malignant astrocytomas.

Our highly physiological relevant mouse model also allowed us to address the question of how glioma is maintained in vivo: whether tumors are maintained by a subpopulation of cells with self-renewal capacity that supplies tumor bulk, or whether the majority of tumor cells have the capacity to maintain the tumor. In our spontaneous somatic mouse model of glioma, a Nestin-ΔTK-IRES-GFP transgene labels the primary tumor cells that are required for tumorigenicity in allograft assays. Ablating endogenous Nes-ΔTK-positive cells significantly extended the survival of tumor-bearing mice by decreasing tumor proliferation and infiltration. We show that the glioma drug, temozolomide,

selectively targets endogenous CSC-derived proliferating cells. Furthermore, a combination therapy targeting both dividing cells and the CSCs arrests tumor progression.

TABLE OF CONTENTS

PRIOR PUBLICATIONS

1. Alcantara Llaguno, S.*, **Chen, J.***, Kwon, C. H.*, Jackson, E. L., Li, Y., Burns, D. K., Alvarez-Buylla, A., and Parada, L. F. (2009a). Malignant astrocytomas originate from neural stem/progenitor cells in a somatic tumor suppressor mouse model. ***Cancer cell*** 15, 45-56. (*Authorship equally shared)

2. Alcantara Llaguno, S. R., **Chen, J.**, and Parada, L. F. (2009b). Signaling in malignant astrocytomas: role of neural stem cells and its therapeutic implications. ***Clin Cancer Res*** 15, 7124-7129.

3. **Chen, J.***, Kwon, C. H.*, Lin, L., Li, Y., and Parada, L. F. (2009). Inducible site-specific recombination in neural stem/progenitor cells. ***Genesis*** 47, 122-131. (* Authorship equally shared)

4. Kwon, C. H., Zhao, D., **Chen, J.**, Alcantara, S., Li, Y., Burns, D. K., Mason, R. P., Lee, E. Y., Wu, H., and Parada, L. F. (2008). Pten haploinsufficiency accelerates formation of high-grade astrocytomas. ***Cancer Res*** 68, 3286-3294.

5. Li, Y., Luikart, B. W., Birnbaum, S., **Chen, J.**, Kwon, C. H., Kernie, S. G., Bassel-Duby, R., and Parada, L. F. (2008). TrkB regulates hippocampal neurogenesis and governs sensitivity to antidepressive treatment. ***Neuron*** 59, 399-412.

6. Lin, L., **Chen, J.**, Richardson, J. A., and Parada, L. F. (2009). Mice lacking neurofibromin develop gastric hyperplasia. ***Am J Physiol Gastrointest Liver Physiol*** 297, G751-761.

7. Llaguno, S. A., **Chen, J.**, Kwon, C. H., and Parada, L. F. (2008). Neural and Cancer Stem Cells in Tumor Suppressor Mouse Models of Malignant Astrocytoma. ***Cold Spring Harb Symp Quant Biol.***

8. Lush, M. E., Li, Y., Kwon, C. H., **Chen, J.**, and Parada, L. F. (2008). Neurofibromin is required for barrel formation in the mouse somatosensory cortex. ***J Neurosci*** 28, 1580-1587.

9. Nie, Y., Wang, P., Shi, X., Wang, G., **Chen, J.**, Zheng, A., Wang, W., Wang, Z., Qu, X., Luo, M., et al. (2004). Highly infectious SARS-CoV pseudotyped virus reveals the cell tropism and its correlation with receptor expression. ***Biochem Biophys Res Commun*** 321, 994-1000.

10. Wang, P.*, **Chen, J.***, Zheng, A.*, Nie, Y., Shi, X., Wang, W., Wang, G., Luo, M., Liu, H., Tan, L., et al. (2004). Expression cloning of functional receptor used by SARS coronavirus. ***Biochem Biophys Res Commun*** 315, 439-444. (*Authorship equally shared)

11. Yi, L., Li, Z., Yuan, K., Qu, X., **Chen, J.**, Wang, G., Zhang, H., Luo, H., Zhu, L., Jiang, P., et al. (2004). Small molecules blocking the entry of severe acute respiratory syndrome coronavirus into host cells. ***J Virol*** 78, 11334-11339.

12. Yuan, K., Yi, L., **Chen, J.**, Qu, X., Qing, T., Rao, X., Jiang, P., Hu, J., Xiong, Z., Nie, Y., et al. (2004). Suppression of SARS-CoV entry by peptides corresponding to heptad regions on spike glycoprotein. ***Biochem Biophys Res Commun*** 319, 746-752.

LIST OF FIGURES

LIST OF TABLES

LIST OF APPENDICES

LIST OF DEFINITIONS

BrdU –Bromodeoxyuridine

CldU –Chlorodeoxyuridine

IDU –Idoxuridine

MSP –Methylation specific PCR

CHAPTER ONE
Introduction

RECENT ADVANCES IN GLIOMA RESEARCH

Although the total incidence of primary central nervous system (CNS) tumors is only about 18.7 per 100,000 persons in US, 80% of primary malignant tumors in the CNS are gliomas, which are generally incurable (CBTRUS, 2009). According to the 2007 WHO classification, gliomas can be classified histologically as astrocytomas, oligodendrogliomas, and oligoastrocytomas. More than half of gliomas are glioblastoma multiforme (GBM, grade IV astrocytoma), one of the most aggressive cancers (Louis et al., 2007). Even after decades of advances in surgery and radiation and chemotherapies, the five-year survival rate of GBM is still less than 5%, a rate that typically decreases with older age at diagnosis (CBTRUS, 2009). This dismal clinical outcome makes glioma an urgent subject of cancer research.

Glioma core signaling pathways

In the past two decades, cytogenetics and molecular genetics have identified a number of chromosomal abnormalities and genetic alterations in malignant gliomas, particularly in GBM. Advances in molecular technologies, especially high-density microarray and genome sequencing, make it possible to evaluate genetic and epigenetic changes in the tumors at the genome-wide level. One of the most comprehensive studies, carried out by The Cancer Genome Atlas (TCGA) project, sequenced 601 cancer-related candidate genes in more than 200 human GBM samples (Network, 2008). As part of this multidimensional study, the project also analyzed genome-wide DNA copy number

changes, DNA methylation status, and protein-coding and non-coding RNA expression (Network, 2008). A similar but complementary study by Parsons et al. sequenced 20,661 protein-coding genes in 22 GBM samples and integrated the genetic alteration information with DNA copy number and gene expression profiles (Parsons et al., 2008).

These integrative genomic studies confirmed much of the data from previous molecular genetic studies. They also provided a comprehensive view of the complicated genomic landscape of GBM, revealing the core pathways of GBM (Figure 1-1): the P53 pathway, RB pathway and RTK pathway (Network, 2008; Parsons et al., 2008). Furnari et al. have written a detailed review of those pathways in glioma (Furnari et al., 2007). As expected, at the core pathway level the spectrum of mutations in the tumors echoes the traditional analogy of the cancer cell as an uncontrolled racecar. The majority of GBM tumors have genetic alterations in all three pathways, which helps to fuel cell proliferation and enhance cell survival while at the same time, allowing the cell to escape from cell cycle checkpoints, senescence and apoptosis. However, at the single gene level, many components of the same pathways were found to be mutated across tumor samples, most of which were rare mutations (Network, 2008). Interestingly, in the same tumor, alterations of components in the same pathway exist in a mutually exclusive manner, suggesting the fundamental contribution of the core pathways, rather than a common gene, to tumorigenesis.

In addition to confirming known genetic events in GBM, the large amount of sequencing data from TCGA also provided somatic mutation information at the base pair level,

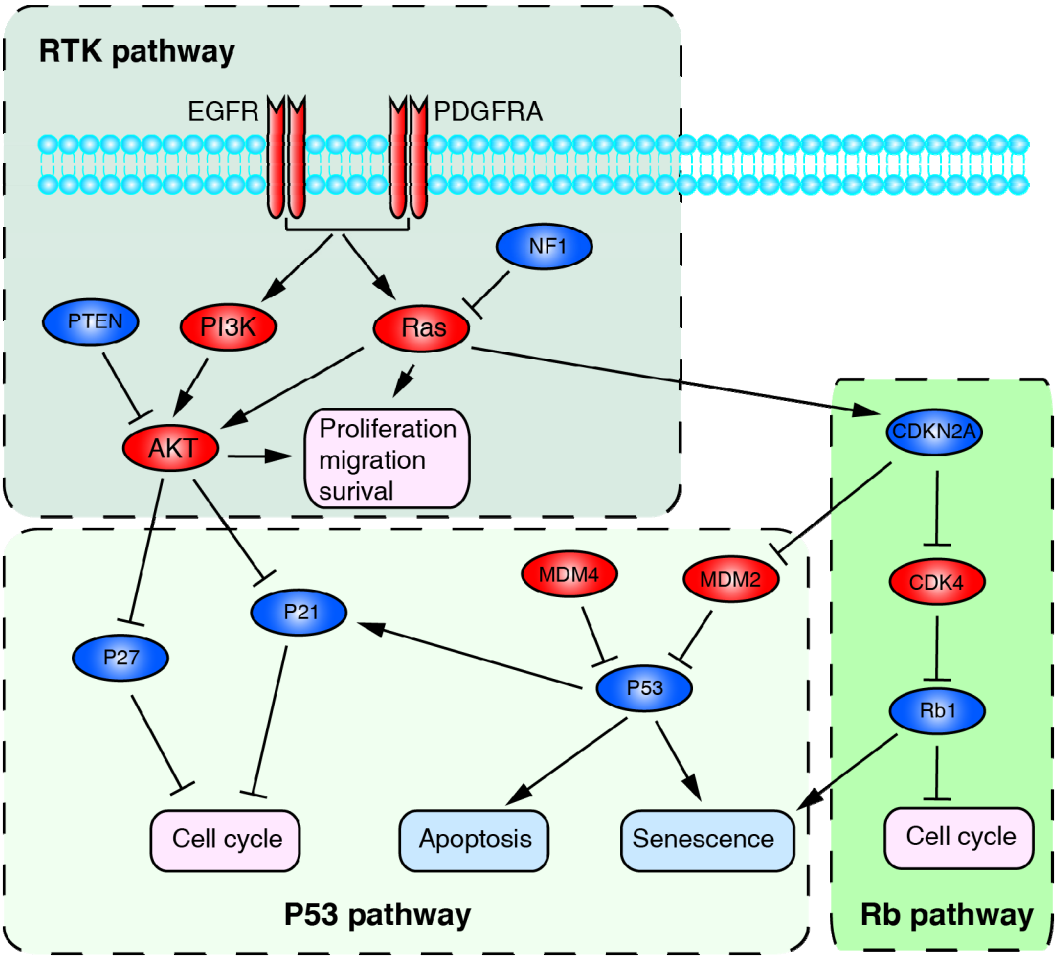

Figure 1-1. Core signaling pathways of glioma tumorigenesis. The receptor tyrosine kinase (RTK), p53 and Rb pathways are the core signaling pathways in glioma oncogenesis. Red color indicates oncogenes that are either overexpressed or amplified in GBM samples while blue color labels tumor suppressor genes that are somatically mutated or deleted (except for P27 and P21).

revealing new roles for known tumor supressors/oncogenes in GBM as well as completely novel cancer driver genes. For example, it has been observed that patients with neurofibromatosis type 1 (NF1) have an increased incidence of malignant glioma (Kyritsis et al., 2010). Studies in genetic mouse models have also strongly suggested a causal role of NF1 mutation in glioma tumorigenesis (Alcantara Llaguno et al., 2009; Kwon et al., 2008a; Zhu et al., 2005a). The involvement of NF1 mutation in human GBM was underappreciated until the TCGA project, which reported that 47 of the 206 patient samples, or 23%, have NF1 inactivating mutations or deletions, ranking it third among somatic mutation frequencies of all the 601 sequenced genes (Network, 2008).

Role of IDH mutations in gliomas

Among the genomic effort to characterize gliomas, the biggest surprise came from the genome-wide exon sequencing project, where R132 mutations of isocitrate dehydrogenase 1 (IDH1) were observed in 12% of the GBM samples (Parsons et al., 2008). Subsequently, the same mutation was also reported to be frequently found in acute myeloid leukemia (AML) (Green and Beer, 2010). Further studies showed that some gliomas also contain IDH2 R172 mutations, an analog to IDH1 R132, at a lower frequency (Yan et al., 2009). Interestingly, two new point mutations, IDH1 R100 and IDH2 R140, were found in AML but were never observed in glioma samples (Green and Beer, 2010).

Normally, IDH1 and IDH2 convert isocitrate to α-ketoglutarate (α-KG) while at the same time reducing NADP+ to NADPH in the cytosol and mitochondria, respectively (Figure

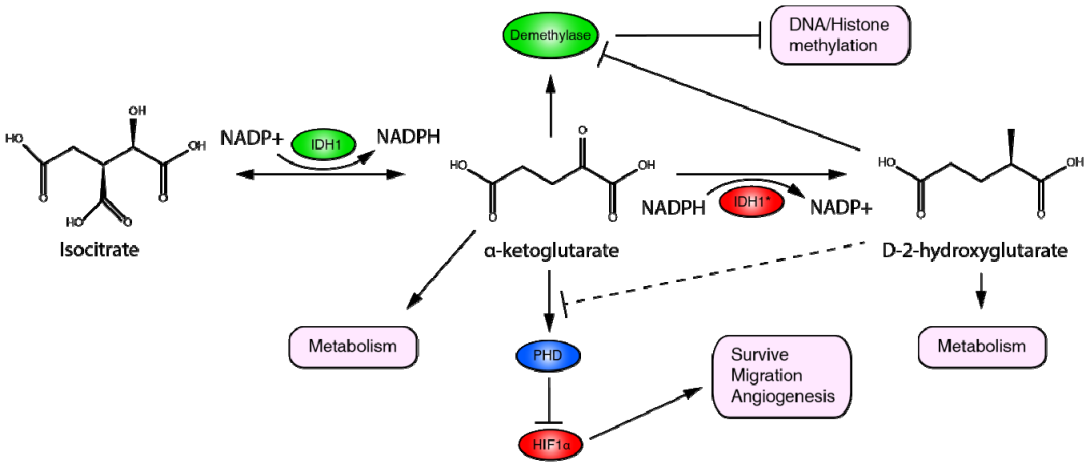

Figure 1-2. Function of normal and mutated IDH1. Wild type IDH1 catalyzed isocitrate to form alpha-ketoglutarate and convert NADP+ to NADPH at the same time. A mutated form of IDH1 has been found to be able to convert alpha-ketoglutarate to D2-hydroxyglutarate in an NADPH-dependent manner. Excessive D2-hydroxyglutarate will result in cellular stress as well as metabolic changes. It could also potentially act as a competitive substrate to inhibit DNA/histone demethylase and prolyl hydroxylases (PHDs), resulting in DNA/histone hypermethylation or activation of HIF1alpha, which can be further accelerated by lack of alpha-ketoglutarate, as alpha-ketoglutarate is a key substrate for both DNA/histone demethylases and PHDs.

1-2) (Yen et al., 2010). It was initially hypothesized that the IDH1 R132 and IDH2 R172 mutations reduced the enzyme's ability to make α-KG (Yan et al., 2009). Subsequent studies reported a dominant-negative role for IDH1 R132 and suggested a tumor suppressor function for IDH1/2 (Zhao et al., 2009). However, human genetic data showed that the mutations were always observed on a specific residue and only one copy of the gene was altered, strongly suggesting the possibility that it acts as a gain of function mutation (Green and Beer, 2010; Reitman et al., 2010; Yan et al., 2009). Follow-up studies discovered that the IDH1/2 mutations had an NADPH-dependent ability to convert α-KG to D-2-hydroxyglutarate (D-2HG) (Figure 1-2), supporting a pro-oncogenic role for IDH1/2 (Dang et al., 2010; Gross et al., 2010; Ward et al., 2010). Furthermore, knocking down wild type IDH1 in a glioma cell line slowed down cell growth, which is the opposite of a tumor suppressive function (Ward et al., 2010). Consistent with the biochemical data, levels of 2HG were found to be ten-fold higher in IDH1/2 mutated glioma or leukemia samples (Dang et al., 2010).

Despite this new intriguing data, the exact mechanism by which IDH1/2 mutations transform cells is still far from clear. The discovery of a neomorphic enzymatic function for IDH1/2 raises the possibility that D-2HG may act as an onco-metabolite (Dang et al., 2010; Gross et al., 2010; Ward et al., 2010). It has been reported that increased levels of D-2HG in cells caused oxidative stress in rat brains (Latini et al., 2003), which could potentially promote oncogenesis. In the clinic, high levels of 2HG have been linked to a rare neurometabolic disorder called D-2-hydroxyglutaric aciduria (Struys, 2006). It has been recently reported that a subset of patients with this disease harbors the IDH2 R140

mutation (Kranendijk et al., 2010). Interestingly, although the D-2-hydroxyglutaric aciduria patients with IDH2 mutations showed significantly higher levels of D-2HG compared to leukemia or glioma patients with IDH1/2 mutations, they did not develop gliomas, leukemia or other malignancies in a limited follow-up study (Kranendijk et al., 2010). However, in glioma patients, IDH1/2 mutations usually co-exist with TP53 mutations (Yan et al., 2009). It is possible that like other oncogenic stresses that trigger cell death and senescence, cells with extremely high levels of 2HG may be restrained from further malignant transformation by a similar checkpoint mechanism.

Additionally, other substrates/products affected by the IDH1/2 mutations may also be involved in oncogenesis. Disrupting the balance of NADP+/NADPH is likely to result in a broad spectrum of cellular reactions, and α-KG is a key component of multiple pathways. For example, α-KG is a key substrate for prolyl hydroxylases (PHDs) to catalyze hydroxylation of hypoxia inducible factor (HIF), a key regulator of angiogenesis (Figure 1-2) (Semenza, 2010). This hydroxylation allows HIF to be recognized and targeted for ubiquitin-mediated protein degradation. It has been observed that overexpression of IDH1 R132 in glioma cell lines resulted in increased levels of HIF-1α (Zhao et al., 2009). However, whether cells with IDH1/2 mutations have lower levels of α-KG is still controversial (Dang et al., 2010; Zhao et al., 2009). Given the structural similarity of α-KG and D-2HG, it is also possible that the new product D-2HG can compete with α-KG. Such competition has been linked to the oncogenetic mechanism of succinate dehydrogenase (SDH) and fumarate hydratase (FH) mutations, where accumulated succinate and fumarate compete with α-KG to inhibit the activity of prolyl

hydroxylase domain proteins (PHDs) (Semenza, 2010). In addition, α-KG is a substrate for particular histone- and DNA-demethylation enzymes (Figure 2). Reducing α-KG levels or levels of competing substrate would likely affect global gene expression. Indeed, 2-HG can inhibit multiple α-KG-dependent dioxygenases, which are important for DNA/histone demethylation (Xu et al., 2011). In AML patients, IDH1/2 mutations and mutations of the DNA-demethylating enzyme TET2 are mutually exclusive. Expression of IDH2 R140 inhibited TET2 function and resulted in hypermethylation of the genome, leading to impaired hematopoietic differentiation (Figueroa et al., 2010). Consistent with this idea, gliomas with IDH1 mutations showed significantly higher frequency of CpG island methylator (CIM) phenotype and increased histone methylation (Noushmehr et al., 2010; Xu et al., 2011). Interestingly, according to the COSMIC database, unlike in leukemia, mutations in TET2 are not frequently observed in brain tumors (http://www.sanger.ac.uk/genetics/CGP/cosmic/).

Molecular subclassification of gliomas

Classification of gliomas by molecular profile is another hot topic in the field of glioma genomic research. A detailed summary of the recent progress and problems related to this topic can be found in a recent review by Vitucci et al (Vitucci et al., 2010). In general, these genome-wide studies have revealed that distinct tumor histology is reflected in distinct gene expression signatures. Furthermore, molecular profiles can identify subclasses of tumors that would otherwise be indistinguishable by standard morphological methods. One such example is primary and secondary GBM. Although the histology of both types of GBM is identical, GBM has traditionally been further divided

into primary GBM and secondary GBM according to the clinical history, i.e. the history of disease progression (Ohgaki and Kleihues, 2007). It was believed that patients with primary GBM did not have previous lesions in the brain, while secondary GBM progressed from lower-grade tumors. Recently, however, several groups have used genome-wide analyses to successfully categorize these two subtypes based on their gene expression profiles (Godard et al., 2003; Maher et al., 2006; Shai et al., 2003; Tso et al., 2006).

Depending on the sample pool and analysis methods, different studies have reported different numbers of sub-classes. The prognostic value of the molecular subclassification was also frequently evaluated, with several studies suggested that gliomas with expression of genes involved in neurogenesis (proneural subtype) are generally associated with better survival (Freije et al., 2004; Li et al., 2009a; Phillips et al., 2006). In contrast, gliomas with mesenchymal gene expression (mesenchymal subtype) usually have poor outcome (Li et al., 2009a; Phillips et al., 2006; Tso et al., 2006). However, the proneural subtype has a significantly higher proportion of grade III gliomas, which is known to have a more favorable outcome compared to GBM (Cooper et al., 2010; Phillips et al., 2006), thus it is not clear whether the difference in patient survival merely reflects the known survival differences associated with tumor grade. In addition, the supervised marker selection process could also be problematic. These problems were reemphasized by TCGA's study in which only GBM samples were analyzed. Unsupervised clustering analysis of TCGA dataset grouped the tumors into four different subtypes, Proneural (PN), Neural (NL), Mesenchymal (MES) and Classical (CL)

(Verhaak et al., 2010). The PN and MES subtypes shared significant overlap with previous studies. Integration of genetic alteration events revealed that PN, MES, and CL subtypes were associated with aberrant PDGFRA/IDH1, NF1, and EGFR status respectively. However, no prognosis differences were observed between each subtype (Verhaak et al., 2010). Very recently, Gravendeel et al. used a completely unsupervised algorithm to classify profiles of 276 gliomas into 24 subtypes. A similar proneural subtype (Cl17) was also identified. Either all the gliomas or GBM alone in this group have significant superior survival, suggesting that the previous prognosis value of the molecular markers was not just the consequence of the selection methods, where markers were chosen based on their association with outcome in the training data sets (Gravendeel et al., 2009).

Although gliomas with proliferative or mesenchymal characteristics generally have poor outcome, several studies have confirmed that these subtypes are more sensitive to radiation and chemotherapy combinational therapy, which could potentially be due to the higher proliferative index or higher levels of microvascular endothelial proliferation (Gravendeel et al., 2009; Verhaak et al., 2010). Clinical trials designed upon this molecular subtype information are ongoing.

The numerous molecular subclassification studies have no doubt confirmed the value of this tool. A certain degree of consistency has been reported from these studies, however there are also some large variations in the numbers of subtypes and the signature genes identified in each subtype, which could potentially be caused by differences in the

statistical model and the data sets utilized by different studies. These variations make it extremely difficult to perform meaningful follow up studies. For example, initial studies of the proneural subclass using TCGA dataset failed to show better prognosis, while the proneural subtype in the same dataset identified using pre-selected markers from Phillips et al. or unsupervised clustering from Gravendeel et al. showed significantly longer survival (Gravendeel et al., 2009; Verhaak et al., 2010). Furthermore, prediction and validation of molecular subclassification is usually based on genome-wide expression data, but it remains difficult to perform DNA microarray analysis on every newly-diagnosed glioma considering the technical and cost issues, not to mention the sample processing and "lab affect" when pooling profiles from multiple sources (Irizarry et al., 2005). Algorithms to translate these discoveries into more reliable and convenient assays are needed. Recently, quantitative PCR-based methods testing nine marker genes were developed and are currently being tested in clinical trials to see if they successfully predict sensitivity to an angiogenesis inhibitor (Colman et al., 2010).

Lessons from genomic studies

The wealth of genomic data now available for glioma provides tremendous opportunity to impact both basic research and clinical outcomes. Obviously, new genetic alterations provide opportunities for drug development against novel therapeutic targets. IDH1/2 mutations are one such example. Another example is ERBB2, which is frequently amplified in breast cancer (Mendelsohn and Baselga, 2000). Interestingly, 8% of GBM samples in TCGA project were shown to also have alterations in ERBB2, making it a

tempting target for therapeutic intervention by known drugs such as trastuzumab (Network, 2008).

Currently, genetic information is more useful in making a clinical diagnosis and formulating treatment plans. While decisions regarding glioma treatment are still mainly based on traditional pathology, which relies on histology, over the past 10 years genetic assessment has been playing an increasing role to facilitate this process (Jansen et al., 2010). One such successful example in glioma is 1p/19q loss, which frequently occurs in oligodendrogliomas (Smith et al., 1999). Patients with high-grade oligodendrogliomas that also harbor these genetic events have a better prognosis (Kouwenhoven et al., 2009; Smith et al., 2000). In low-grade oligodendrogliomas patients, 1p/19q loss dictates favorable progression-free survival after temozolomide treatment (Kouwenhoven et al., 2006). It has also been reported that co-expression of EGFRvIII and the tumor suppressor Pten associates with clinical response to EGFR kinase inhibitor in a recent clinical trial (Mellinghoff et al., 2005). The discovery of core signaling pathways in gliomas and the observation that several components of the same pathway are subject to mutagenesis in tumors also suggested a pathway targeting strategy rather than targeting a single gene, for future drug discovery efforts (Network, 2008; Parsons et al., 2008). Consistent with this concept, co-activation of several tyrosine kinases was observed in both xenograft and primary human GBM specimens. In a cell culture system, targeting these RTKs concurrently using combinations of inhibitors and/or RNAi showed significantly better response than treating with a single agent alone (Stommel et al., 2007).

Detailed molecular information about tumors also led to a reshaping of the classification scheme. For example, it was initially discovered that lower-grade GBMs have a higher frequency of TP53 mutation and PDGFRA expression, thus classifying these two events as markers of secondary GBM (Ohgaki and Kleihues, 2007). However, TP53 was also found to be the most frequent somatically mutated gene by the TCGA project, where predominantly primary GBM samples were studied (Network, 2008). Likewise, in the same dataset, a subset of GBMs was also found to over-express PDGFRA (Network, 2008; Verhaak et al., 2010). These findings, on one hand, demonstrate the need to identify additional markers for secondary GBM. Examples of additional markers are the recently identified IDH1/2 mutations, which have mainly been found in grade II-III gliomas (Parsons et al., 2008; Yan et al., 2009). On the other hand, it is conceivable that primary GBMs actually develop way before the patient becomes symptomatic. It is thus very tempting to develop diagnostic techniques to identify those early events for therapeutic intervention because patients with secondary GBM, which is usually diagnosed at a younger age compared to primary GBM, have a significantly better prognosis (Ohgaki and Kleihues, 2007). Genome-wide sequencing techniques plus sophisticated bioinformatic tools now enable us to reconstruct the evolutionary history of tumor cells. For example, it has been suggested that it takes more than a decade between the first genetic mutation and formation of the first non-metastatic pancreatic tumor cells (Campbell et al., 2010; Yachida et al., 2010). Bioinformatic efforts to reconstruct the temporal sequence of mutations in GBM using the TCGA dataset also indicated that the TP53 gene is likely mutated first in the tumorigenic process (Attolini et al., 2010), a finding consistent with mouse model studies (Zhu et al., 2005a).

Genetic mouse models of glioma

The laboratory mouse shares extensive molecular and physiological similarities to humans and is a very powerful tool for studying cancers. Unlike invertebrate model systems, tumor development in mice is accompanied by other complex processes such as angiogenesis and metastasis, similar to those in human cancer. More importantly, mouse tumor models provide temporally and genetically controlled systems for studying the tumorigenic process and response to treatment. However, initial efforts to create mouse models of glioma using single tumor suppressor knockouts or overexpression of single oncogenes mostly failed (Reilly and Jacks, 2001). It was subsequently found that, as confirmed by TCGA project, the core signaling pathways are crucial for gliomas: genetically engineered mice that activate RTK pathways in the brain, along with simultaneous loss of genes involved in cell cycle control develop glioma with high penetrance (Hambardzumyan et al., 2011). Also, like human gliomas, additional loss of the tumor suppressor PTEN causes higher-grade malignancy and reduced survival in mouse glioma models (Kwon et al., 2008a; Nickerson et al., 2002). Catalyzed by the profusion of genetic information arising from a number of genome-wide studies that revealed mutations present in human gliomas, as well as advances in molecular biology tools including retroviral/lentiviral techniques, dozens of genetic mouse glioma models have been generated over the last two decades (summarized in table 1-1).

Table 1-1: Summary of mouse models of glioma

Genetics	Techniques	Tumor type	Grade	Incidences
$NF1^{+/-}$;$P53^{+/-}$ (Reilly et al., 2000)	gKO	AST	II-IV	30-75%a by 15-55 wks
$ARF^{-/-}$ (Kamijo et al., 1997)	gKO	AST	NA	9% by 18-20 wks
$P53^{f/f}$ (Wang et al., 2009)	cKO (GFAP-Cre)	AST/MED (13%)	NA	88% by 24-52 wks
$NF1^{f/+}$;$p53^{-/+}$ (Zhu et al., 2005a)	gKO,cKO (GFAP-Cre)	AST	II-IV	100% by 14-40 wks
$NF1^{f/+}$;$p53^{-/f}$ (Zhu et al., 2005a)	gKO,cKO (GFAP-Cre)	AST	II-IV	100% by 14-40 wks
$NF1^{f/+}$;$p53^{-/+}$;$pten^{f/+}$ (Kwon et al., 2008a)	gKO,cKO (GFAP-Cre)	AST	III-IV	100% by 12-24 wks
$NF1^{f/+}$;$p53^{-/f}$;$Pten^{f/+}$ (Kwon et al., 2008a)	gKO,cKO (GFAP-Cre)	Ast	III-IV	100% by 11-24wks
$NF1^{f/+}$;$p53^{f/f}$;$pten^{f/+}$ (Unpublished observation)	cKO (GFAP-Cre)	AST	III-IV	100% by 11-24wks
$NF1^{f/+}$;$p53^{f/f}$;$pten^{f/+}$ (Alcantara Llaguno et al., 2009)	cKO (Nes-CreERT2, E13.5 induce)	AST	III-IV	100% by 11-24wks
$NF1^{f/+}$;$p53^{f/f}$;$pten^{f/+}$ (Alcantara Llaguno et al., 2009)	cKO (Nes-CreERT2, 4wk induce)	AST	III-IV	100% by 28-56 wks
$P53^{f/f}$;$pten^{f/+}$ (Zheng et al., 2008)	cKO (GFAP-Cre)	AST	III-IV	73% by 15-40 wks
GFAPZT121 (Xiao et al., 2002)	TG (bActin-Cre)	AST	II-III	100% by 25 wks
GFAPZT121;$Pten^{f/+}$ (Xiao et al., 2002)	TG, cKO (bActin-Cre)	AST	II-III	100% by 11wks
GFAPZT121;$pten^{f/f}$ (Xiao et al., 2005)	TG; cKO; MSCV-Cre virus	AST	NA	100%

GFAPHRasV12 (Ding et al., 2001)	TG	AST	II-IV	20-100% by 2-24 wks
GFAP-HRASV12;GFAP-EGFRvIII (Ding et al., 2003)	TG	OLIG/MIXED	III	100% by 2-13 wks
GFAP-HRASV12;Ad-EGFRvIII (Wei et al., 2006)	TG; virus	AST/MIXED	II-IV	95% by 12wk
GFAP-HRASV12;Pten$^{f/+}$ (Wei et al., 2006)	TG; cKO, Ad-Cre virus	AST	III-IV	73% by 8 wk
S100-v-erbB (Weiss et al., 2003)	TG	OLIG	II	60% by 52 wk
S100-v-erbB;INK4aARF$^{-/-}$ (Weiss et al., 2003)	TG; cKO	OLIG	III	90% by 24 wk
S100-v-erbB;p53$^{+/-}$ (Weiss et al., 2003)	TG, gKO	OLIG	III	80% by 24 wk
PDGF-B (Uhrbom et al., 1998)	MoMuL virus	AST/OLIG/PNET	NA	40% in 14-29 wk
PDGF-A (Jackson et al., 2006)	Infusion	NA	NA	100% in 6 days
PDGF-B;Ntv-a (Dai et al., 2001)	TG; RCAS virus	OLIG	Mianly II	60% by 12 wks
PDGF-B;Gtv-a (Dai et al., 2001)	TG; RCAS virus	OLIG	Mianly II	39% by 12 wks
PDGF-B;P53$^{-/-}$;Ntv-a (Dai et al., 2001)	gKO, TG; RCAS virus	GBM	IV	100% by 8 wks
GFAP-PDGFB;P53$^{-/-}$ (Dai et al., 2001)	TG gKO	GBM;OLIG	III-IV	43-68% by 24 wks
PDGF-B;INK4a/ARF$^{-/-}$;Ntv-a (Dai et al., 2001)	gKO, TG; RCAS virus	OLIG/MIXED/GBM	Mainly III-IV	57% by 12 wks
PDGF-B;INK4a/ARF$^{-/-}$;Gtv-a (Dai et al., 2001)	gKO, TG; RCAS virus	OLIG/MIXED/GBM	Mainly III-IV	70% by 12 wks
EGFRVIII;INK4a/ARF$^{-/-}$;NTV-a (Holland et al., 1998)	gKO, TG; RCAS virus	NA	NA	42% by 8-10 wk
EGFRVIII;INK4a/ARF$^{+/-}$;NTV-a (Holland et al., 1998)	gKO, TG; RCAS virus	NA	NA	52% by 8-10 wk
Kras;Akt;Ntv-a (Holland et al., 2000)	TG; RCAS virus	AST	IV	26% by 9 week
Kras;Akt;INK4a/ARF$^{-/-}$;Ntv-a (Uhrbom et al., 2002)	gKO, TG; RCAS virus	AST	Mainly IV	49% by 12 weeks

Kras;Akt;INK4a/ARF$^{-/-}$;Gtv-a (Uhrbom et al., 2002)	gKO, TG; RCAS virus	AST	Mainly IV	42% by 12 wks
HrasV12;AKT (Marumoto et al., 2009)	TG (GFAP-Cre); Lentivirus	AST	III-IV	42% by 16-20 wks
HrasV12;AKT;p53$^{+/-}$ (Marumoto et al., 2009)	gKO, TG (GFAP-Cre); Lentivirus	AST	Mianly IV	100% by 22 wks
EGFRvIII/vIII;INK4a/ARF$^{-/-}$;Pten$^{f/f}$ (Zhu et al., 2009)	TG; cKO, gKO, Ad-Cre virus	GBM	IV	100% by 10 wks
EGFRvIII/wt;INK4a/ARF$^{-/-}$;Pten$^{f/f}$ (Zhu et al., 2009)	TG; cKO, gKO, Ad-Cre virus	GBM	IV	100% by 13 wks
NF1$^{f/f}$ (Bajenaru et al., 2003; Zhu et al., 2005b)	TG (GFAP-cre)	AST	I	

gKO: germline knockout; cKO: conditional knockout; TG: transgenic animal; Ad-Cre: Cre expressing adenovirus
OLIG: oligodendroglioma; AST: astrocytoma; GBM: glioblastoma; MED: medulloblastoma; MIXED: oligodendroastrocytoma

Despite the success of re-creating glioma development in the mouse brain, many challenges still remain. Obviously, the guideline for creating mouse glioma models should be the molecular genetic information from human glioma studies. The interpretation of data from mouse model research and the subsequent translation of those findings to human studies rely on how faithfully a mouse model recapitulates the human disease. However, unlike human gliomas, gliomas from mouse models were usually poorly characterized. For example, it is clear that patients with oligodendrogliomas typically have a better prognosis compared to patients with astrocytoma of the same grade. However, in mouse models, such discrimination was frequently masked by the use of the general term, "malignant gliomas". Similarly, hundreds of genomic profiles of human glioma samples are now publically available and several molecular subclasses have been identified. In contrast, similar molecular information for each mouse glioma model is still scarce, as is the molecular subclassification of these tumors (Freije et al., 2004; Li et al., 2009a; Phillips et al., 2006; Verhaak et al., 2010). One intriguing finding from the TCGA dataset suggested that mutations in PDGFRA, NF1 and EGFR, although activating the same RTK pathway, correlate with the PN, MES or CL subtype, respectively (Verhaak et al., 2010). However, whether a certain genetic event determines a specific molecular subtype remains to be tested and genetic mouse models are an excellent system for testing such correlations.

In the near future, ever more faithful mouse glioma models that better recapitulate the complex genomic landscape of human gliomas are expected to be generated, and will be very powerful tools for the pre-clinical testing of personalized therapy. For example,

genome-wide sequencing efforts revealed that an average of more than 40 mutations was present in each GBM sample (Parsons et al., 2008). It is thus urgent to determine the driver mutations that are causal to oncogenesis rather than "passenger" mutations, which do not confer any selective advantage to the tumor cells. Mouse modeling will obviously be a useful tool for validating candidate driver mutations that are identified in statistical, cell biological, and biochemical studies from human gliomas. In addition, although it is arguable that alterations in a particular signaling pathway are more important for tumor formation, subtle differences in the phenotypic consequences of certain gene mutations may greatly confound the clinical value of using mouse models for identifying new targets or validating new therapeutic strategies. For example, several mouse glioma models using overexpression of mutated Ras oncogene have been established (Holland et al., 2000; Marumoto et al., 2009; Uhrbom et al., 2002; Uhrbom et al., 2005). However, only about 2% of human GBM samples have mutations in Kras, Nras or Hras (Knobbe et al., 2004; Network, 2008). In human GBM, activation of the RAS-MAPK pathway is usually driven by mutations in the tumor suppressor NF1, amplification of EGFR, or by the presence of the EGFRvIII mutation or overexpression of PDGFRA, which have been shown to be mutually exclusive genetic events (Network, 2008; Parsons et al., 2008; Verhaak et al., 2010). Biochemical studies implied that unlike Ras oncogene overexpression, the NF1 deletions and EGFRvIII mutation only slightly, although persistently, activate the MAPK pathway (Huang et al., 2009; Li et al., 2009c). Both mutations were also found to signal through the TOR2 complex instead of the TOR1 complex (Johannessen et al., 2005; Li et al., 2009c). Important details like these should always be considered when interpreting results from mouse models of glioma.

Furthermore, both human genetic data and mouse modeling confirmed that multiple genetic alterations are required for glioma formation. It takes more than a decade from the initial appearance of the first somatic mutation for a cell to acquire additional mutations and become a tumor cell in humans (Campbell et al., 2010; Yachida et al., 2010). Most current mouse models, on the other hand, have mainly focused on the final phenotype and histology of the disease but not on the kinetics of disease progression. Compound mutant mice with biallelic deletion of tumor suppressors throughout the brain were frequently used (Frese and Tuveson, 2007). This approach clearly promotes rapid tumor occurrence but fails to address the process of tumor evolution. In addition, gene function is usually studied by generating complete knocks out while somatic mutations in human tumor samples create a variety of neomorphic or hypomorphic alleles, which could act as gain of function as well as loss of function mutations. Mutations in P53 and IDH1 are prime examples of this category (Dang et al., 2010; Goh et al., 2011; Ward et al., 2010).

Understanding the temporal and spatial limitations of mutations in human cases of brain cancer is vital for answering key questions such as the cell of origin of sporadic gliomas, which usually arise clonally in adults from cells with somatic mutations (Visvader, 2011). Furthermore, pediatric gliomas and adult gliomas display unique properties and are clinically considered to be different diseases, while most mouse models utilize germline deletions or transgenic mice that activate mutations early on, during embryonic development or neonatally. These differences can cause development of completely

different tumor types. For example, injecting an EGFRvIII-expressing adenovirus into the cortex of GFAP-HrasV12 mice at 4 weeks of age yields mainly astrocytomas, while overexpressing both simultaneously using the GFAP promoter, which drives expression as early as E9 in the developing brain, resulted in oligodendrogliomas (Ding et al., 2003; Wei et al., 2006). In the future, these concerns can be addressed using different site-specific recombination systems as well as different inducible gene activation/deletion techniques.

Glioma stem cells

In addition to the overwhelming amount of genomic information that has recently become available, another rapidly progressing yet controversial area in glioma research is the cancer stem cell field. Cancer stem cells (CSCs), as defined by the American Association for Cancer Research (AACR) workshop on CSCs, are a subpopulation of cells in the tumor that have self-renewal capacity and can give rise to heterogeneous cancer cells that comprise the tumor (Clarke et al., 2006). Gliomas have been a favorite cancer for investigating the CSC hypothesis. It has long been observed that gliomas are highly heterogeneous, which is reflected in the name given to grade IV gliomas – glioblastoma "multiforme". Glioma stem cells (GSCs) were one of the first such type of cells isolated from solid tumors (Singh et al., 2004). In the original report, as few as 100 GSCs were shown to be sufficient to give rise to tumors with histology that recapitulated the parental tumors in immunodeficient mice. In contrast, as many as 1,000,000 non-glioma stem cells were required to achieve comparable tumorigenic potential (Singh et al., 2004).

Unlike traditional glioma cell culture with serum, GSCs were cultured in vitro as monolayer or as spheroids using serum-free medium containing EGF and FGF (Lee et al., 2006; Singh et al., 2004). Interestingly, the glioma stem cells isolated from human tumors and then cultured in vitro showed remarkable similarities to normal neural stem cells (NSCs). For example, cultured GSCs express neural stem/progenitor markers such as Nestin, Sox2 and Olig2. Upon induction, they can be differentiated to cells with neuronal or glia markers. Using cells derived from the same primary GBM tissues, Lee et al. performed an extensive comparison of traditional serum-containing culture versus serum-free GSC culture (Lee et al., 2006). They reported that the genetic content of parental tumors can be stably preserved under stem cell culture conditions while cells maintained in serum-containing medium underwent dramatic genetic and epigenetic changes over time. More importantly, transplanting glioma stem cells into immunodeficient mice yielded tumors that shared similar histology and global gene expression patterns with their parental tumors. By contrast, in serum-containing medium, early passage glioma cells were completely incapable of tumor formation after transplantation while late passage glioma cells gave rise to morphologically distinct tumors containing a different molecular signature than the original tumors (Lee et al., 2006). The glioma stem cell culture thus provided a more reliable and physiological relevant model to study the mechanism of the disease.

Controversies in the glioma stem cell field

Initially, GSCs were cultured as spheroids in EGF- and FGF-containing medium and it was reported that CD133/prominin-1-positive cells were enriched for CSCs (Singh et al., 2004). However, subsequent studies have suggested that CD133 was not as reliable a CSC marker as originally thought: two different groups reported that CD133-negative tumor cells isolated from GBMs can be stably passaged under the same stem cell conditions. Interestingly, similar to the previously identified CD133+ cells, these cells also showed "stem cell" properties such as self-renewal and differentiation in vitro, and formed transplantable tumors in a xenograft model (Beier et al., 2007; Joo et al., 2008). Interestingly, unlike the CD133+ cells, which can form floating spheroids in culture, the CD133- cells tend to grow as adherent spheres. Recently, a small population of CD133- cells that can give rise to CD133+ cells was reported, suggesting a possible stem cell hierarchy in the spheroid culture system (Chen et al., 2010). To complicate matters even further, it was reported that the CD133 antibody used to isolate CD133+ GSCs was most likely binding to a specific configuration of the glyco-modified protein that has no correlation with the mRNA level, thus making it unsuitable for other model systems where different antibodies are used (Kemper et al., 2010). As a result, more generally applicable stem cell markers were suggested, such as CD44, CD15 and integrin alpha 6 (Anido et al., 2010; Lathia et al., 2010; Son et al., 2009). CD44 is a mesenchymal lineage marker that was used as a CSC marker in several solid tumors (Al-Hajj et al., 2003; Collins et al., 2005; Dalerba et al., 2007; Li et al., 2007). However, whether CD44 is expressed in all GBM tumors, especially in molecular subtypes other than mesenchymal, is unknown (Phillips et al., 2006). CD15 was used as a surface marker for identifying normal adult neural stem cells as well as neural stem cells that differentiated from

embryonic stem cells (Capela and Temple, 2002). Reya et al. reported CD15 as a CSC marker in a mouse model of medulloblastoma (Read et al., 2009). It was then discovered that CD15 can also be used to enrich for GSCs from both CD133-positive and negative GBMs (Son et al., 2009). However, this epitope was not expressed on cells isolated from tumors in our mouse models of glioma driven by co-deletion of NF1, P53 and Pten, although it is detected in medulloblastomas created by the same set of mutations (unpublished observation). The possibility that integrin alpha 6 could be a CSC marker arose from the hypothesis that glioma stem cells are located in endothelial niches, which are known to express laminin (Lathia et al., 2010). However, the existence of such a niche is still under dispute (discussion below).

It is known that normal NSCs reside in specific anatomic regions of the brain: the subventricular zone (SVZ) and subgranular layer (SGZ) (Zhao et al., 2008). In those regions, specific cells, including endothelial cells and ependymal cells, form a niche that nourishes the NSCs and supports their self-renewal (Ramirez-Castillejo et al., 2006; Shen et al., 2004). This “seed-and-soil” relationship has been adapted in CSC research, as CSCs also require a specific microenvironment to maintain their “stem cell” properties. If this is the case, then targeting the CSC niche should result in depletion of the CSCs. Like normal NSCs, Nestin+ and CD133+ GSCs have been reported to reside in a vascular niche (Calabrese et al., 2007). Co-culturing CD133+ GSCs with endothelial cells enhanced their proliferation in vitro. Co-implantation of both CD133+ and endothelial cells promoted tumor growth in a xenograft model while angiogenesis antagonists eradicated GSCs and significantly slowed tumor growth (Calabrese et al., 2007).

However, the in vitro observation from the co-culture experiment could potentially be compromised by the strong mitogenic effect of endothelial cell growth factor in the endothelial cell culture medium. On the other hand, the putative "stem cell" markers Nestin and CD133 are also expressed by endothelial cells, making the immunohistochemistry results unreliable (Kelly et al., 2007; Klein et al., 2003). Furthermore, a "chicken first or egg first" paradox exists in the vascular niche hypothesis, as GCSs themselves can elicit angiogenic effects by secreting factors such as SDF-1 and VEGFA (Folkins et al., 2009; Li et al., 2009d). Under certain conditions, GSCs can even directly transdifferentiate into the endothelial lineage, making it difficult to determine whether the vascular niche is required for glioma stem cell maintenance (Ricci-Vitiani et al., 2010; Soda et al.; Wang et al., 2010). Finally, the vascular niche hypothesis failed to explain several clinical and experimental observations. First, glioma cells are notorious for infiltration: malignant gliomas invariably recur after surgical removal of the tumor indicating that the peripheral regions of the tumor contain cancer stem cells. However, histological observations from both human GBM samples and mouse tumor models suggested that glioma cells typically migrate along white matter (WM) tracts and not their proposed vascular niches (David N. Louis, 2007). Second, it is known that hypoxic conditions facilitate self-renewal of both NSCs and GSCs in culture (Clarke and van der Kooy, 2009; Li et al., 2009d). Hypoxia factor 2a was reported to regulate tumorigenic potential of GSCs and its expression correlates with poor clinical outcome of glioma patients (Li et al., 2009d). A high percentage of CD133-positive cells were also observed in the pseudopalisade formations that delineate the necrotic center of GBMs, which was thought to be caused by hypoxia (Christensen et al., 2008). In vivo, deletion of HIF-1a

resulted in a decline in hippocampal neurogenesis (Mazumdar et al., 2010). It is thus difficult to reconcile the function of hypoxia in neural/glioma stem cells with the vascular niche hypothesis, where high levels of oxygen are supplied to neighboring stem cells. Third, in several mouse tumor models, although inhibition of angiogenesis can shrink the original tumor, it also promotes malignant progression by increasing tumor cell invasion and metastasis (Ebos et al., 2009; Keunen et al., 2011; Paez-Ribes et al., 2009). Similar findings have been observed in bevacizumab-treated GBM patients where the tumor phenotype shifted to a predominantly infiltrative pattern (de Groot et al., 2010; di Tomaso et al., 2011). As a result, bevacizumab treatment leads to an increase in length of a progression-free stage but not in overall survival time (T. F. Cloughesy, 2008 (May 20 suppl; abstr 2010b)). Therefore, there could be more than one defined niche for GSCs (Figure 1-3). A hypoxic environment could be one such niche. Hypoxia promotes glioma stem cell (most likely quiescent because of a lack of nutritional supply) infiltration. The infiltrating GSCs, under certain conditions, can home to vascular niches or recruit endothelial cells by secretion of chemokines such as stromal-derived factor 1 (SDF-1). Similar to what has been observed for normal NSCs (Kokovay et al., 2010), the newly established nutritional source then activates the quiescent cancer cells to proliferate and colonize new tumors.

CSCs were defined as cells that maintain the tumor in vivo (Clarke et al., 2006), however, due to technical or ethical limitations, the current demonstration of CSCs usually involves prospective isolation of a subpopulation of cells from tumors and tumorigenic assays using immunodeficient rodents (Clarke et al., 2006). Although the tumorigenic

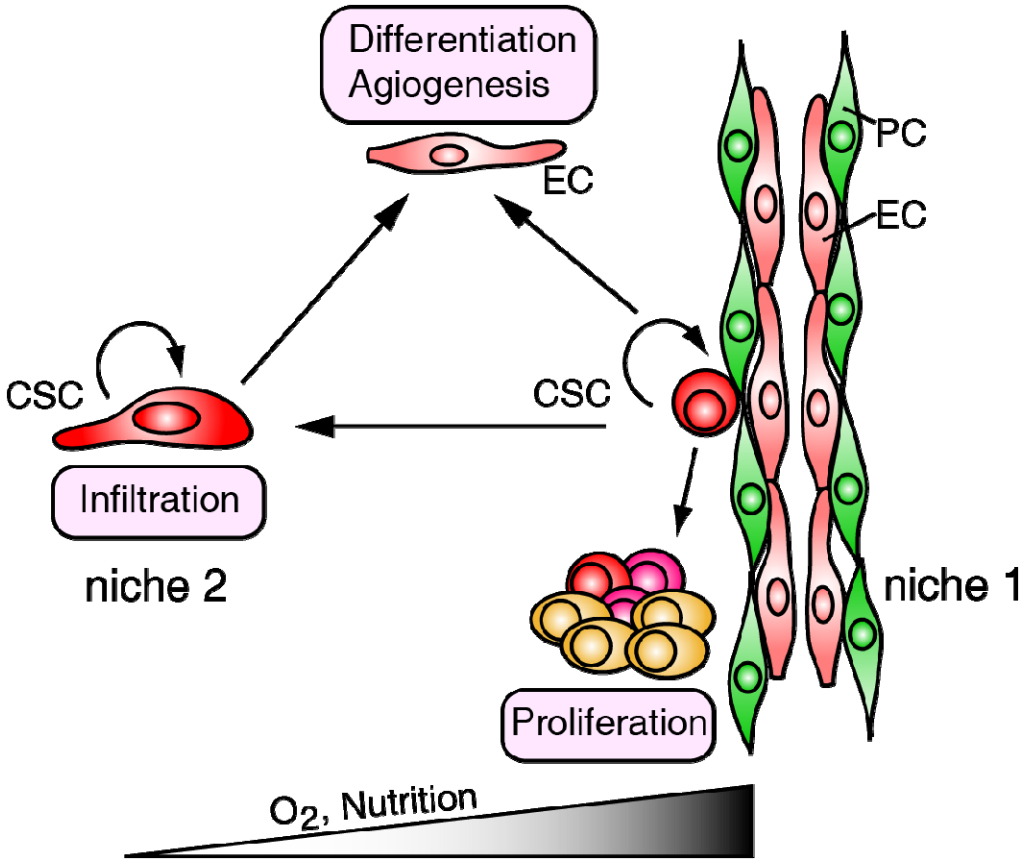

Figure 1-3. Vascular niche and hypoxia niches of glioma stem cells (GSCs). The vascular niches (niche 1) are found to be important for glioma growth probably due to the secreted niche factors from the endothelial cells as well as nutrition supply from the blood vessels. On the other hand, constantly infiltrating glioma stem cells probably maintain their stemness through activation of hypoxia-related pathway (niche 2). At the same times, GSCs can recruit endothelial cells by secreting angiogenesis factors or directly differentiating into endothelial lineage, which in turn supports glioma growth.

assay of serially transplanting cells into immunodeficient hosts is considered the "gold standard" assay for the validation of CSCs, the ability to form a tumor in an immunodeficient host does not necessarily correlate with the true definition of CSCs, which is defined by its tumor maintenance function in vivo (Gupta et al., 2009; Quintana et al., 2008). In fact, primary glioma cells, as well as glioma cell lines, under serum-containing "non-stem cell" culture condition, can form tumors when transplanted. Recently, it has also been reported that the variability of the transplantation assay could greatly impact the estimation of CSC frequency (Boiko et al., 2010; Ishizawa et al., 2010; Kelly et al., 2007; Quintana et al., 2008). In some tumor types, a large fraction of the tumor cells can initiate tumor formation in more severely immunodeficient mice if supplied with an artificial microenvironment (Quintana et al., 2008). As the field was still in its early stages, experiments were performed using various conditions; however the term "cancer stem cell" was ubiquitously applied, making it difficult to compile results from different sources. Finally, the "cancer stem cell" nomenclature was first borrowed from normal tissue stem cells to describe the abilities required for maintaining tumor growth: self-renewal and giving rise to other tumor cells. The CSC concept and properties are frequently confused with the dogma of normal tissue stem cells (Jordan, 2009). The hierarchy of normal tissue stem cells is always well defined and conserved. In contrast, tumors have always shown a huge degree of diversity. For example, CSCs in mouse models of lung cancer driven by different mutations express distinct surface antigens (Curtis et al., 2010).

The inconsistent findings observed in GSC research could be potentially explained by the fact that gliomas can be classified into several subtypes according to either pathology or molecular genetics. In fact, it was reported that GSC spheroids cannot be derived from secondary GBMs (Beier et al., 2007). CD133- GBMs usually showed different histology, and the GSCs isolated from these tumors harbored distinct molecular signatures compared to CD133+ tumors (Beier et al., 2007; Joo et al., 2008). Additionally, although spheroid cultures can be established from various brain tumor types in addition to glioma, these cultures can display distinct properties. For example, addition of BMP4 to GSCs isolated from astrocytic tumors and GBM can efficiently differentiate these cells while it has only a minor effect on spheroids isolated from oligodendrogliomas (Persson et al., 2010; Piccirillo et al., 2006). Likewise, even in the same tumor, CSCs are not likely to be a static population: multiple clones of CSCs with diverse genetic alterations could exist, and those stem cells would be under selective pressure at the same time (Figure 1-4). Such genetic variation has been observed for leukemia stem cells by single cell fluorescence immunohybridization and DNA copy number profiling (Anderson et al., 2011; Notta et al., 2011). It has been suggested that the tumor is maintained by a cellular hierarchy that is similar to Darwin's evolutionary tree structure rather than a linear hierarchical structure (Greaves, 2010). Consistent with this idea, Piccirillo et al. isolated two "stem-like" cell populations, from the periphery and the core of the same GBM samples, that display distinct tumorigenic potential and cytogenetic profiles (Piccirillo et al., 2009). The heterogeneity of tumor phenotypes is thus likely to be determined by both the clonal diversity of CSCs and their differentiation capacity. Another possible layer of complexity, which has yet to be demonstrated in vivo, suggests that the progeny of cancer

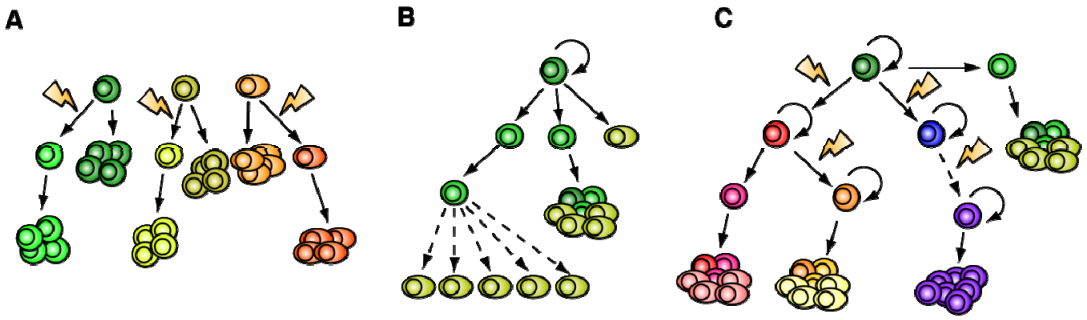

Figure 1-4. Cancer maintenance models. A) Clonal evolution model. Tumor cells are equivalent and a majority of the tumor cells have the ability to sustain tumor growth. B) Traditional view of cancer stem cell model. A stable hierarchical structure exists in tumor cells and only cancer stem cells have the ability to self-renew and contribute to long-term maintenance of tumor growth. C) Evolutionary view of cancer stem cell model. The hierarchical structure of cancer stem cells is constantly evolving due to natural selection and genomic instability. New cancer stem cell clones with different genetic alterations emerge over time. Certain genetic events will ultimate grant most tumor cells self-renewal capacity without reliance on niches or stemness factors (Dash arrow).

stem cells are plastic and can revert back to a stem cell-like state. In melanoma, it was reported that a slow-cycling JARID1B-positive population that can give rise to JARID1B-negative cells is essential for tumor growth and for preventing growth exhaustion (Roesch et al., 2010). However, in contrast to the typical unidirectional hierarchy of cancer stem cells, the JARID1B-expressing population is not pre-determined and can be dynamically changed. Furthermore, Weinberg et al. proposed another hypothesis: that a process similar to epithelial to mesenchymal transition (EMT) could lead to conversion of the non-cancer stem cells and CSC compartments (Gupta et al., 2009; Mani et al., 2008). EMT is a developmentally regulated process and believed to be involved in breast cancer metastasis. It has been reported that breast epithelial cells that have undergone EMT showed characteristics resembling CSCs (Mani et al., 2008). It is known that sphere-forming cells in wild type SVZ neural stem cell culture are mostly derived from the progenitor cells that respond to EGF and FGF stimulation (Doetsch et al., 2002). Whether similar processes are also involved in glioma development in vivo is still unclear. Finally, it is formally possible that the majority of late stage carcinoma cells can acquire enough mutations making them capable of giving rise to new tumors (Figure 1-4). It was reported that CD271-positive cells in melanoma were enriched for tumor-propagating cells while the majority of melanoma cells isolated from late stage tumors or tumors that have been expanded through xenograft transplantation fulfilled criteria of CSCs (Boiko et al., 2010; Quintana et al., 2008).

Targeting glioma stem cells

The genetic diversity of CSCs and the potential plasticity of non-cancer stem cells revealed more commonalities between the two tumor maintenance models - the cancer stem cell model and the clonal evolution model - posing a serious problem for targeted therapy designed for a single genetic alteration. In contrast to the clonal evolution model, in which drug resistant clones would be random and unpredictable, the common "stem-like" properties of the tumor-propagating cells provide an additional angle for therapeutic intervention. Zhou et al. have provided a detailed report summarizing the ongoing clinical and pre-clinical studies targeting CSCs (Zhou et al., 2009). Here, we briefly describe a few of the potential strategies that can be utilized to target CSCs.

1). Targeting self-renewal pathways. Self-renewal is the fundamental difference between CSCs and non-CSCs in tumors. CSC researchers have therefore focused much attention on important developmental signaling pathways as possible therapeutic targets in cancer. Numerous studies have shown that pathways such as Sonic hedgehog, Notch and Wnt, as well as key "stemness" factors such as Olig2, Bmi1 and Nanog, play important roles in glioma stem cell maintenance (Anido et al., 2010; Bruggeman et al., 2007; Ligon et al., 2007; Piccirillo et al., 2006; Po et al., 2010; Stiles and Rowitch, 2008; Zbinden et al., 2010; Zheng et al., 2010; Zhou et al., 2009). Chemical compounds or RNAi constructs that block components of those pathways have been shown to slow down glioma stem cell growth in vitro and attenuate tumor formation in transplantation assays. On the other hand, factors that promote differentiation can be another viable approach to eliminate CSCs. One such example mentioned earlier is BMP4, which induces astrocytic differentiation of GSCs and dramatically reduces the tumorigenic potential of CD133+

human GSCs (Piccirillo et al., 2006). Another approach to inhibit CSC self-renewal is to target the CSC niche, which is believed to support CSC self-renewal. Consistent with this idea, preclinical studies that target the vascular niches using angiogenesis inhibitors, or by blocking the CSC-niche interaction with laminin antibodies effectively delay tumor formation in xenograft models (Calabrese et al., 2007; Lathia et al., 2010).

2) Inhibiting glioma stem cell survival pathways. GBM is notoriously refractory to chemotherapy and radiation. It is believed that GSCs may be an underlying cause for this resistance to chemo- and radiation therapy. Indeed, studies have revealed that CD133+ glioma stem cells in vitro were more resistant to radiation compared to the CD133- population due to activation of DNA repair pathways by CHK1/CHK2 (Bao et al., 2006). The role of CHK1/CHK2 in radiation resistance has recently been validated in a mouse model of glioma driven by PDGF-B overexpression in combination with P53 loss (Squatrito et al., 2010). Several CHK1/CHK2 inhibitors have been developed and their effectiveness remains to be examined (Zhou and Sausville, 2003). Another property of certain stem cell populations as well as cancer stem cells is the ability to efflux Hoechst dye which serves as the basis of the "side population" (SP) assay (Golebiewska et al., 2011). This property is thought to be caused by the expression of ATP-binding cassette transporters (ABCTs) (Golebiewska et al., 2011). Consistent with this idea, Eric Holland's group showed that glioma stem cells in a PDGF-induced mouse model were enriched in side population that also expressed ABCG2 (Bleau et al., 2009). In addition, the expression of ABCG2, as well as the drug resistant phenotype of GSCs, were found to be regulated by the PTEN/PI3K/AKT pathway and could be blocked by AKT

inhibitors (Bleau et al., 2009). However, whether GSCs are enriched in the SP is still controversial. Both SP and non-SP cells from cell lines as well as human glioma tissues were reported to be tumorigenic (Bleau et al., 2009). Inconsistency between SP and ABCG2 expression has also been reported: Patrawala et al. demonstrated that both the ABCG2+ and ABCG2- population can initiate tumors after transplantation (Patrawala et al., 2005). More interestingly, the ABCG2- population was found to express higher levels of "stemness" genes and to be more clonogenic (Patrawala et al., 2005).

3). Targeting stem cell surface markers. The ability to isolate CSCs using cell surface epitopes also provides an opportunity for therapeutic interventions, especially for immunotherapy. Monoclonal antibodies can be used to elicit antibody-dependent cellular toxicity or complement-dependent toxicity. They can also be used to target cellular receptors that are important for CSC self-renewal, survival, and evasion of host immunosurveillance. Furthermore, antibody-chemo/radiation drug conjugates can be designed to achieve more specific drug delivery with lower toxicity. Several successful preclinical studies using this strategy to treat leukemia models have been reported. For example, CD44 antibody can efficiently block leukemia CSCs from homing to their bone marrow niche, resulting in attenuated BCR-ABL-induced leukemia in recipient mice (Charrad et al., 1999; Jin et al., 2006). In addition, both mouse and human leukemia CSCs were eliminated by a CD47 antibody that triggered phagocytosis by macrophages (Jaiswal et al., 2009; Majeti et al., 2009). As we gain a better understanding of GSCs and their surfacome, similar strategies are likely to be applied in glioma research and treatment.

4). Eliminating quiescent cancer stem cells. Cancer is considered a disease of abnormal cell proliferation and so most therapeutic strategies have been designed to target rapidly dividing cells. However, recent studies from leukemia and several solid cancers suggested that CSCs are a relatively slow-cycling population that is not targeted by those drugs. In order to completely block tumor reemergence, understanding the mechanisms underlying this relative quiescence is necessary. For example, melanoma cells in culture are maintained by a population of slow-cycling cells that express the histone H3 lysine 4 demethylase JARID1B. Knocking down this enzyme by RNA interference temporarily increases cell proliferation but is then followed by exhaustion of cell proliferation (Roesch et al., 2010). Furthermore, a combinational strategy can be used that first induces quiescent CSCs to re-enter the cell cycle followed by treatment with conventional radiation/chemo-therapy that targets the dividing cells. This method has been shown to significantly prolong survival of mice that had undergone leukemia cell transplantation compared to leukemia cell transplanted mice treated with chemotherapy alone (Saito et al., 2010). It is well known that normal GFAP-positive stem cells are mainly quiescent in the brain (Doetsch et al., 1999). Secreted factors that help to maintain the quiescence have been reported (Lim et al., 2000; Ramirez-Castillejo et al., 2006). Given the similarity between NSCs and GSCs in vitro and in vivo, it would be interesting to see whether the quiescent cancer stem cell theory also holds up in gliomas.

It is important to state that the application of a particular GSC targeting strategy to a specific case should be examined very carefully as the properties of CSCs can be greatly

affected by the genetic and pathologic nature of the tumor, as well as the heterogeneity within the tumor. The controversy surrounding stem cell surface antigens is one such example. Another example is the differentiation-inducing agent BMP4. As discussed earlier, BMP4 very efficiently induces astrocytic differentiation of glioma stem cells from GBM, but has only minor or no effect in treating GSCs from oligodendrogliomas or GSCs that have had their BMP receptor silenced epigenetically (Lee et al., 2008; Persson et al., 2010; Piccirillo et al., 2006). The integration of molecular genetics with CSC research in the future will yield more informative and practical guidelines for clinical applications.

Cell of origin of glioma

Besides the difference in genetic alterations, another potential factor contributing to tumor subtype diversity and heterogeneity is the tumor cell of origin. Cells of origin are the normal cells in which tumorigenic mutations first occur and accumulate to form a full-blown malignancy. CSCs, on the other hand, are defined as the cells that maintain an already formed tumor. However, the two concepts are frequently confused, especially when CSCs are also referred to as “tumor-initiating cells”. As Jane E. Visvader pointed out, the term “tumor-initiating cells” is more in line with the “cells of origin”, while CSCs would more accurately be referred to as “tumor-propagating cells” (Visvader, 2011).

Prior to the discovery of adult NSCs, astrocytes were thought to be the origin of gliomas as they were the only known replication-competent population (Figure 1-5). The

malignant transformation process requires a “dedifferentiation” process by which differentiated cells regain immature glial and progenitor properties. The feasibility of this dedifferentiation process is supported by recent findings demonstrating that a certain transcription factor cocktail can reprogram terminally differentiated cells back to pluripotent embryonic stem cells (Takahashi and Yamanaka, 2006). Indeed, early cortical astrocytes in culture can be reverted back to a neural stem/progenitor-like status by deleting the tumor suppressors INK4a/ARF or prolonging treatment with growth factors (Bachoo et al., 2002; Ghashghaei et al., 2007; Sharif et al., 2007). Several studies reported successful generation of gliomas by transforming early cortical astrocytes in vitro and in vivo (Bachoo et al., 2002; Uhrbom et al., 2002). However, evidence supporting mature astrocytes as possible cells of origin of gliomas is still lacking. In vivo efforts using genetically engineered mice or viral delivery were limited by the lack of a good mature astrocyte marker. It is now well known that the widely used “astrocyte” marker GFAP is also expressed by adult NSCs (Figure 1-5) (Doetsch et al., 1999). In vitro, culturing mature astrocytes is extremely difficult and astrocyte cultures from neonatal mouse cortex were reported to contain immature progenitor cells (Laywell et al., 2000). Additionally, transformation of neonatal astrocytes relies on deletion of INK4a/ARF in many studies. Given their roles in reprogramming and aging (Li et al., 2009b; Molofsky et al., 2006; Utikal et al., 2009), whether the germline deletion of INK4a/ARF itself affects glial maturation is still unclear, and thus further compromises the interpretation of these studies.

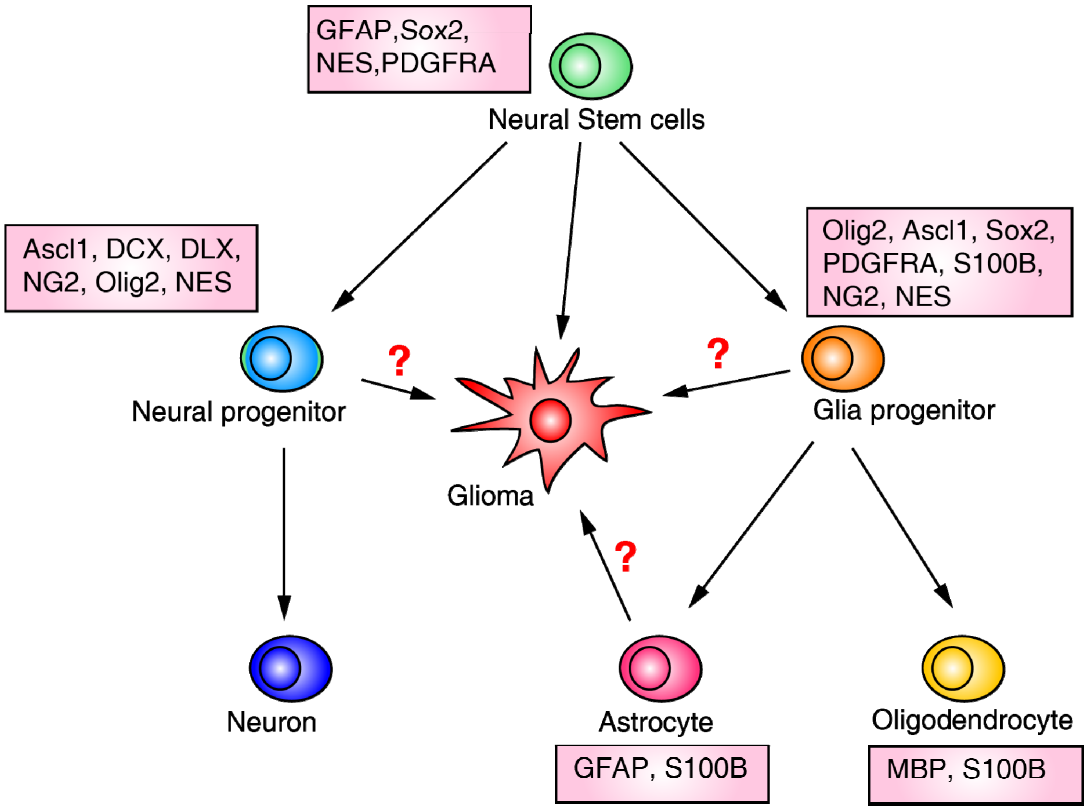

Figure 1-5. Cell of origin of gliomas. Mutations in adult neural stem cells are sufficient to drive malignant glioma formation in vivo. Evidences of progenitors or mature astrocytes origination has been presented in vitro and in vivo however strict proof has not been shown due to the lack of specific lineage markers (pink boxes) in vivo.

The discovery of self-renewing NSCs in postnatal mammalian brains (Zhao et al., 2008), provided an attractive alternative candidate for the cell of origin of gliomas (Figure 1-5). Self-renewal capacity gives the NSCs a natural "advantage" in accumulating oncogenic mutations. The oncogenic process can then be viewed as NSCs losing control over their self-renewal and differentiation properties. Several lines of evidence now suggest that the NSCs are more susceptible to malignant transformation. 1) Abnormalities first occur in the NSC niches of pretumorigenic mice in spontaneous mouse models of glioma (Kwon et al., 2008a; Zhu et al., 2005a). 2) An RCAS virus expressing active forms of Kras and Akt can transform nestin-positive progenitor cells far more efficiently than the GFAP-positive population in neonatal mouse brains (Uhrbom et al., 2002). 3) Temporally deleting the tumor suppressors P53, NF1 and Pten specifically in postnatal mouse neural stem/progenitor cells using a tamoxifen-inducible Nestin-Cre results in glioma formation with 100% penetrance, while ablation of the same combination of tumor suppressors in non-neurogenic adult brain regions using Cre adenovirus did not produce tumors (Alcantara Llaguno et al., 2009). Similarly, ablation of P53, Pten and/or Rb in SVZ stem cells but not in the peripheral astrocytes yielded gliomas (Jacques et al., 2010). It should be noted that these experiments were unable to distinguish the more quiescent, long term self-renewing NSCs from the more rapidly-dividing progenitor cells with limited self-renewal potential. Studies involving different forms of leukemia have demonstrated that lineage restricted progenitors are able to regain the property of self-renewal and cause tumor formation or disease progression (Cozzio et al., 2003; Jamieson et al., 2004; Krivtsov et al., 2006; So et al., 2003). In fact, the NG2+, PDGFRA+ oligodendrocyte progenitor cells (OPCs) in mouse brain were susceptible to oncogenic events and

oligodendroglioma formation (Persson et al., 2010). Oligodendroglioma in human patient samples was also found to be associated with white matter (WM) and expressed oligodendrocyte progenitor markers (Persson et al., 2010). Nevertheless, similar caveats also exist in those studies. Human glioma cells are known to migrate through the WM tracts, and the oligodendrocyte lineage marker PDGFRA is expressed by both NSCs and OPCs (Figure 5) (Jackson et al., 2006). A population of multipotent NG2+ cells was also identified in the mouse brain (Aguirre et al., 2004; Rivers et al., 2008; Zhu et al., 2008); it is still unknown whether those cells have long-term self-renewal capacity. Finally, SVZ NSCs can differentiate into oligodendrocytes and migrate into the WM (Menn et al., 2006). This process can be greatly enhanced by EGF infusion (Aguirre et al., 2007; Gonzalez-Perez and Alvarez-Buylla, 2011), and amplification of EGFR was frequently identified in both astrocytomas and oligodendrogliomas (Persson et al., 2010).

Mouse models are important tools for investigating and validating the cell of origin of cancers, and it is critical that genetic alterations and physiological setting of tumor development closely resemble that seen in human patients. In addition, cell of origin studies address tumor development and progression, which usually takes years if not decades in human patients. An ideal model system for studying the cell of origin should not only address whether the cells are capable of transformation following a set of simultaneous oncogenic events but also by accumulation of mutations over time. Knowledge of cell-specific markers combined with technologies that achieve more precise temporal and spatial somatic gene manipulation could greatly facilitate future studies. Histopathology and higher resolution molecular genetic analyses (e.g. single cell

analysis) of patient samples at different stages will also provide valuable information. For example, microarray studies of human GBM samples suggested that different molecular subtypes share similarity with profiles of different neural lineages, suggesting potentially different origins (Verhaak et al., 2010). However, studies in other solid tumors including breast cancer, pancreatic tumors, and basal cell carcinomas reported that histopathology and molecular markers of malignant tumors can be misleading. Breast cancers with BRCA1 mutations usually show basal cell-like marker expression even though they arise from luminal progenitor cells (Lim et al., 2009). And early abnormalities were observed in the acinar cells from Kras-driven pancreatic duct carcinomas (De La et al., 2008). It has yet to be determined whether a similar phenomenon occurs in the origin of gliomas.

Concluding Remarks

In summary, although many questions and controversies remain, our understanding of glioma has increased dramatically in recent years. For the first time, we have a clear picture of the human GBM genomic landscape. This information is being validated and incorporated into sophisticated animal models that further advance our knowledge of disease origin, progression and treatment. At the same time, the cancer stem cell theory not only provides novel cancer targeting strategies from aspects of developmental biology, but also provides insights into tumor maintenance, therapy resistance and recurrence. The accumulation of this knowledge provides great opportunities to improve and even revolutionize current diagnosis and treatment of human malignant gliomas, especially GBM, which typically causes lethality within 1 year.

CHAPTER TWO

MOLECULAR CHARACTERIZATION OF A MOUSE MODEL OF GLIOMA

Introduction

The mouse genome and human genome share more than 80% sequence similarity (Gregory et al., 2002). It is generally believed that the same genetic alterations can result in similar phenotypes in both human and mouse. Various human cancers can thus be recreated in the mouse by either overexpression of oncogenes or deletion of tumor suppressors in order to facilitate the study of tumor development and treatment (Frese and Tuveson, 2007). However, it is still unknown to what extent these mouse models can reproduce the cognate human cancer. For example, homozygous Rb deletion in human is necessary to cause retinoblastoma, however, loss of Rb alone is not sufficient to produce the same type of tumor in mice. Additional deletion of p107, another Rb-related tumor suppressor, is also required (Robanus-Maandag et al., 1998).

Over the last few years, our lab has established a series of mouse models of glioma (Alcantara Llaguno et al., 2009; Kwon et al., 2008a; Zhu et al., 2005a). These mouse models utilize a brain-specific hGFAP-Cre that selectively ablates a combination of tumor suppressors including NF1, P53 and Pten, the most frequent somatic mutations found in human GBMs (Network, 2008). When only NF1 and P53 were deleted, the mice developed low-grade gliomas that eventually progressed to high-grade gliomas (Zhu et al., 2005a). The additional loss of one Pten allele further accelerated tumor formation and

resulted in predominantly high-grade gliomas (Kwon et al., 2008a). Tumors from these mouse models were shown to have undergone similar oncogenic events as human gliomas, such as spontaneous loss of heterozygosity, and also shared indistinguishable histological features (Alcantara Llaguno et al., 2009; Kwon et al., 2008a; Zhu et al., 2005a). However, the global gene expression signature of these mouse model tumors and their degree of similarity to human glioma samples at the molecular level remained unknown.

As discussed in chapter 1, molecular genetics and global gene expression profiling have been used for detailed classification and characterization of glioma subtypes. Chapter 1 summarized several studies. For example, the analysis of gene expression profiles from human GBM samples undertaken by the TCGA project classified GBM further into 4 subtypes: the proneural (PN), neural (NL), classical (CL) and mesenchymal (MES) subtype (Verhaak et al., 2010). Furthermore, integration of the gene expression data with genomic alteration information suggested that the PN, CL and MES subtypes correlate with mutations in the PDGFR/IDH, EGFR and NF1 genes, respectively (Verhaak et al., 2010). However, it is unclear whether certain genetic mutations are causal events leading to this distinct molecular subclassification. The defined genetic background of our mouse glioma models offers the ideal setting to investigate this question.

Unfortunately, complicated experimental variables embedded in the microarray dataset make it impossible to directly compare expression profiles of the same biological phenotype using the same microarray platform from different labs (Irizarry et al., 2005).

Cross-species comparisons using the public datasets not only requires dealing with the "lab effect", but also handling homology assignments between species as well as cross-platform comparison (Hong and Breitling, 2008; Irizarry et al., 2005; Lu et al., 2009). Many sophisticated bioinformatic methods have been developed to overcome these issues. One of these methods is Gene Set Enrichment Analysis (GSEA), which has been successfully applied to evaluate similarity between Kras-driven mouse lung cancer and human lung adenocarcinoma (Subramanian et al., 2005; Sweet-Cordero et al., 2005). Basically, differentially expressed genes (DEGs) were obtained in each dataset and GSEA treats each gene as either differentially expressed or not. DEGs were sorted according to a differential expression score. For a predefined list of genes (GOI), an enrichment score (ES) is calculated to determine whether members of GOI are randomly distributed throughout the sorted DEGs or primarily located on the top or bottom. For cross-species comparison between our mouse model of glioma and other human tumors, we first calculated the DEGs by comparing our mouse tumors to the normal brain tissues and mapped them to their human homologs. The mapped DEGs were then used as GOI. Additionally, gene expression values of various human cancers compared to their normal tissue control are rank ordered. An ES is derived by comparing the GOI to each rank ordered gene list from human cancer datasets. A higher positive ES suggests higher enrichment for up-regulated genes, while a lower negative ES suggests better similarity for down-regulated genes.

Results

Molecular profiling of mouse gliomas

Six malignant mouse glioma samples from hGFAP-Cre;NF1$^{f/+}$;P53$^{-/+}$ (hGFAP-Cre;Mut3) mice were used for gene expression profiling studies. As a control group, we dissected out similar anatomic brain regions from 6 age-matched Cre-negative animals. RNA samples were processed and hybridized to Illumina WG6v2 array. Initial data analysis revealed that 2387 upregulated probes and 2516 downregulated probes were found to be changed at least 2 fold, which represented 1477 upregulated (Appendix A) and 1541 downregulated (Appendix B) uniquely annotated genes respectively. Functional clustering by gene ontology analysis suggested that genes involved in categories such as DNA replication and cell cycle were enriched in the up-regulated gene list (Appendix C); genes with functions related to synapse, GTPase activation were enriched in the down-regulated gene list (Appendix D).

Mouse gliomas share similar molecular signature as human GBMs

In order to test which human cancers most closely share a common molecular signature with our mouse glioma model tumors, expression profiles of various tumor tissues and their normal tissue controls were obtained from public databases (Table 2-1). The 1477 up-regulated and 1541 down-regulated differentially expressed genes in the mouse gliomas were mapped to probes of different platforms used in the human studies. This process yielded a total of 833 non-redundant upregulated and 847 non-redundant downregulated genes that also have common probes in all the human tumor profiles.

Table 2-1. Human tumor expression dataset summary

Tumor Type	Source	Tumor	Control	Platform	Array	GEO	Citation	Organization
Lung Adenocarcinoma	Boston	34	60	Affymetrix	HGU95Av2	NA	Nat Genet. 37(1):48-55	Broad Institute
Prostate cancer	Boston	49	46	Affymetrix	HGU95Av2	NA	Cancer Cell.1(2):203-9	Broad Institute
Breast cancer	Boston	40	7	Affymetrix	HGU133Plus2	GSE3744	Cancer Cell 9(2):121-32	Brigham and Women's Hospital
Neurofibroma cells	Cincinnati	22	10	Affymetrix	Hs133P_ref8v2	GSE14038	EMBO Mol Med 1(4):236-48	Cincinnati Children's Hospital Medical Center
Melanoma	San Diego	45	7	Affymetrix	HGU133A	GSE3189	Clin Cancer Res	Veridex
Pancreatic Cancer	Rochester	36	16	Affymetrix	HGU133Plus2	GSE16515	Cancer Cell16(3):259-66	Mayo Clinic
Ovary Tumor	Boston	53(52)	10	Affymetrix	HGU133Plus2	GSE18520	NA	Massachusetts General Hospital
Colon Cancer	Singapore	24	24	Illumina	Human Ref8v2	GSE10972	Cancer Cell 13(6):529-41.	Genome Institute Of Singapore
Primitive Neuroectodermal Tumors (PNET)	Toronto	33	7 (Fetal)	Illumina	Human WG6v2	GSE14295	NA	Hospital for Sick Children
GII Astrocytoma	Bethesda	7	23	Affymetrix	HGU133Plus2	GSE4290	Cancer Cell 9(4):287-300	National Cancer Institute
GIII Astrocytoma	Bethesda	19	23	Affymetrix	HGU133Plus2	GSE4290	Cancer Cell 9(4):287-300	National Cancer Institute
GII Oligodendroglioma	Bethesda	38	23	Affymetrix	HGU133Plus2	GSE4290	Cancer Cell 9(4):287-300	National Cancer Institute
GIII Oligodendroglioma	Bethesda	12	23	Affymetrix	HGU133Plus2	GSE4290	Cancer Cell 9(4):287-300	National Cancer Institute
GBM	Bethesda	47	23	Affymetrix	HGU133Plus2	GSE4290	Cancer Cell 9(4):287-300	National Cancer Institute

Gene enrichment scores for up-regulated or down-regulated gene list were calculated for each human tumor type (Table 2-2).

Table 2-2. Enrichment score of different human tumors compared to mouse glioma

	Mut3 upregulated set			**Mut3 downregulated set**		
Tumor Type	**ES**	**NES**	**Nominal *p***	**ES**	**NES**	**Nominal *p***
GBM	**6.46E-01**	2.00E+00	0.00E+00	-7.20E-01	-1.97E+00	0.00E+00
PNET	6.14E-01	1.40E+00	1.04E-02	**-7.90E-01**	-1.46E+00	6.28E-03
GIII Astrocytoma	6.08E-01	1.88E+00	0.00E+00	-7.27E-01	-2.07E+00	0.00E+00
GIII Oligodendroglioma	5.97E-01	1.84E+00	6.00E-03	-7.29E-01	-2.04E+00	0.00E+00
GII Astrocytoma	5.36E-01	1.77E+00	0.00E+00	-6.84E-01	-1.91E+00	0.00E+00
GII Oligodendroglioma	5.09E-01	1.70E+00	7.68E-03	-6.66E-01	-1.79E+00	0.00E+00
Pancreatic Cancer	4.22E-01	1.62E+00	1.79E-03	-2.77E-01	-1.24E+00	1.40E-01
Colon Cancer	4.13E-01	1.97E+00	0.00E+00	-4.87E-01	-1.91E+00	0.00E+00
Prostate cancer	3.77E-01	1.21E+00	4.26E-02	-2.15E-01	-1.10E+00	2.76E-01
Breast cancer	3.67E-01	1.45E+00	3.01E-02	-3.84E-01	-1.40E+00	2.67E-02
Melanoma	3.53E-01	1.71E+00	1.67E-03	-2.60E-01	-1.33E+00	4.72E-02
Primary Neurofibroma cells	2.89E-01	1.10E+00	2.78E-01	3.50E-01	1.37E+00	5.58E-03
Ovary Tumor	1.96E-01	8.19E-01	7.93E-01	-3.26E-01	-1.68E+00	5.39E-03
Lung Adenocarcinoma	-2.28E-01	-9.18E-01	5.83E-01	-1.88E-01	-9.04E-01	6.72E-01

Compared to the profiles of human tumors from different organs, the mouse glioma profiles shows obviously higher similarity to tumors in the nervous system. Within different WHO grades of gliomas compared, our mouse model generally has a more similar signature to higher-grade tumors (Grade IV/III vs grade II). Consistent with the pathology diagnosis, gene expression patterns in the mouse gliomas resemble astrocytic tumors more than oligodendrogliomas. Interestingly, what ranked first in the down-

regulated gene list and second in the upregulated gene list was a pediatric neural crest tumor called primitive neuroectodermal tumor (PNET). This could partially be attributed to the fact that our mouse gliomas display some undifferentiated neural progenitor-like properties (Alcantara Llaguno et al., 2009; Kwon et al., 2008a; Zhu et al., 2005a).

Table 2-3. TCGA tumor sample summary

Subtype	**Sample Number**
CL	47
MES	57
NL	28
PN	56
CTL	10

Mouse gliomas express higher PN markers in general

It has been reported that GBM can be classified into 4 subtypes according to their molecular profiles (Verhaak et al., 2010). Samples with somatic NF1 mutations have been associated with the MES subtypes. To test whether the molecular signature of our mouse gliomas is similar to the MES subtypes, expression profiles of GBM samples with known subtypes as well as 10 normal brain controls were retrieved from the TCGA data portal (Table 2-3). Among the differentially expressed genes in mouse glioma samples, 1111 upregulated and 1096 downregulated genes have probes present on the Affymetrix HGU133AHT platform which was used for the TCGA project. Gene set enrichment scores were calculated by comparing each subtype to normal brain controls. Meanwhile, 25 tumor samples from each subtype were pooled to generate a reference dataset as an internal control. The Bethesda glioma dataset where molecular subtype information was

unavailable was also used as an additional control (Sun et al., 2006). To our surprise, the PN subtype showed the highest enrichment score for both upregulated and downregulated genes in our mouse model of glioma (Table 2-4). The enrichment score was higher than both reference controls, suggesting that a proneural signature fits our mouse model better than a general GBM profile.

Table 2-4. Enrichment score of different glioma subtypes compared to mouse glioma

	Mut3 upregulated set			**Mut3 downregulated set**		
Subtype	**ES**	**NES**	**Nominal *p***	**ES**	**NES**	**Nominal *p***
PN	6.40E-01	1.61E+00	0.00E+00	-7.93E-01	-1.55E+00	2.00E-03
NIH GBM	6.37E-01	2.05E+00	0.00E+00	-7.22E-01	-2.05E+00	0.00E+00
Combined	6.14E-01	1.67E+00	0.00E+00	-7.84E-01	-1.57E+00	0.00E+00
NL	6.10E-01	1.47E+00	2.13E-03	-7.67E-01	-1.42E+00	4.23E-03
MES	6.07E-01	1.63E+00	0.00E+00	-7.88E-01	-1.52E+00	0.00E+00
CL	6.05E-01	1.60E+00	2.02E-03	-7.90E-01	-1.58E+00	0.00E+00

Mouse gliomas can be further classified into PN and MES subtypes

Since every mouse harbors the same tumor initiation mutations in our mouse model, relatively homogeneous expression profiles were expected. It was intriguing to observe that tumor profiles cluster into two groups in hierarchical clustering (Fig. 2-1A). K-means clustering also suggested that potentially two subgroups existed in the 6 tumor samples (Fig. 2-1B). One possibility was that those two groups represent two different molecular subtypes in human GBM. To test this hypothesis, DEGs were obtained by comparing profiles of each glioma group to normal control and then mapped to the HGU133AHT platform. GSEA was used to calculate the similarities between each human glioma subtype and the two potential mouse glioma groups (Table 2-5).

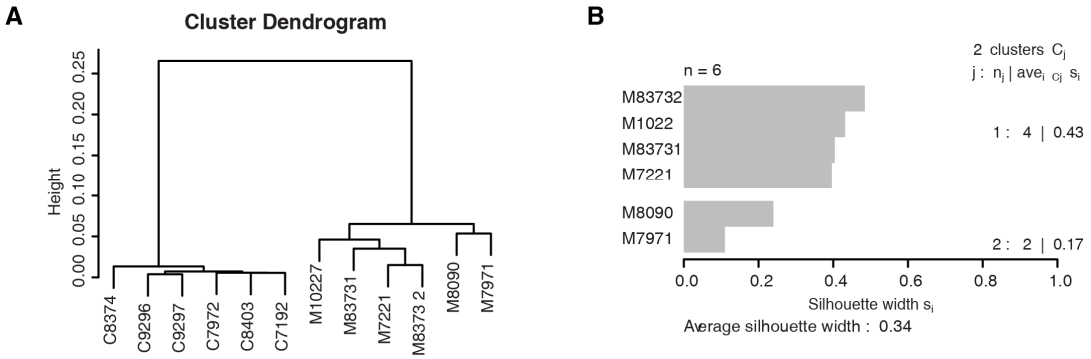

Figure 2-1. The six mouse tumor samples clustered into two groups. A) Average linkage clustering of Mut3 tumor and control expression profiles C: control samples. M: Mut3 glioma samples. B) Silhouette plot of K-means clustering of Mut3 tumor profiles (K=2).

Table 2-5. Enrichment score of different subtypes for each mouse glioma group

		Mut3 upregulated set			Mut3 downregulated set		
	Subtype	**ES**	**NES**	**Nominal *p***	**ES**	**NES**	**Nominal *p***
Group1	PN	**6.59E-01**	1.61E+00	0.00E+00	-7.96E-01	-1.56E+00	0.00E+00
	NIH GBM	6.54E-01	1.97E+00	0.00E+00	-7.34E-01	-1.97E+00	0.00E+00
	MES	6.46E-01	1.60E+00	0.00E+00	**-8.01E-01**	-1.49E+00	0.00E+00
	Combined	6.43E-01	1.69E+00	2.00E-03	-7.93E-01	-1.61E+00	0.00E+00
	NL	6.31E-01	1.47E+00	9.86E-03	-7.69E-01	-1.40E+00	2.05E-02
	CL	6.31E-01	1.54E+00	0.00E+00	-7.98E-01	-1.53E+00	0.00E+00

		Mut3 upregulated set			Mut3 downregulated set		
	Subtype	**ES**	**NES**	**Nominal *p***	**ES**	**NES**	**Nominal *p***
Group2	PN	**6.25E-01**	1.64E+00	0.00E+00	**-7.85E-01**	-1.59E+00	0.00E+00
	NIH GBM	6.23E-01	1.94E+00	0.00E+00	-7.08E-01	-1.90E+00	0.00E+00
	NL	5.97E-01	1.46E+00	2.14E-03	-7.56E-01	-1.42E+00	4.29E-03
	MES	5.90E-01	1.58E+00	0.00E+00	-7.76E-01	-1.50E+00	0.00E+00
	Combined	5.95E-01	1.68E+00	2.09E-03	-7.73E-01	-1.65E+00	2.12E-03
	CL	5.88E-01	1.57E+00	2.02E-03	-7.79E-01	-1.56E+00	0.00E+00

We found that the PN subtype still had the most similarity with both mouse glioma groups for the up-regulated genes. Interestingly, for the down-regulated genes, more similarity was obtained with the MES subtype in group 1 while the enrichment score for the PN subtypes remained the highest for the group 2 mouse gliomas (Table 2-5), suggesting that different molecular subtypes can derive from the same initiating mutations. The initial GBM subtype classification was done by comparing between tumor samples. To confirm the MES characteristic of group 1, we mapped the markers of each TCGA subtype to their mouse orthologs and calculated GSEA by comparing group 2 with group 1. Indeed, group 1 and group 2 showed the highest enrichment scores for the MES and PN markers, respectively (Table 2-6).

Table 2-6. GSEA of two mouse glioma subgroups in TCGA subtypes

	Group 2 vs Group 2			**TCGA PN vs MES**		
	ES	**NES**	**Nominal p**	**ES**	**NES**	**Nominal p**
PN	2.92E-01	**2.35E+00**	0.00E+00	7.90E-01	**9.38E+00**	0.00E+00
CL	3.16E-01	2.25E+00	0.00E+00	-3.70E-01	-3.31E+00	0.00E+00
NL	-1.42E-01	-1.30E+00	9.40E-02	-1.80E-01	1.80E+00	7.00E-03
MES	-2.15E-01	**-2.72E+00**	0.00E+00	-8.50E-01	**-8.87E+00**	0.00E+00

Human PN and MES glioma subtype can be classified using 20 markers

Molecular subclassification of tumors usually utilizes the global gene expression profile, which is neither cost effective nor easily expandable. We therefore decided to select a handful of representative markers for each subtype from the original 841 genes used for classification of the TCGA dataset. As described in chapter 1, the number of subtypes

and their markers vary from study to study, however, it is generally accepted that one subset of the gliomas express genes that are related to neurogenesis (proneural or PN) and another subset of tumors have a mesenchyme (mesenchymal or MES) related gene profile (Freije et al., 2004; Li et al., 2009a; Phillips et al., 2006; Verhaak et al., 2010; Vitucci et al., 2010). In addition, after using the original 841 genes to cluster the TCGA dataset, Genentech dataset and Bethesda dataset, we noticed that samples in the CL subtype generally expressed high levels of MES markers at the same time. The NL subtype, on the other hand, expressed either high levels of PN or MES genes in addition to NL markers (Figure 2-2). We then decided to focus on PN and MES only. To determine the number of genes that is required to identify each subtype, we calculated cross-validated error (CVE) to identify the TCGA subtypes using a range of 1-20 genes per subtype. Based on the CVE, we then manually picked up 10 genes each as PN (DCX, NKX2-2, GPR17, MYT1, FLRT1, NRXN1, SOX2, OLIG2, ASCL1, CNTN1) and MES (CHI3L1, CD44, COL5A1, CEBPB, TGFBI, TNFRSF1A, MVP, PLA2G5, S100A13, TIMP1) markers. Hierarchical clustering revealed that all of the TCGA MES subtype tumors and 53 out of 56 PN subtype tumors were successfully identified by the 20 marker genes, respectively (Figure 2-3A). Since we were planning to evaluate gene expression of these markers by quantitative PCR (QPCR), where gene expression is usually normalized to housekeeping genes such as GAPDH, we first tested whether this relative value can still be used to classify tumor subtypes. The subtraction of log2-transformed gene expression values to the log2 transformed GAPDH value of the same sample was used for hierarchical clustering. 52 out of 57 of the TCGA MES subtype and 55 out of 56 the PN subtype samples were correctly classified even without normalizing the original

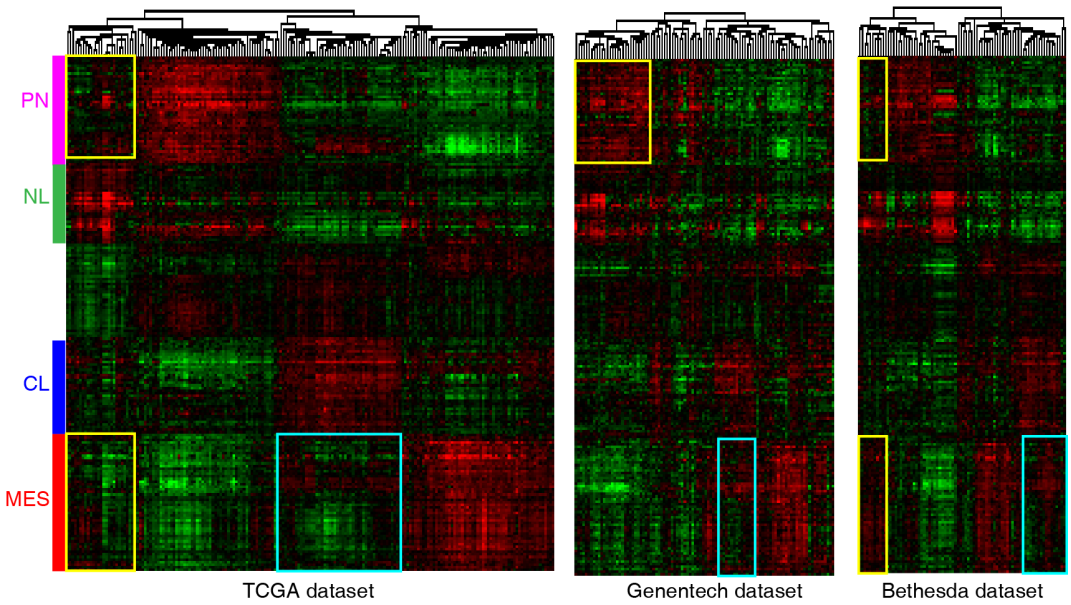

Figure 2-2. Hierarchical clustering analysis of TCGA dataset, Genentech dataset and Bethesda dataset using the 841 genes that were used to classify TCGA dataset. Note that NL subtype also showed high level expression of PN or MES genes (yellow rectangle), while CL subtype expresses high level of MES markers (light blue rectangle）.

expression values across samples (Figure 2-3B). To test whether these 20 genes can be applied to more general datasets, we then applied similar analysis to two other glioma microarray datasets. Phillips et al. has classified high-grade gliomas into proneural (PN), mesenchymal (MES) and proliferative (PROLIF) subtypes (Phillips et al., 2006). We found that these 20 gene markers can successfully identified 33 out of 37 of the PN and 30 out 35 of the MES subtype gliomas reported by Phillips et al (Figure 2-3C) (Phillips et al., 2006). In addition, we also found that these markers can segregate the 80 GBM profiles from the Bethesda dataset into two distinct groups (Figure 2-3D) (Sun et al., 2006).

Gliomas from hGFAP-Cre;NF1$^{flox/+}$;P53$^{flox/flox}$;Pten$^{flox/+}$ also showed distinct molecular subtypes

These 20 gene markers allowed us to expand our studies to more tumor samples using QPCR. As an independent verification, we used gliomas from the hGFAP-Cre;NF1$^{flox/+}$;P53$^{flox/flox}$;Pten$^{flox/+}$ (Mut7) mice. Consistent with clinical observation, tumors in this mouse model progressed more rapidly than in the one without Pten mutation (Kwon et al., 2008a; Phillips et al., 2006). In addition, the predominant tumor type presenting in symptomatic mice is high-grade gliomas (Kwon et al., 2008a). Clustering analysis using the ΔCT of each marker gene revealed three subgroups in the nine tumors tested (Figure 2-4A). Three tumors showed generally high levels of PN gene expression while another three tumors were enriched for MES marker expressions. A similar trend was observed in the gene expression fold changes compared to wild type mouse cortex (Figure 2-4B).

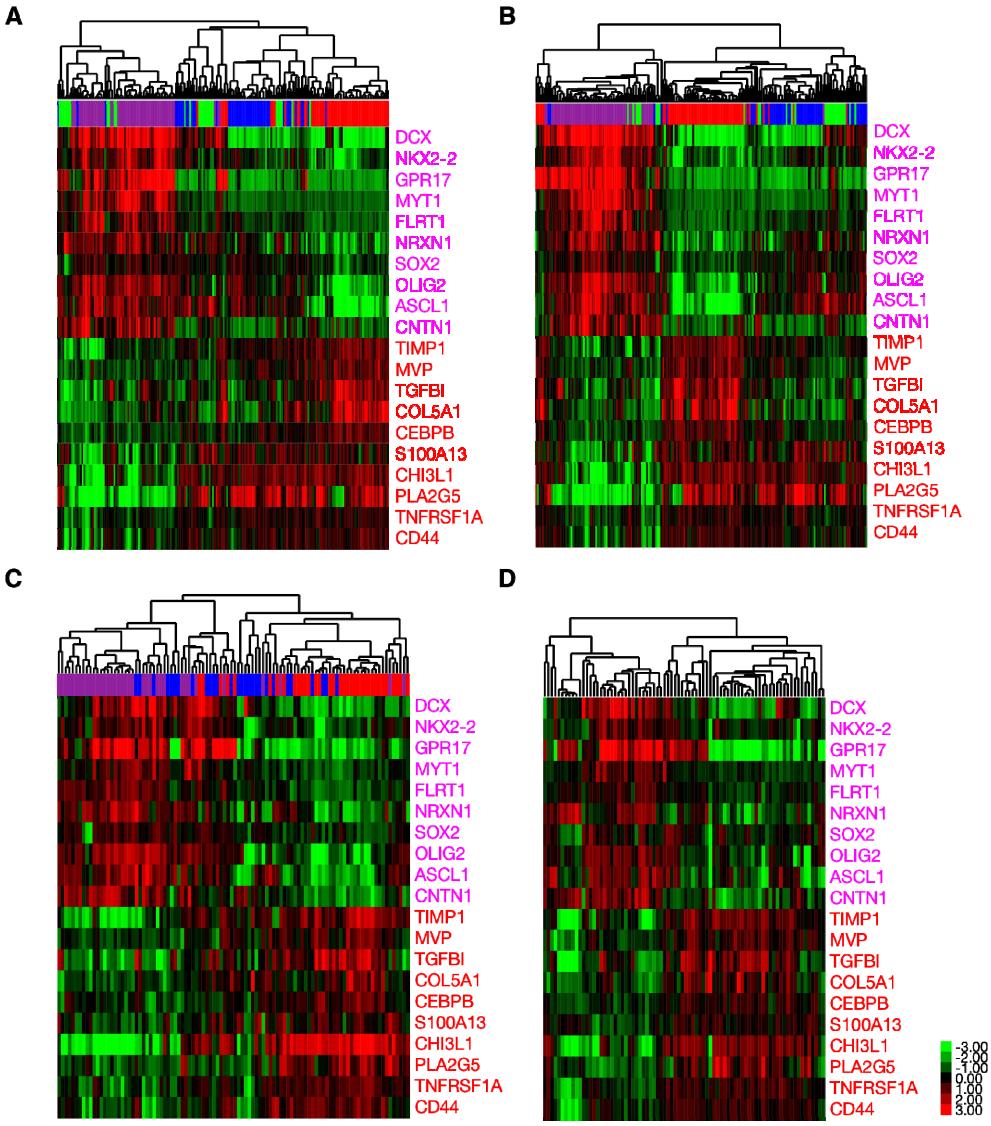

Figure 2-3. Classification of PN and MES based on 20 gene markers. A) Hierarchical clustering result of TCGA dataset using absolute expression value (log2 transformed) of the 20 selected marker genes. B-D) Hierarchical clustering of glioma profiles from TCGA (B), Genentech (C) and Bethesda (D) dataset using relative expression value of the selected marker genes that have been normalized to internal GAPDH expression. Green, red, blue, purple color on the header correspond to NL, MES, CL and PN subtypes of the TCGA dataset (A&B). For the Genentech dataset, red, blue and purple on the header indicate original MES, PROLIF and PN subtypes identified by Phillips et al (C).

To further validate whether the markers of the two tumor subtypes can arise from the same genotype, we evaluated expression of the PN marker Olig2 and MES marker CD44 on six additional grade III astrocytomas from the Mut7 mice. Similar to the conclusions from the microarray and QPCR experiments, we observed co-existence of both markers in gliomas of the same brains (Figure 2-4C). Moreover, the expression patterns of the two antigens in the same tumor brain are mutually exclusive, which is consistent with the idea that the two markers belong to different subtypes (Figure 2-4C).

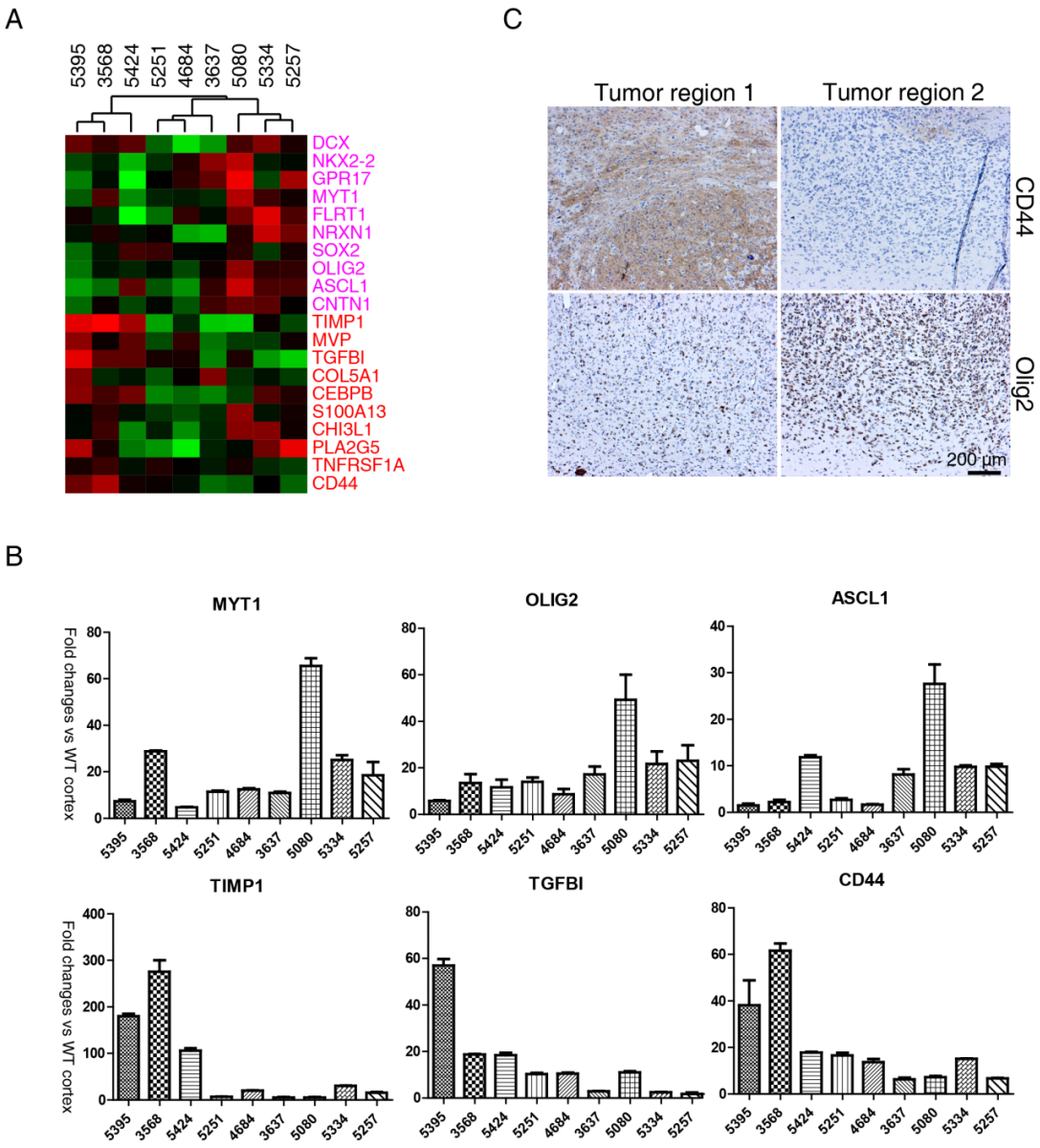

Figure 2-4. Gliomas from hGFAP-Cre; NF1$^{flox/+}$;P53$^{flox/flox}$;Pten$^{flox/+}$ (Mut7) mice can be classified into distinct PN or MES subtypes. A) Hierarchical clustering of nine Mut7 mice using ΔCT values of the 20 gene markers. B) Relative marker gene expression (MYT1, OLIG2, ASCL1 as examples of PN markers and TIMP1, TGFBI and CD44 as examples of MES markers) of the tumor samples compared to normal mouse cortex. C) PN and MES markers co-exist in different tumor regions from the same tumor-bearing mouse. Adjacent selections were selected to perform PN marker (OLIG2) and MES marker (CD44) staining.

Discussion

The integrative comparison between mouse glioma expression profiles and different human cancer profiles suggested that our mouse model of glioma faithfully recapitulated human GBM. The mouse model thus provides an ideal platform for pre-clinical study of tumor development, maintenance and treatment (Alcantara Llaguno et al., 2009; Kwon et al., 2008a; Zhu et al., 2005a).

Whether GBMs can be classified into strictly distinctive subtypes or subtypes that co-exist in the same tumor is clinically important. Distinct tumor subtypes have been associated with different prognoses. For example, patients with PN subtype gliomas generally have a better outcome (Gravendeel et al., 2009; Phillips et al., 2006). In addition, subtype classification could also be potentially used as a guide for treatment plans. For example, it has been observed that patients with MES subtype gliomas have better response to radiation therapy (Gravendeel et al., 2009; Verhaak et al., 2010).

In contrast to the report by Verhaak et al., gliomas in our NF1;P53-deleted mouse model displayed a predominantly PN characteristic, with part of the samples also showing MES marker expression. It is unlikely that a subtype is predetermined by the genetic mutations of the tumor cells. How these two subtypes emerge is still unknown. The TCGA subtype classification by expression profile correlates well with the observation that NF1 mutations, EGFR amplification and PDGFR overexpression are mutually-exclusive events as demonstrated by somatic mutation and gene copy number analysis (Network, 2008; Verhaak et al., 2010). On the other hand, as also indicated by the TCGA studies,

all these genetic alteration events lead to activation of the same glioma core signaling pathways, the RTK pathway, based on TCGA studies(Network, 2008). For example, although PDGFRA overexpression was considered to be a PN maker, its ligand, PDGFA, belongs to the CL subtype (Verhaak et al., 2010), indicating the conversion of downstream pathways. Analysis of the TCGA dataset suggested that each glioma subtype shared similar molecular profile with a certain neural cell type in the brain (Vitucci et al., 2010). It is possible that the distinct tumor subtypes resulted from the transformation of different cell types, where a certain genetic alteration is "preferred" by a specific cell type. A similar phenomena has been observed during *in vitro* reprogramming: induced pluripotent stem cells (iPS) still maintain some signature of their tissue of origin after being reprogrammed into embryonic stem cells (Kim et al., 2010; Polo et al., 2010).

Our finding that different subtypes can co-exist within the same brain tumor also suggests the potential risks of a treatment plan that is based solely on tumor subtype classification, as the biopsy is usually taken from one region of the tumor. The underrepresented tumor subtypes are thus likely to evade this subtype-specific therapy. In addition, it is still unclear whether the molecular subtypes can be changed during tumorigenesis or upon treatment. Phillips et al. observed that recurrent gliomas are mostly mesenchymal subtype, which has a worse prognosis, supporting the hypothesis of subtype shifting (Phillips et al., 2006). Consistent with this observation, earlier passage gliomas from serial transplantation of glioma microexplants that had been transplanted into immunodeficient rat brain revealed an infiltrative signature with more neurogenic gene expression. However, tumors from late passage experiments had an angiogenesis

signature with more proliferative gene expression (Sakariassen et al., 2006). In contrast, it has also been reported that gliomas maintain their original subtypes even after xenograft, which suggests a relatively stable phenotype (Verhaak et al., 2010). Further studies are required to clarify these issues.

CHAPTER THREE

MUTATIONS IN ADULT NEURAL STEM/PROGENITOR CELLS ARE SUFFICIENT FOR MALIGNANT ASTROCYTOMA FORMATION

Introduction

As mentioned in Chapter 1, historically, astrocytes were thought to be the origin of gliomas as they were the only known replication-competent population. The discovery of neural stem/progenitor cells (NSCs) in mammalian brains provided an attractive alternative origin owing to the fact that NSCs have long-term self-renewal potential thus facilitating mutation accumulation. In adult rodents, neurogenesis in the subventricular zone (SVZ) of the lateral ventricles serves to replenish olfactory bulb (OB) interneurons via the rostral migratory stream (RMS). In the dentate gyrus, neurogenesis in the subgranular layer (SGL) generates synaptically active granule neurons and has been implicated in learning, memory and mood disorders (Ming and Song, 2005; Zhang et al., 2008; Zhao et al., 2008).The NSC origin of astrocytoma was supported by several lines of evidence arising from studies using mouse glioma models in our lab (Kwon et al., 2008a; Zhu et al., 2005a). For example, tumors are usually found in the periventricular region or continuous with the subventricular region where NSCs are located (Zhu et al., 2005a). In addition, abnormal migration of NSCs was found weeks before the malignant tumors emerge (Kwon et al., 2008a). However, the hGFAP-cre, which was used for tumor suppressor deletion in our previous mouse models, was expressed as early as E9 and targeted the majority of cells in the mouse brain (Zhuo et al., 2001). To circumvent this problem and enable gene ablation specifically in adult NSCs, we took advantage of

the tamoxifen inducible Cre recombinase technique. In this system, the Cre recombinase protein is fused together with a modified estrogen receptor ligand-binding domain (ER^{T2}), which causes sequestering of the fusion protein in the cytoplasm where it cannot mediate loxP recombination. Application of estrogen or estrogen analogs however causes translocation of the Cre-ER^{T2} fusion protein to the nucleus and recombination can be achieved (Figure 3-1).

To permit temporal ablation of genes in the neural stem cell lineage, we utilized a neurogenic lineage-specific promoter/enhancer of the nestin gene to drive the Cre-ER^{T2} fusion protein expression. Nestin is an intermediate filament protein specifically expressed in neural stem/progenitor cells in both developing central nervous system and adult brain. The regulatory element driving neural specific nestin expression has been mapped to the 2nd intron of the nestin gene (Lendahl et al., 1990; Zimmerman et al., 1994). Here we show that the transgene is silent in the absence of estrogen analog induction. Upon activation the expression is robust and recombination is elicited primarily in the principal neurogenic niches. Additional expression is confined to the cerebellum, certain peripheral nerves, and to potentially novel sites of neurogenesis. Furthermore, using this Cre to inactivate NF1, P53 and Pten specifically in adult NSCs resulted in malignant astrocytoma formation with 100% penetrance.

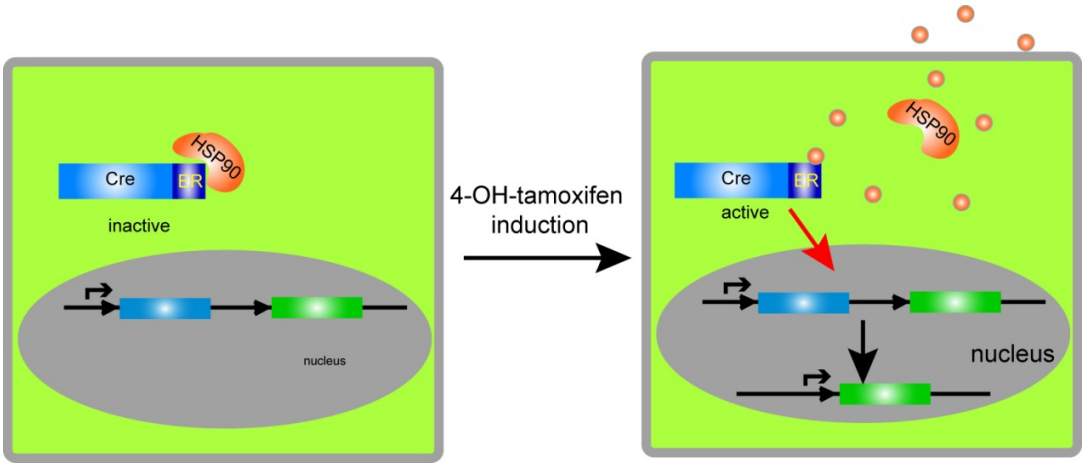

Figure 3-1. Mechanism of the tamoxifen-inducible Cre system. Bacteriophage P1 Cre recombinase is fused with a fragment of mutated estrogen receptor (ER). Under normal conditions, the fusion protein is sequestered in the cytoplasm by the HSP90 protein. The inhibition is released upon 4-OH-tamoxifen treatment and the Cre protein can then enter the nucleus to carry out recombination.

Results

Generation of transgenic lines

The Cre-ER^{T2} cDNA was placed under the control of a 5.6 kb rat nestin 5' regulatory element and followed by the 668 bp inverse nestin 2nd intron (Figure 3-2A). Six transgenic lines were obtained after pronuclear injection and four underwent germline transmission. To assay Cre recombinase activity after induction, we crossed the CreER^{T2} lines with Rosa26-stop-lacZ (Rosa26^{lacZ}) reporter mice. The Rosa26^{lacZ} mice require Cre-mediated recombination for β-galactosidase gene activation due to a stop cassette flanked by loxP sites upstream of the lacZ gene. To assess inducibility of the Cre transgene, sunflower oil vehicle (150 μl) or the estrogen analog tamoxifen (1 mg) was injected into pregnant mice at embryonic day 12.5 (E12.5) and the embryos were dissected out at E14.5 for whole mount X-gal staining. In a Rosa26lacZ reporter background, exposure of the four transgenic lines to tamoxifen revealed that only two of the lines (line 8 and line 73) exhibited recombination activity (Figure 3-2B). Moreover, comparison of Cre activity upon induction was similar although line 8 was leaky, having minor but detectable Cre activity in the absence of tamoxifen. In contrast, line 73 (Nes73-CreER^{T2}) showed no signs of Cre activity in the absence of tamoxifen and the blue X-gal staining was found predominantly in embryonic brain and spinal cord where most nestin-positive neural progenitors are located (Figure 3-2B).

Embryonic and neonatal stem/progenitor-specific Cre induction

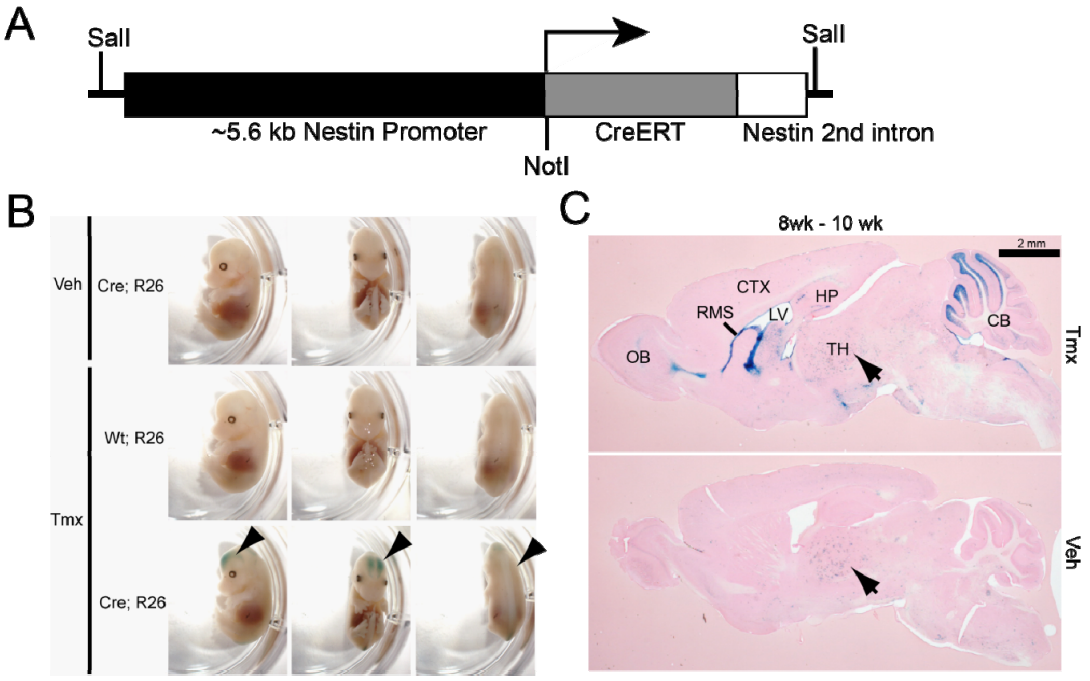

Figure 3-2. Transgene construct and tamoxifen inducibility. A) Structure of the Nestin-CreER^{T2} transgene consisting of the rat nestin promoter/enhancer, cDNA encoding the CreER^{T2} fusion protein and inversely oriented Nestin 2nd intron. B) Transgene induction during embryogenesis. Representative whole-mount, X-gal-stained E14.5 embryos (induced at E12.5) show no X-gal signal in vehicle-treated (Veh) Nes73-CreER^{T2};Rosa26^{lacZ} embryos (top panels) or tamoxifen-treated (Tmx) Rosa26^{lacZ} embryos (middle panels). Only Tmx-treated Nes73-CreER^{T2};Rosa26^{lacZ} embryos show blue staining in the developing CNS (black arrowheads). C) Transgene induction in adult. Representative X-gal-stained brain sections from 10 week-old mice show that five days of Tmx injection into 8 week-old Nes73-CreER^{T2};Rosa26^{lacZ} mice induced recombination as evidenced by X-gal signal in the hippocampus (HP), lateral wall of lateral ventricle (LV), rostral migratory stream (RMS), olfactory bulb (OB) and anterior cerebellum (CB). Vehicle-injected Nes73-CreER^{T2};Rosa26^{lacZ} mice have no X-gal activity. Diffuse, low-level X-gal signal was observed in the thalamus (TH) of both Veh- and Tmx-injected mice (black arrow).

The temporal control of Cre activity allowed us to induce Cre-mediated recombination for the purpose of tracing NSCs and their progeny at various time points. The pattern observed upon embryonic induction closely reflected the course of brain development. Tamoxifen induction at E13.5 labeled almost the entire cortex in the forebrain as well as the entire cerebellum including neurons and glia (Figure 3-3A). This coincides with the initiation of neural progenitor migration that contributes to different cortical layers in embryonic neural development (Sun et al., 2002). Induction at E17.5, when neurogenesis in the forebrain reaches completion, resulted in labeling of only the outer most layers of the cortex (Figure 3-3B), which stands in line with the "inside-out" pattern of cortex layer formation (Sun et al., 2002). Additionally, the thalamus and hindbrain were labeled at this time point. In the neonatal mouse brain, there is persistent mild but widespread lacZ activity, indicative of residual but rare progenitor cells throughout the parenchyma (Figure 3-3C&D). The most active neurogenic region at this time is the cerebellum (Herrup and Kuemerle, 1997), which showed intense lacZ staining following induction at E17.5 through P7 (Figure 3-3B-D). Mouse cerebellum development is considered to be complete by three weeks after birth, however our Nes73-CreER^{T2};Rosa26^{lacZ} mice showed strong Cre activity in the anterior part of cerebellum when induced four and eight weeks after birth (Figure 3-2C, Figure 3-3E&F, Figure 3-6A-C; and see below). Nonetheless, in the anterior brain, by four weeks of age the SVZ and SGL are the most neurogenic regions as assayed by tamoxifen-induced Cre activity (Figure 3-3E&F).

Adult induction and neurogenesis

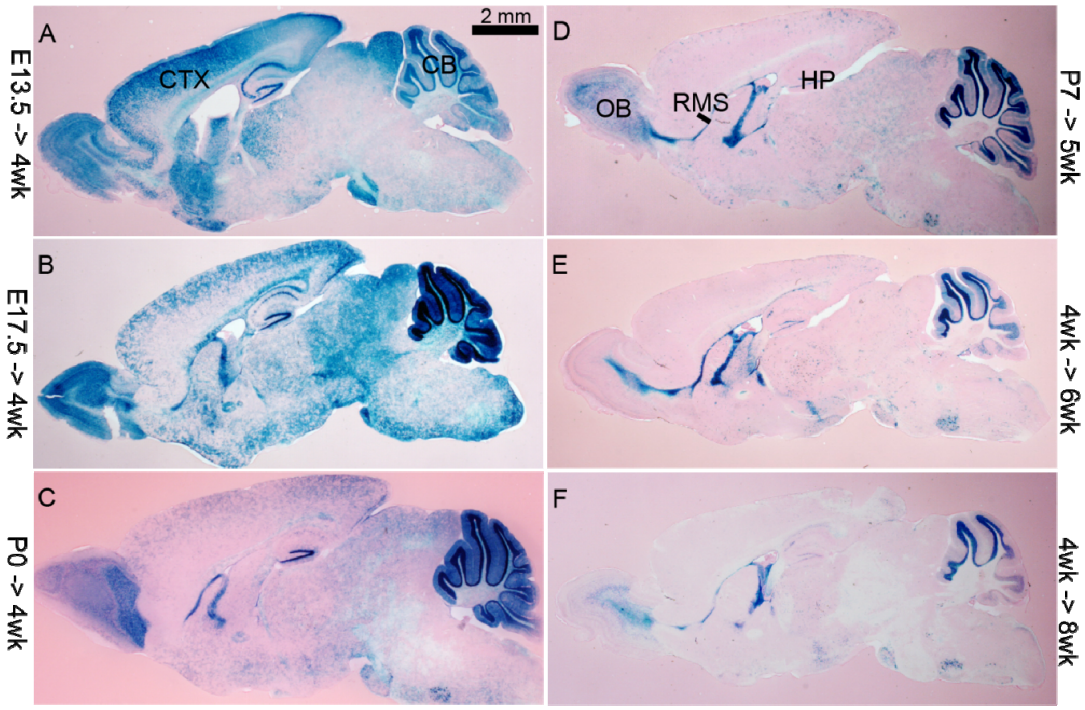

Figure 3-3. Tmx induction at various time points during mouse development reflects neurogenesis at different stages. In utero induction of Nes73-CreER^{T2};Rosa26^{lacZ} (A, B) results in Cre activity in the cerebral cortex (CTX) and cerebellum (CB); neonatal induction (C, D) shows labeling of the whole cerebellum (CB); adult induction (E, F) results in signal that is restricted to the neural stem cell niches and their migration targets as well as to the anterior part of cerebellum (CB).

Adult NSCs modify their gene expression as they migrate and differentiate. In the SVZ, glial fibrillary acidic protein (GFAP) positive cells are considered to be stem cells (Doetsch et al., 1999). When differentiation starts and neuronal fate of the progenitor cells has been specified, cells begin to express doublecortin (DCX) and migrate into the OB through the RMS to finally become NeuN-positive mature neurons (Doetsch et al., 1999; Ming and Song, 2005). To determine the sites of primary Cre recombinase activity, we examined the SVZ of 4-week-old Nes73-CreER^{T2};Rosa26^{lacZ} mice 48 hours after a short pulse of tamoxifen, since both GFAP-positive neural stem cells and some transient amplifying progenitor cells express nestin. X-gal staining followed by immunohistochemistry (IHC) with GFAP or DCX antibody revealed that the majority of Cre activity resides in GFAP-positive SVZ cells close to the lateral ventricle, with only rare DCX-positive SVZ or RMS cells showing recombination (Figure 3-4A). This was further confirmed using an estrogen receptor antibody to show double labeling of Cre-ERT2-positive cells with the stem cell marker GFAP, and with S100β, a marker of radial glia-derived ependymal cells (Figure 3-4B) (Spassky et al., 2005). These studies indicate that the primary site of tamoxifen-activated Cre recombinase is the GFAP-positive, SVZ stem cell population.

To measure the efficiency of tamoxifen-induced recombination in our Nes73-CreER^{T2} mice, we crossed them with the Rosa26^{YFP} reporter line to generate Nes73-CreER^{T2};Rosa26^{YFP} mice and then induced these mice with tamoxifen at four weeks of age. We then harvested brain sections from the induced mice at six weeks of age, and performed immunofluorescent double-labeling with GFP and Sox2 antibodies (Figure 3-

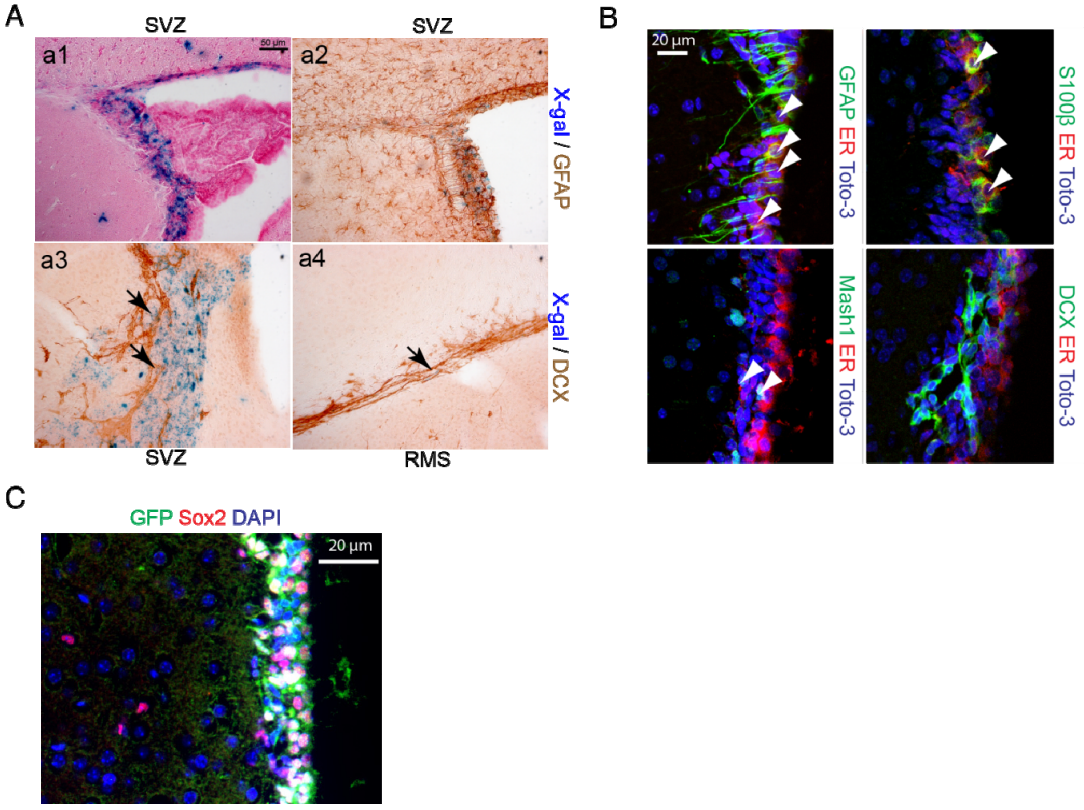

Figure 3-4. Early Cre activity in adult neural stem cell niche upon tamoxifen induction. A) Representative X-gal stained brain sections from mice 48 hours after two tamoxifen administrations at P28 (12 hour interval). X-gal signal was mainly restricted to SVZ (a1), with little or no signal observed in rostral migratory stream (RMS) (a1, a4). Immunohistochemistry following X-gal staining revealed that the majority of X-gal positive cells express glial fibrillary acidic protein (GFAP). A few X-gal positive cells (black arrows) also express doublecortin (DCX) in subventricular zone (SVZ) (a3) and RMS (a4). B) Cre-ER^{T2} fusion protein expression in the SVZ of 4-week-old uninduced Nes73-CreER^{T2} mice. GFAP-positive type B neural stem cells and S100β-positive ependymal cells have the highest level of Cre-ER^{T2} protein expression (white arrows). Some Mash1-positive type C cells also expressed Cre-ER^{T2} protein (white arrowheads). The majority of doublecortin (DCX)-positive neuroblasts were Cre-negative. C) Representative immunofluorescence staining of GFP and Sox2 in Nes73-CreER^{T2};Rosa26^{YFP} mice 2 weeks after tamoxifen induction.

4C). The percentage of GFP/Sox2 double-positive cells divided by the number of Sox2 positive cells in the SVZ was used to determine recombination efficiency. This quantification analysis revealed that 75±4% of Sox2-positive cells in the SVZ have been targeted 2 weeks after a 5-day tamoxifen induction.

In order to further study the dynamics of stem/progenitor cell migration and differentiation, Nes73-CreER^{T2};Rosa26^{lacZ} mice were induced at four weeks of age and examined by X-gal staining two or four weeks later (Figure 3-3E&F & Figure 3-5A). The dynamics of Cre-active cells in the hippocampus over time was not very dramatic (Figure 3-5A&B), however in the SVZ, an increase in the number of Cre active cells in an expanded ventricular area was evident four weeks after induction (Figure 3-5A). These results suggest a precursor-progeny relationship in which, after two weeks of induction, a significant number of new progenitor cells have been generated by stem cells and are beginning to disperse from the SVZ. Similarly, in the OB two weeks after induction, the X-gal positive cells were confined to a central cluster, whereas four weeks post induction the cells were dispersed throughout the OB (Figure 3-5A). We interpret this result to indicate that at two weeks post-induction, cells are just arriving to the OB via the RMS and are confined to this central area, while at four weeks post induction, these labeled cells have now dispersed throughout the OB. A similar, although more restricted, migration was also observed in hippocampus, where β-Gal and NeuN double-positive neurons first appear close to the subgranular layer (SGL) two weeks after induction but by four weeks post-induction have migrated deeper into the granular layer (Figure 3-5B).

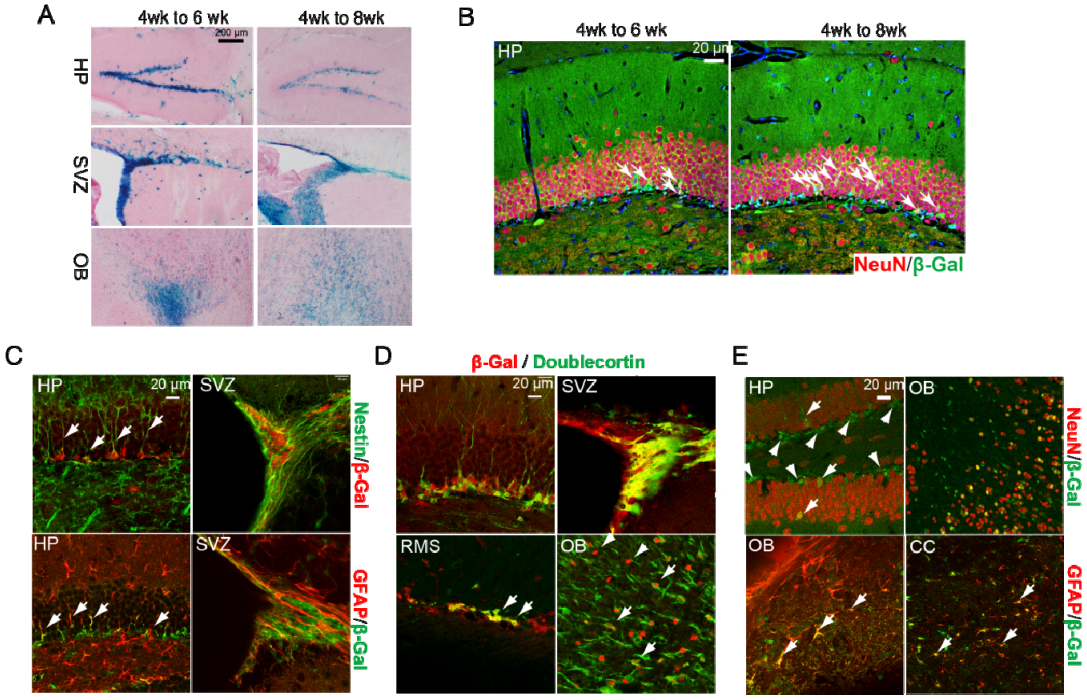

Figure 3-5 Cre activity in adult NSC niches and migration targets. A) Representative X-gal-stained brain sections from 6 or 8 week-old Nes73-CreER^{T2};Rosa26^{lacZ} mice that were induced at 4 weeks of age show the dynamics of X-gal-positive cells in the hippocampus (HP), SVZ and olfactory bulb (OB). B) Representative β-galactosidase (β-Gal) and NeuN staining of hippocampus 2 or 4 weeks after tamoxifen induction at 4 weeks of age. Newly generated β-Gal-positive neurons slowly migrate into the granular cell layer (white arrows). (C - E): Representative immunofluorescence staining showing the presence of β-galactosidase (β-Gal)-expressing (hence, Cre active) cells in Nes73-CreER^{T2};Rosa26^{lacZ} mice 4 weeks after tamoxifen induction. C) Expression of β-Gal was observed in NSCs that also express nestin and GFAP (white arrows, for example). D) DCX-positive neural progenitor cells also expressed β-Gal in the SVZ, HP, rostral migratory stream (RMS) and OB (white arrows, for example). In the OB, some β-Gal-positive cells were DCX-negative, and thus possibly represent mature neurons (white arrowheads, for example). E) Multiple lineages of differentiated cells with β-Gal expression. Top panels: mature neurons (generated by adult NSCs) that migrated into the hippocampal (HP) granular layers were rare (white arrows, for example), while the majority of β-Gal-positive cells were NeuN-negative (white arrowheads, for example). In the OB, a significant number of mature neurons were contributed by adult neurogenesis as shown by β-Gal and NeuN double labeling. Bottom panels: adult NSCs were also found to differentiate into GFAP-positive astrocytes (white arrows, for example) in the OB and corpus callosum (CC).

To explore the identity of the Cre-active cells, immunofluorescent double labeling was used to characterize Nes73-CreER^{T2};Rosa26^{lacZ} mice four weeks after induction (Figure 3-5C-E). β-Gal immunoreactivity was found in nestin and GFAP-positive neural stem/progenitor cells in the SVZ and SGL (Figure 3-5C). In the anterior part of the SVZ and SGL, DCX-positive neural progenitors also showed Cre activity (Figure 3-5D). In addition, a majority of the cells in the RMS express both β-Gal and DCX (Figure 3-5D). Furthermore, NeuN-positive mature neurons that also retained β-Gal immunoreactivity could be found in the HP and OB (Figure 3-5E). A small number of GFAP-positive astrocytes in the OB and the corpus callosum (CC) also expressed the reporter gene β-Gal (Figure 3-5E), indicating the presence of Cre activity in multiple cell types in the NSC lineage. This result is consistent with recent quantitative lineage tracing studies (Lagace et al., 2007).

Additional tamoxifen inducible Cre activity

The significant amount of Cre activity induced in anterior cerebellum of adult mice was unexpected (Figure 3-2C & Figure 3-3). Figure 3-6A shows a representative eight-week-old brain from a mouse that was induced with tamoxifen at four weeks of age. The β-Gal positive cells were mostly NeuN-positive inner granular layer (IGL) granule cells and Bergmann glia that extend long processes to the surface of the cerebellum (Figure 3-6A-C). Consistent with previous reports that Bergmann glia express NSC markers such as nestin and Sox2(Mignone et al., 2004; Sottile et al., 2006), we found that Cre-active Bergmann glia also expressed the NSC marker nestin (Figure 3-6B). However, the Cre-ERT2 fusion transgene was also expressed in some Sox2-negative cells in the IGL

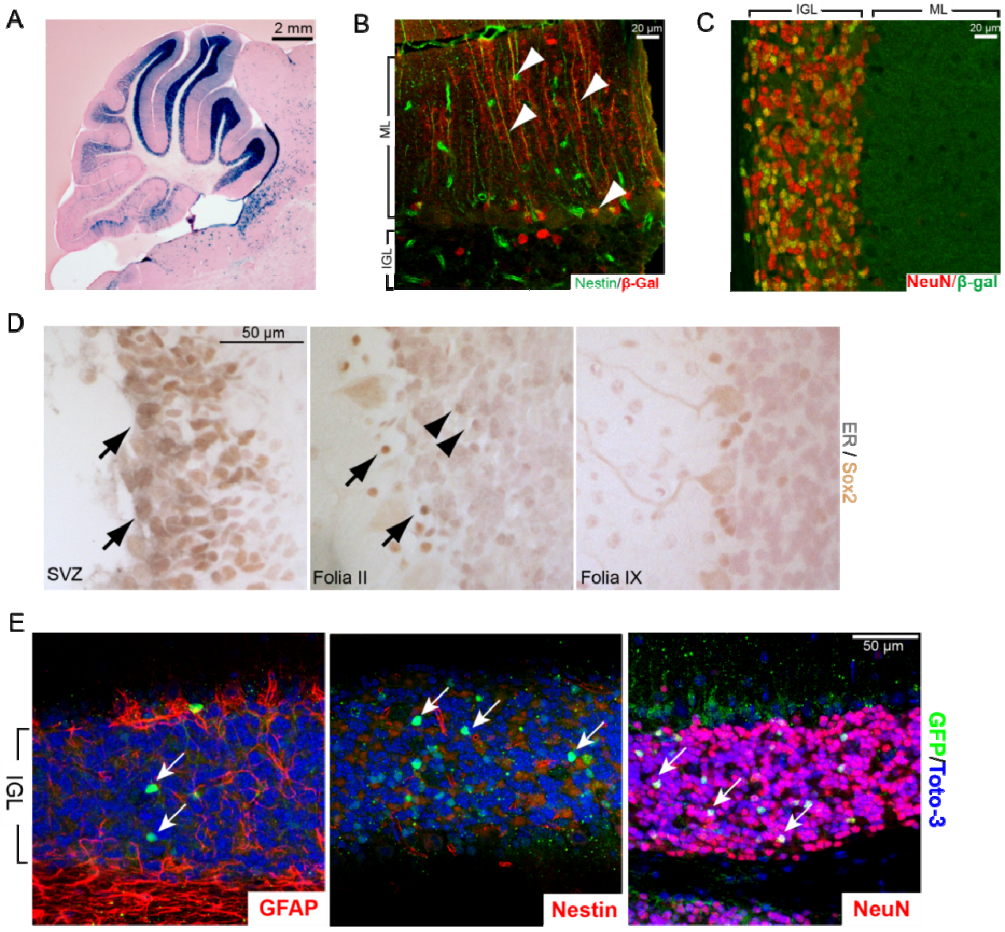

Figure 3-6 Novel Cre activity in adult cerebellum. Nes73-CreER^{T2};Rosa26^{lacZ} mice were treated with tamoxifen at 4 weeks of age and analyzed at 8 weeks. Abundant β-Gal expression was detected in the anterior part of cerebellum of tamoxifen-treated mice (A - C) X-gal staining (A) and immunostaining (B & C) reveal that in cerebellum a majority of β-Gal-expressing cells are nestin-positive Bergmann glia in the molecular layer (ML) (B) or NeuN-positive granule neurons in the inner granular layer (IGL) (C). D) Representative estrogen receptor (ER) and Sox2 immunohistochemistry staining from 4 week old Nes73-CreER^{T2};Rosa26^{lacZ} mice. The Cre-ER^{T2} fusion transgene was expressed in Sox2-positive cells in SVZ (black arrows in left panel), anterior part of cerebellum (black arrows in folia II in middle panel, for example) and also some Sox2-negative cells in cerebellum (black arrowheads in middle panel). No Cre-ER^{T2} fusion protein was detected in the IGL of posterior cerebellum (folia IX in right panel). E) Cre activity after acute induction in NeuN-positive mature neurons in cerebellum. 3 Month old Nes73-CreER^{T2};Rosa26^{YFP} mice were induced by 2 acute tamoxifen administration and perfused 2 days later. The brains were cut sagittally into 50 µm thick vibratome sections and subjected into dual immunofluorescence labeling.

(Figure 3-6D, middle panel), suggesting potential aberrant expression of the Nestin-CreERT2 transgene. Mild but reproducible tamoxifen-induced Cre activity was also observed in the piriform cortex (Figure 3-7A&B), which has also been reported to be a potential neurogenic region (Pekcec et al., 2006). We next assessed tamoxifen-induced Cre activity in other regions using whole mount X-gal staining, and found that the dorsal root ganglia (DRG) but not the spinal cord showed Cre activity (Figure 3-7C). Histological examination revealed that less than half of the DRG neurons undergo Cre-mediated recombination (Figure 3-7D). In addition, Cre activity was detected in the optic nerve and trigeminal ganglia in mice induced at neonatal (Figure 3-7E, middle panel) or adult stages (Figure 3-7E, right panel). Collectively these data indicate that the nestin promoter/enhancer employed to generate this tamoxifen inducible transgene, exhibits remarkable fidelity to the endogenous neural expression with only a few potential sites of discrepancy.

Detailed analysis of traditional Nestin-Cre transgenic lines has revealed Cre activity outside the CNS such as in the kidney and somite-derived tissues (Dubois et al., 2006). To determine whether Cre activity in the Nes73-CreER^{T2} mice was restricted to the neural system, Nes73-CreER^{T2}; Rosa26^{lacZ} mice were induced for 5 days from P0 and analyzed at eight weeks of age by whole-mount X-gal staining of internal organs including the heart, lung, liver, thymus, spleen, kidney, pancreas and stomach. With the exception of the esophagus where neonatal but not adult exposure to tamoxifen induced Cre activity (Figure 3-8) and stomach where spontaneous lacZ activity is present in

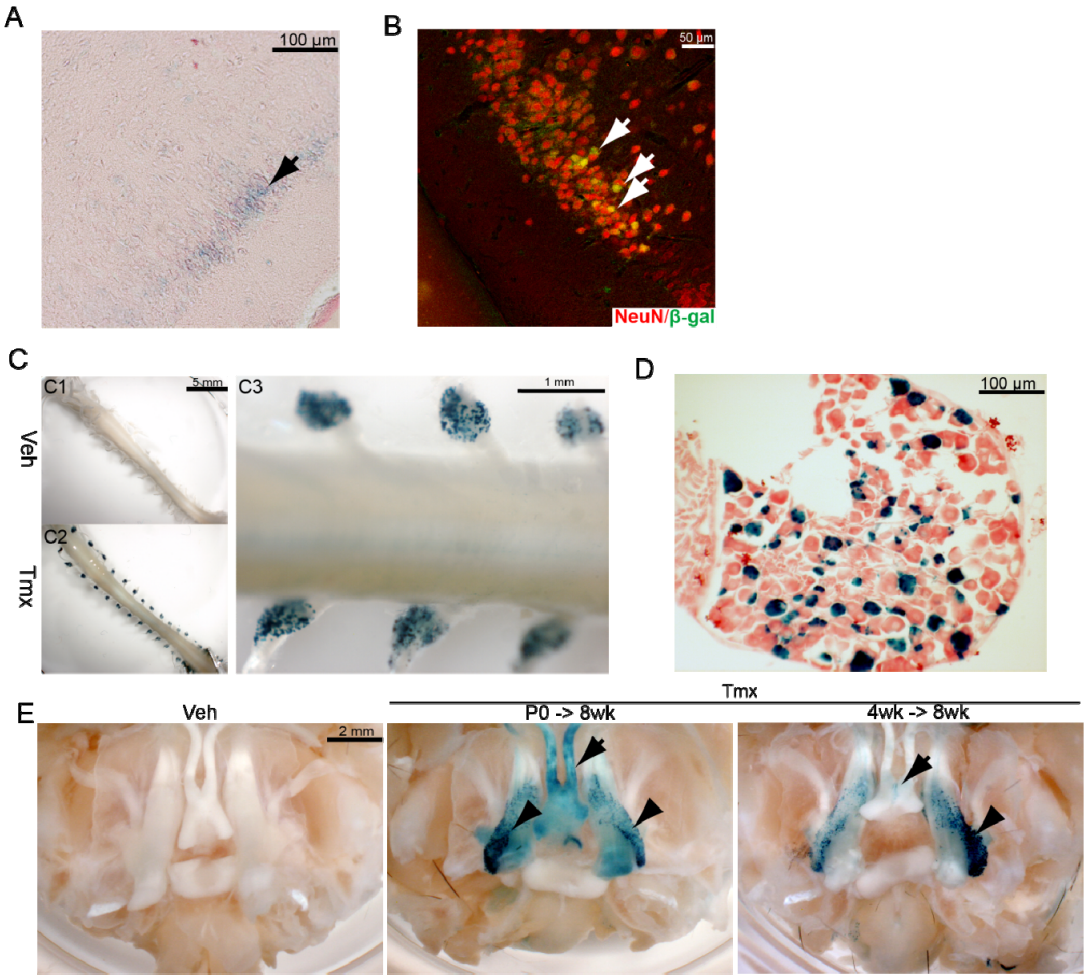

Figure 3-7. Additional Cre activity in piriform cortex, dorsal root ganglia (DRG), optic nerve and trigeminal ganglia. Weak β-Gal expression (black arrow) was also found in the piriform cortex (A and co-localized with NeuN-positive neurons (white arrows) (B). Outside of the brain, X-Gal signal was detected in the dorsal root ganglia (DRG) (C & D), optic nerve (black arrows) and trigeminal ganglia (black arrowheads) (C). No obvious signal was detected in the spinal cord by whole mount X-gal staining (C2 & C3). Further sectioning of DRG showed that some small, medium, and large-sized DRG neurons were positive for β-Gal staining (D). Vehicle-treated controls were negative for β-Gal expression (C1 and E, left panel).

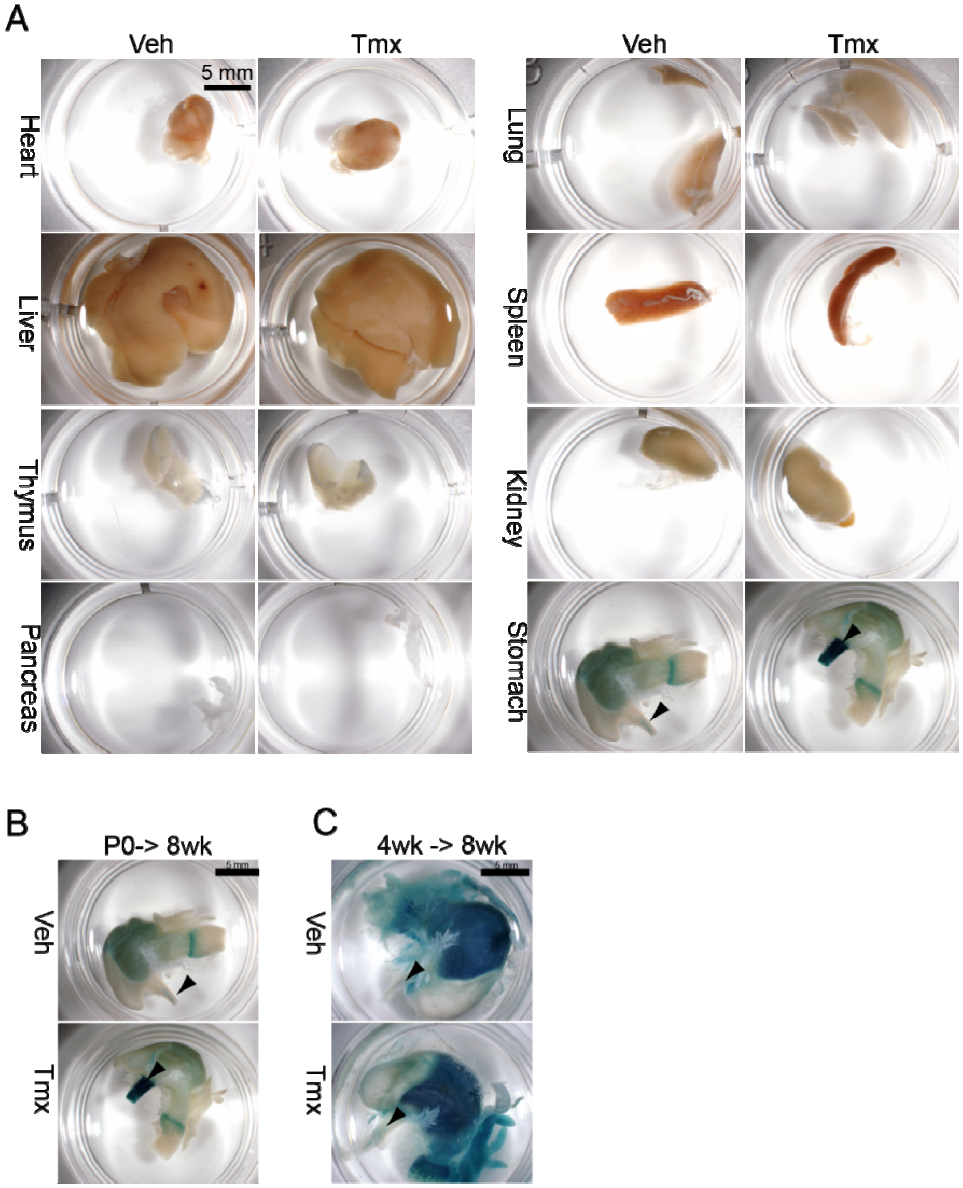

Figure 3-8. Cre activity is not observed in internal organs. A - B) Nes73-CreER^{T2};Rosa26^{lacZ} mice were treated with vehicle (Veh) or tamoxifen (Tmx) at P0 for 5 days. Different organs were then dissected out at 8 weeks and subjected to whole mount X-gal staining. Endogenous X-gal signal is present in the stomachs of both treatment groups. Except for the Cre activity shown in the esophagus (B) of the Tmx-treated mice (black arrowheads), no obvious difference was found elsewhere between genotypes (not shown) or treatments. C) Cre activity in esophagus (black arrowheads) is not presented when tamoxifen was administrated at 4 week of age.

controls (Kwon et al., 2006), we found no evidence of reporter expression in the absence or presence of tamoxifen (Figure 3-8).

Genetic Tumor Suppressor Targeting of Neural Stem/Progenitor Cells Induces Astrocytomas

To directly examine whether tumor suppressor depletion in neural stem/progenitors was sufficient to induce astrocytoma formation, we bred the inducible Nes73-creER^{T2} mice to incorporate the tumor suppressor floxed (flox) alleles (either Nf1$^{flox/+}$;P53$^{flox/flox}$;Pten$^{flox/+}$ or Nf1$^{flox/flox}$;p53$^{flox/flox}$) and injected pregnant females with tamoxifen at E13.5 or adult mice at 4 weeks of age. All tamoxifen-treated (TMX) mutant mice developed high-grade astrocytomas, while vehicle-treated (Veh) mice did not (Figure 3-9A). E13.5-tamoxifen-treated mutant mice developed tumors at a similar rate as the previously reported hGFAP-cre;Nf1$^{flox/+}$;P53$^{-/flox}$;Pten$^{flox/+}$ mouse strain (Kwon et al., 2008a), with a median survival of around 16 weeks. Mutant mice injected with tamoxifen at 4 weeks of age developed tumors with a median survival of around 46 weeks. Hematoxylin and eosin (H&E) staining of these tumors showed the classical features of diffusely infiltrating astrocytomas, including nuclear atypia and prominent mitoses, as well as necrosis (Figure 3-9B). Both E13.5- and adult-treated mutant mice developed tumors diagnosed as Grade III or Grade IV (glioblastoma multiforme) astrocytomas based on the World Health Organization classification system (Figure 3-9C, Table 3-1). These tumors had large numbers of Ki67-positive cells, indicating robust proliferation, and were immunoreactive for Gfap, nestin and Olig2 (Figure 3-10A), acknowledged markers in human astrocytic tumors (Furnari et al., 2007). Consistent with

Table 3-1 Glioma grades of inducible tumor

Mouse NO.	Genotype	Gender	Timing of injection	Age (weeks)	Tumor Grade*
9830	Nes-CreER^{T2};Nf1$^{flox/+}$;p53$^{flox/flox}$;Pten$^{flox/+}$	F	4wk	41	GIII
9888	Nes-CreER^{T2};Nf1$^{flox/+}$;p53$^{flox/flox}$;Pten$^{flox/+}$	F	4wk	45	GIII
9890	Nes-CreER^{T2};Nf1$^{flox/+}$;p53$^{flox/flox}$;Pten$^{flox/+}$	F	4wk	29	GIII
10469	Nes-CreER^{T2};Nf1$^{flox/+}$;p53$^{flox/flox}$;Pten$^{flox/+}$	M	4wk	28	No BT
10544	Nes-CreER^{T2};Nf1$^{flox/+}$;p53$^{flox/flox}$;Pten$^{flox/+}$	M	4wk	33	GIII
11478	Nes-CreER^{T2};Nf1$^{flox/+}$;p53$^{flox/flox}$;Pten$^{flox/+}$	M	4wk	25	GIII
11544	Nes-CreER^{T2};Nf1$^{flox/+}$;p53$^{flox/flox}$;Pten$^{flox/+}$	M	4wk	60	GIII
14561	Nes-CreER^{T2};Nf1$^{flox/+}$;p53$^{flox/flox}$;Pten$^{flox/+}$	M	4wk	57	No BT
10529	Nes-CreER^{T2};Nf1$^{flox/+}$;p53$^{flox/flox}$;Pten$^{flox/+}$	F	4wk	37	GIII
15574	Nes-CreER^{T2};Nf1$^{flox/+}$;p53$^{flox/flox}$;Pten$^{flox/+}$	M	4wk	47	GIV
15791	Nes-CreER^{T2};Nf1$^{flox/+}$;p53$^{flox/flox}$;Pten$^{flox/+}$	M	4wk	44	GIII
15793	Nes-CreER^{T2};Nf1$^{flox/+}$;p53$^{flox/flox}$;Pten$^{flox/+}$	F	4wk	32	GIII
15794	Nes-CreER^{T2};Nf1$^{flox/+}$;p53$^{flox/flox}$;Pten$^{flox/+}$	F	4wk	30	GIII
15862	Nes-CreER^{T2};Nf1$^{flox/+}$;p53$^{flox/flox}$;Pten$^{flox/+}$	M	4wk	30	GIII
15867	Nes-CreER^{T2};Nf1$^{flox/+}$;p53$^{flox/flox}$;Pten$^{flox/+}$	F	4wk	34	GIII
15875	Nes-CreER^{T2};Nf1$^{flox/+}$;p53$^{flox/flox}$;Pten$^{flox/+}$	M	4wk	44	GIII
16591	Nes-CreER^{T2};Nf1$^{flox/+}$;p53$^{flox/flox}$;Pten$^{flox/+}$	M	4wk	37	GIV
13003	Nes-CreER^{T2};Nf1$^{flox/+}$;p53$^{flox/flox}$;Pten$^{flox/+}$	M	E13.5	21	GIII
13039	Nes-CreER^{T2};Nf1$^{flox/+}$;p53$^{flox/flox}$;Pten$^{flox/+}$	F	E13.5	15	GIII
13042	Nes-CreER^{T2};Nf1$^{flox/+}$;p53$^{flox/flox}$;Pten$^{flox/+}$	M	E13.5	16	GIII
17654	Nes-CreER^{T2};Nf1$^{flox/+}$;p53$^{flox/flox}$;Pten$^{flox/+}$	M	E13.5	14	GIII
17913	Nes-CreER^{T2};Nf1$^{flox/+}$;p53$^{flox/flox}$;Pten$^{flox/+}$	F	E13.5	15	GIV
19568	Nes-CreER^{T2};Nf1$^{flox/+}$;p53$^{flox/flox}$;Pten$^{flox/+}$	F	E13.5	13	GIV
19516	Nes-CreER^{T2};Nf1$^{flox/+}$;p53$^{flox/flox}$;Pten$^{flox/+}$	F	E13.5	15	GIII
19519	Nes-CreER^{T2};Nf1$^{flox/+}$;p53$^{flox/flox}$;Pten$^{flox/+}$	F	E13.5	12	GIV
19523	Nes-CreER^{T2};Nf1$^{flox/+}$;p53$^{flox/flox}$;Pten$^{flox/+}$	M	E13.5	15	GIII
11477	Nes-CreER^{T2};Nf1$^{flox/flox}$;p53$^{flox/flox}$	M	4wk	61	GIII
18277	Nes-CreER^{T2};Nf1$^{flox/flox}$;p53$^{flox/flox}$	M	4wk	37	GIII

Tumor grade*:
GIII: WHO Grade III astrocytoma
GIV: WHO Grade IV astrocytoma
No BT: No brain tumor was found after serial sectioning and H&E staining.

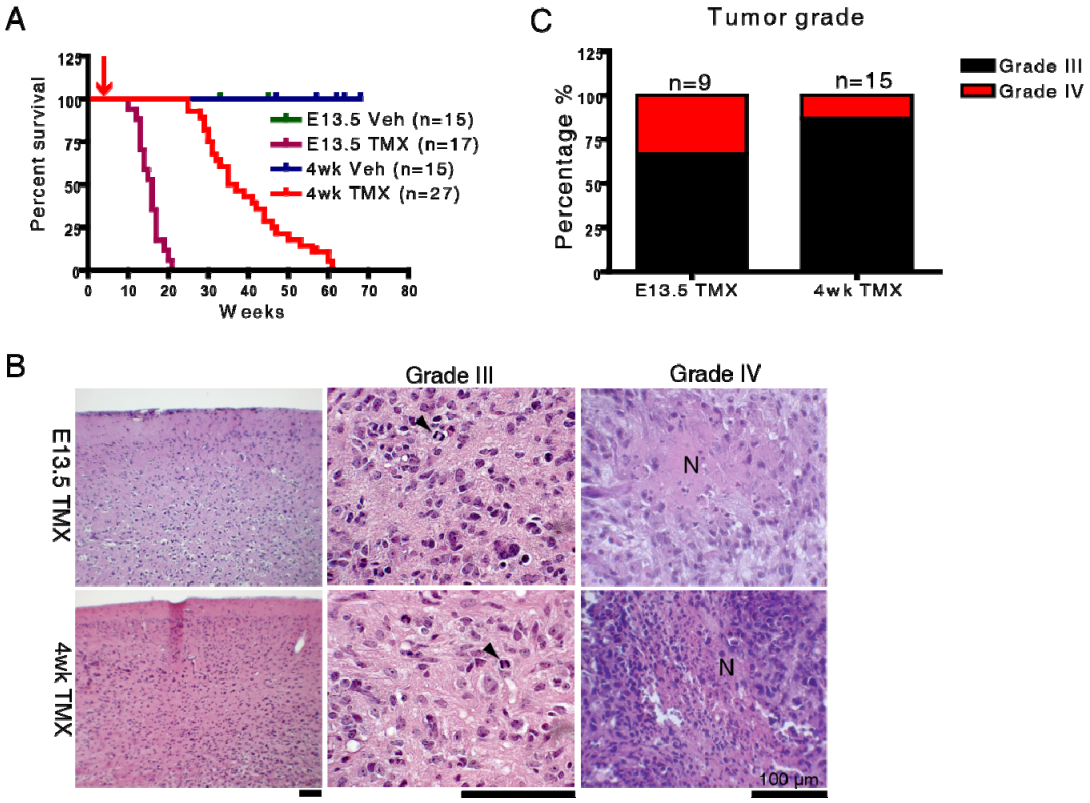

Figure 3-9. Tumor suppressor inactivation in nestin-expressing neural stem/progenitor cells induces high grade astrocytoma formation A) Mice with induced tumor suppressor inactivation (Nes-73-creER^{T2};Nf1$^{flox/+}$;P53$^{flox/flox}$;Pten$^{flox/+}$ or nes73-creER^{T2};Nf1$^{flox/flox}$;P53$^{flox/flox}$) by tamoxifen treatment (TMX) have shortened survival compared to vehicle-treated (Veh) mice. Kaplan-Meier survival curves of Nes73-creER^{T2} mice with tumor suppressor inactivation induced at either E13.5 or 4 weeks of age show median survivals of 16 weeks and 46 weeks, respectively. Red arrow indicates timing of adult injection. B) Histologically identifiable high grade astrocytomas develop in inducible mutant mice. Representative H&E-stained brain sections reveal formation of brain tumors in Nes73-creER^{T2} mice with tumor suppressor inactivation induced at either E13.5 or 4 weeks of age. Grade III or IV astrocytomas with characteristic features of nuclear atypia, mitoses (arrowheads), and necrosis (N) are shown. Scale bars, 100 µm. C) Mutant mice wherein tumor suppressor inactivation is induced by tamoxifen (TMX) at E13.5 or adult ages develop Grade III or Grade IV astrocytomas.

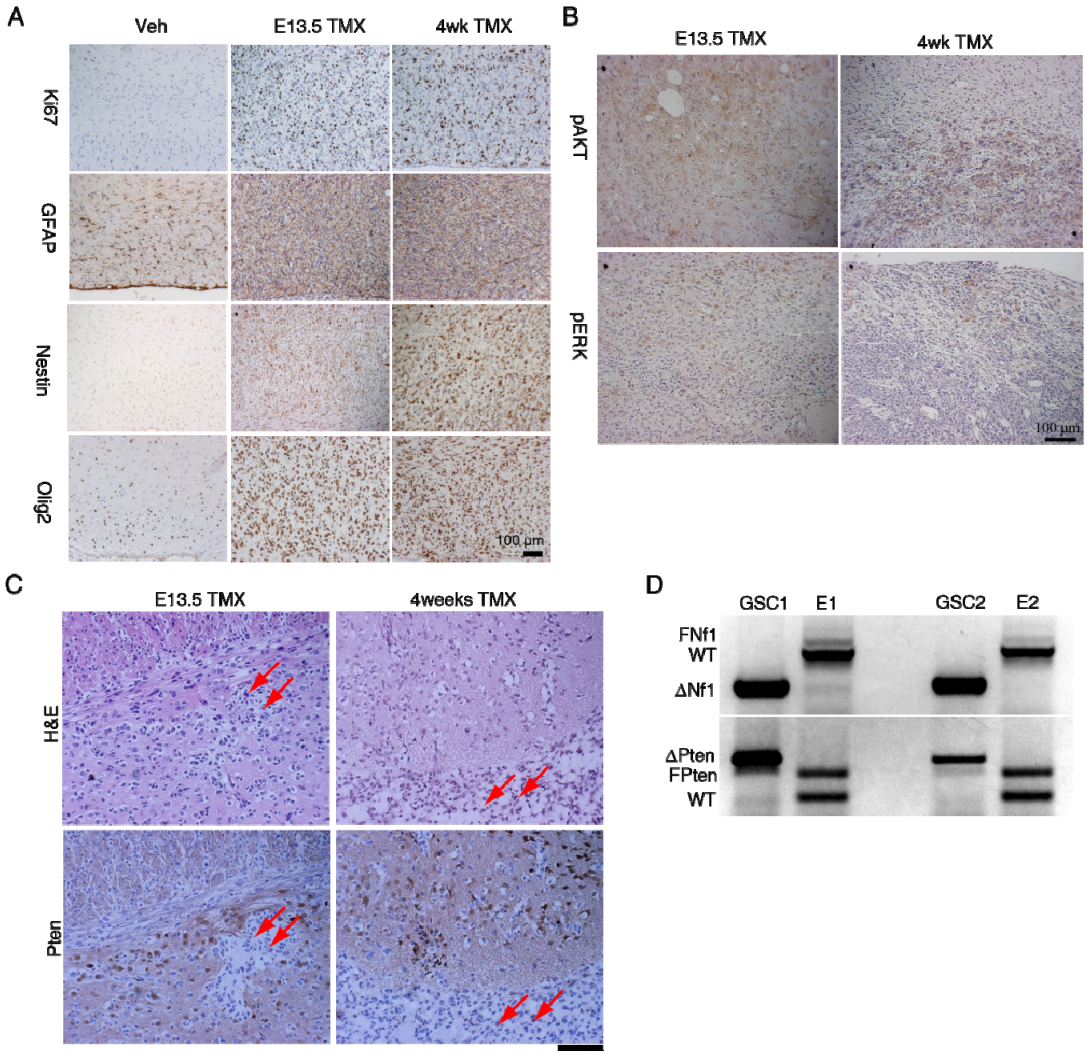

Figure 3-10. Characterization of tamoxifen induced gliomas. A) Tumors express traditional markers of astrocytomas, including Ki67, Gfap, nestin, and Olig2. B) Some tumor regions show robust pErk and pAkt staining, consistent with activation of the Ras and PI3K-Akt signaling pathways, respectively. C) Representative PCR genotyping of tumors from Nes73-creER^{T2} mice with induced tumor suppressor inactivation shows loss of heterozygosity of Nf1 and Pten tumor suppressor alleles. Genomic DNA from tumor-derived neurospheres (GSC) or ear (E) was used to genotype for the floxed (fNf1, fPten), recombined (ΔNf1, ΔPten) and wild type (wt) Nf1 and Pten alleles. Two different representative samples are shown. Scale bar, 100 μm.

activation of the Ras and Akt signaling pathways by loss of Nf1 and Pten, respectively, some tumor regions showed robust pErk and pAkt expression (Figure 3-10B). We further confirmed LOH of the tumor suppressor alleles in tumors by immunostaining and genotyping (Figure 3-10C&D). Thus, cre-mediated somatic mutation of Nf1, p53, and Pten restricted to the neural/stem progenitor compartment is sufficient to replicate the high grade astrocytoma phenotype previously observed using combinations of germline and somatic mutations and a less specific hGFAP-cre driver (Kwon et al., 2008b; Zhu et al., 2005a). Furthermore, loss of Nf1, p53 and/or Pten was present in all tumors and is therefore apparently required for high grade tumor induction (Kwon et al., 2008a).

Cancer-initiating Cells Undergo Infiltration and Spontaneous Differentiation

The presence of the R26-lacZ reporter in the context of the floxed tumor suppressors allows for lineage tracing of cells as they undergo tumorigenic transformation. While normal neural stem cells and their progeny are principally restricted to the SVZ-RMS-OB and SGZ-GL (Figure 3-2C & Figure 3-3), tumors arising from inducible mutant mice were found in adjacent brain regions, including the cortex and striatum, as shown by X-gal staining (Figure 3-11A). The cre transgene is expressed in cerebellum but only one tumor was found in cerebellum and it resembled astrocytoma and not medulloblastoma, which is the idiotypic tumor of this brain region. The β-galactosidase positive tumor cells co-stained with the astrocytoma markers Gfap, nestin, and platelet-derived growth factorα (PDGFRα; Figure 3-11A). Thus, mutant stem cells or their progeny migrate away from their normal niches and invade the parenchyma during tumor development.

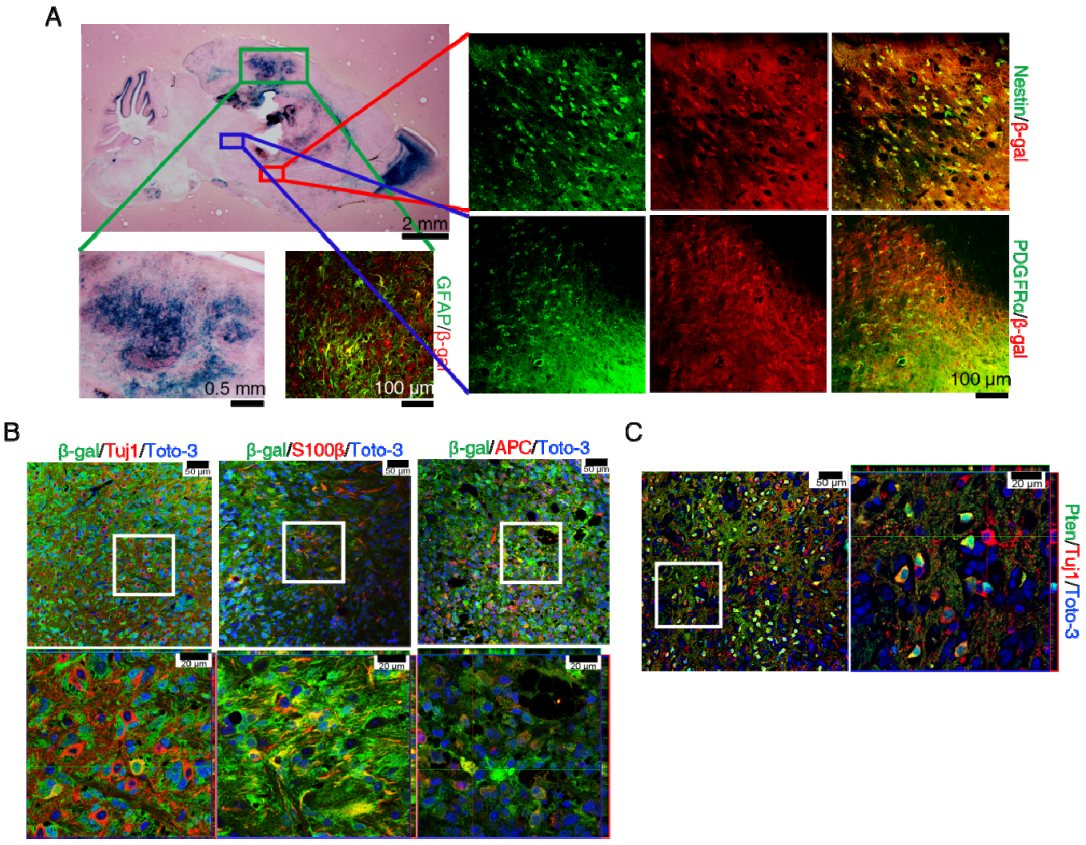

Figure 3-11. Cancer-initiating cells exhibit infiltration and differentiation during tumor development. A. β-galactosidase-positive mutant cells infiltrate into adjacent brain structures, away from their normal neural stem/progenitor niches. A representative X-gal-stained brain tumor section from Nes73-CreER^{T2};Nf1$^{flox/+}$;p53$^{flox/flox}$;Pten$^{flox/+}$;R26^{lacZ} mouse 8 months after tumor suppressor inactivation shows tumor cells found outside their original locations in the SVZ/SGZ niches. β-galactosidase-positive tumor cells, shown here expressing Gfap, nestin, and PDGFRα, are found elsewhere in the forebrain, such as the cortex and striatum. B. Marked astrocytoma cells expressing multi-lineage markers are found in the tumor bulk. β-galactosidase-positive tumor cells in inducible mutant mice, shown here in the thalamus, express markers of neuronal (Tuj1), and glial (S100β and APC) differentiation. Toto-3 marks cell nuclei. C) Pten-negative tumor cells express markers of more differentiated cell types. Pten/Tuj1 double immunofluorescence staining shows a subset of Pten-negative cells within the tumor bulk expressing Tuj1, an immature neuronal marker.

Astrocytomas are heterogeneous tumors, with varying cellular morphologies and presence of immature and mature markers for all neural lineages. Upon examination of the tumor bulk, we found a variety of β-galactosidase-positive cells co-expressing markers of subsets of differentiated cells, such the neuronal marker Tuj1, and the glial markers S100βand adenomatous polyposis coli or APC, as shown in a thalamic tumor in Figure 3-11B. These immunoreactive tumor cells morphologically resembled mature neurons, astrocytes, and myelin-ensheathing oligodendrocytes. In contrast to normal CNS cells which show abundant Pten expression (Kwon et al., 2008b), these marker-positive cells were Pten-negative (Figure 3-11C), confirming that these "differentiated" cells are indeed cancer cells. These data provide formal evidence that tumor cells have the stem/progenitor capacity to exit the cell cycle and at least partially differentiate in situ. This may account for the heterogeneity of tumor cell types that is classically associated with high grade astrocytomas.

Discussion

One interesting observation from the study is the novel sites of nestin-Cre recombinase activity. Whether this activity identifies previously undetected sites of neurogenesis or simply ectopic Cre expression remains to be rigorously determined. However, we note that a second, independently derived transgenic line, *Nes8-CreER*^{T2}, shows a similar pattern of inducible expression. This leads us to favor the conclusion that the expression outside the SVZ and SGZ is not likely due to the consequence of endogenous regulatory elements at the site of transgene insertion but rather is a reflection of the properties of the transgenic construct. Stem cells have been isolated from neonatal cerebellum and they are reported to be prominin/CD133-positive and Math1-negative (Klein et al., 2005; Lee et al., 2005). We observe Cre activity in the cerebellum from E17.5 through 8 weeks of age. Although diminishing over time, a clear gradient is observed that becomes progressively more anterior. The lacZ positive cells resulting from activation of the Rosa26 reporter possess the characteristic morphology of granule cells. In adult cerebellum, the Bergmann glia retain a morphology reminiscent of radial glia which can generate neurons and adult NSCs during brain development (Gotz and Barde, 2005; Merkle et al., 2004). In addition, Bergmann glia still express stem cell markers such as Sox2 and nestin (Mignone et al., 2004; Sottile et al., 2006). On the other hand, rare BrdU-incorporated cells have been observed in adult cerebellum even after growth factor infusion (Grimaldi and Rossi, 2006). The fact that a number of NeuN-positive neurons in the anterior cerebellum were targeted 2 days after acute tamoxifen administration suggested that the cre activity in the IGL was likely due to promoter leakage (Figure 3-6E).

A series of similar inducible Nestin-Cre transgenes have recently been reported, although the extent of expression over time as well as expression outside the nervous system was not described (Table 3-2) (Balordi and Fishell, 2007; Burns et al., 2007; Imayoshi et al., 2006; Kuo et al., 2006; Lagace et al., 2007). Eisch and colleagues recently described a tamoxifen-inducible Cre transgenic mouse line with no obvious Cre activity in the cerebellum upon tamoxifen induction (Lagace et al., 2007). The fact that our transgenic construct included only intron 2 of the nestin gene whereas their construct contained nestin exons 1-3 could account for this discrepancy (Zimmerman et al., 1994). It is possible that our more limited nestin construct might lack cerebellar-specific repressor sequences. Another potentially significant variation is the use of a $Rosa26^{lacZ}$ reporter line versus the $Rosa26^{YFP}$ reporter used by Lagace et al. (Lagace et al., 2007). Both the sensitivity of the reporter and perhaps the recombinogenic efficiency could in principle differ, leading to these discrepancies. We also observe Cre activity in the adult piriform cortex. This is in accordance with previous reports of BrdU incorporation in this region, leading to the suggestion of additional neurogenic niches (Pekcec et al., 2006).

In the same published result, Dr. Sheila Alcantara Llaguno demonstrated that only targeting NSC niches by cre adenovirus injection can yield glioma in several strains of tumor suppressor floxed mice ($Nf1^{flox/flo}x;p53^{flox/flox}$, $Nf1^{flox/flox};p53^{flox/-}$, or $Nf1^{flox/+};p53^{flox/flox};Pten^{flox/+}$) while targeting non-neurogenic region was unable to initiate tumor (Alcantara Llaguno et al., 2009). Collectively, we have suggested that adult neural stem/progenitor cells are major tumor initiating cells of malignant

Table 3-2. Summary of published tamoxifen inducible Nestin-Cre mice

Publication	Transgene structure	Reporter line	Induction protocol	Summary of results
Imayoshi *et al.* *(Imayoshi et al., 2006)* Forni *et al.* *(Forni et al., 2006)*	5.8 kb rat nestin promoter driven Cre-ER^{T2} with 1.8 kb nestin 2nd intron	Rosa26^{LacZ}; Z/EG	Intraperitoneal (I.P.) injection (0.5 mg) or oral gavage (4 mg) to pregnant mice at E9.5, E10.5 and E18.5. No postnatal induction was performed.	Line 1 showed significant leakage without tamoxifen administration. Line 4 showed less but noticeable leakage. Line 1 and 4 mice showed microcephaly and hydrocephaly upon high dosage of tamoxifen induction from E10.5 (8 mg, I.P.). Line 5-1 showed minimal leakage upon oil treatment.
Kuo *et al*. (Kuo et al., 2006)	~5.8 kb rat nestin promoter driven CreER^{Tm} with 2.6 kb nestin 2nd intron	Rosa26^{LacZ}	Single subcutaneous injection (8 mg/40 g body weight) into pregnant mice at E10.5 or postnatal mice at P0, P7 and P14.	No obvious leakage in embryonic induction and SVZ in postnatal induction. Cre transgene was expressed mainly in SVZ astrocytes and ependymal cells. A few Mash1-positive type C cells and DCX-positive neuroblasts expressed Cre. Cre activity and inducibility in other brain regions or non-brain tissues were not studied.
Burns *et al.* *(Burns et al., 2007)*	Nestin 2nd intron/hsp68 mini promoter driven Cre-ER	CAG-CAT-EGFP	I.P. injection (5 mg/40 g body weight) to pregnant mice at E14.5, E16.5 or E19 for embryonic induction. For adult induction, 5 week old mice were injected once a day (4 mg/30 mg body weight) for 4 days and looked at 10 days later.	No obvious leakage in RMS and striatum of the mice without tamoxifen induction. Cre activity was detected in SVZ neural stem cells and their progeny. There is no cre activity in SGL neural stem cell niches. The mini promoter was also aberrantly activated in some neurons in hippocampus and cingulate cortex.

Lagace *et al*. (Lagace et al., 2007)	~5.8 kb rat nestin promoter driven Cre-ER^{T2} with nestin exons 1-3 including 2nd intron	Rosa26^{YFP}	5-7 week-old mice were injected with tamoxifen at 180 mg/kg/d for 5 days and looked at 1, 12, 30, and 65 days after injection.	No obvious expression without tamoxifen treatment. No appreciable number of YFP^{+} cells in non-neurogenic regions such as cortex and cerebellum of tamoxifen treated mice. 2 transgenic lines only showed cre activity in SVZ and 2 additional lines have cre activity in both SVZ and SGL.
Balordi and Fishell. (Balordi and Fishell, 2007)	~1.8 kb Nestin 2nd intron followed by 160 bp HSV-TK promoter driven Cre-ER^{T2}	Rosa26^{LacZ}	I.P. injection (5 mg/35 g body weight) of tamoxifen into pregnant mice at E12.5 for embryonic induction. Adult mice were induced by 3 day I.P. injection (5 mg/35 g body weight) or one single oral gavage (10 mg/35 g body weight).	Low level spontaneous cre activity was observed in both embryonic and adult mouse brain without induction. Both SVZ and SGL neural stem cells were targeted after tamoxifen administration. Cre activity elsewhere was not described.

astrocytomas in our mouse models. However, as discussed in chapter 1, we can not pinpoint whether quiescent neural stem cells or the actively dividing cells contribute to glioma formation due to the fact that both cell populations express nestin. In addition, as many as 2% of rat white matter cells and 4% of human white matter cells are dividing oligodendrocyte progenitors (Dawson et al., 2003; Gensert and Goldman, 2001). In a naturally occurring tumorigenic process where somatic mutations are mostly generated during replication, the larger base of dividing oligodendrocyte progenitors will have more chances to acquire somatic mutations, even though they lack long-term self-renewal potential. This possibility could not be addressed by our cre viral injections as only a limited region of the brain was targeted. Progenitor-specific inducible Cre mice are required to answer those questions.

Gliomas are heterogeneous tumors and grade IV gliomas are called glioblastoma "multiforme", reflecting this heterogeneity. The exact causes of this heterogeneity are still unclear. Several hypotheses have been suggested, including differentiation of cancer stem cells, various cells of origin of cancer, diversity of the genetic mutations, etc. (Visvader, 2011). Our lineage tracing experiment confirmed the differentiation capacity of the cancer cells, suggesting the possible existence of cancer stem cells. More importantly, the fact that the majority of neurons inside a tumor are negative for the tracing marker strongly suggested that a substantial portion of the heterogeneity was caused by the infiltrative nature of the tumor cells that trapped various neural cell types.

Another intriguing observation from the lineage tracing is that the invading cells mostly expressed neural stem cell markers such as nestin and PDGFR-α. Whether the cells are pretumorigenic cells that abnormally migrated out of the neurogenic niches or tumor cells that are expanding their territory is still not clear. However, therapeutic approaches that eradicate these cells should greatly benefit patients, as gliomas invariably recur after surgical removal of the original tumor mass due to infiltrative tumor cells.

CHAPTER FOUR

FUNCTIONAL EVIDENCE OF GLIOMA CANCER STEM CELLS IN VIVO

Introduction

The cancer stem cell (CSC) hypothesis holds that some tumors are composed of a hierarchical cadre of cells of which only a subset retains both self-renewal and differentiation capacity (Clarke et al., 2006). In this model, only CSCs within tumors have the capacity to sustain tumor growth. The "gold standard" for evaluating whether tumors contain a CSC subpopulation is a limiting dilution tumorigenic transplantation assay into immunodeficient animals (Clarke et al., 2006). However, there is variability inherent in transplantation assays that may dramatically affect the frequency of CSCs and there remains considerable controversy particularly in the solid tumor field (Boiko et al., 2010; Ishizawa et al., 2010; Kelly et al., 2007; Quintana et al., 2008). The use of epitope markers such as CD133 and CD15 to identify putative cancer stem cells has also proved problematic (Chen et al., 2010; Prestegarden et al., 2010; Son et al., 2009). To date, no studies have directly addressed *in vivo* whether CSCs in a spontaneous solid tumor functionally contribute to tumor maintenance and progression. Evidence of CSCs in the physiological setting of endogenous solid tumor development would permit evaluation of how these cells hold up to *ex-vivo* assays used by the field and permit investigation into the efficacy of a CSC-targeting therapy.

CSCs have been described for the malignant human brain tumor glioblastoma multiforme (GBM) (Singh et al., 2004). GBM is a devastating disease, with a median survival of

about one year, a prognosis that is relatively unchanged over the past three decades (Network, 2008). In xenograft assays, only a limited proportion of human glioma cells, termed glioma or cancer stem cells, have the ability to initiate tumor growth in immunodeficient rodents (Singh et al., 2004). CSCs defined in this manner express many neural stem cell (NSC) markers such as sox2 and nestin (Bao et al., 2006). We have previously generated physiologically relevant mouse models of GBM that are based on conditional somatic deletion of three of the five most frequently mutated tumor suppressors found in sporadic GBM: p53, NF1 and Pten (Alcantara Llaguno et al., 2009; Kwon et al., 2008a; Zhu et al., 2005a). We have further demonstrated that the adult neurogenic niche, the subventricular zone, is the source of gliomas in these models (Alcantara Llaguno et al., 2009; Zhu et al., 2005a). In this report, we take advantage of a Nestin-ΔTK-IRES-GFP (Nes-ΔTK) transgenic mouse line (Yu et al., 2008), originally devised to mark adult NSCs, to selectively mark and ablate transgene-positive tumor stem cells *in vivo* to assess the role of CSCs in tumor maintenance.

Results

Certain regulatory elements of the nestin gene have been shown to drive transgene expression specifically in NSCs (Chen et al., 2009; Yu et al., 2008) (Figure 4-1A). This transgene contains a modified version of the herpes simplex virus thymidine kinase (ΔTK) allowing for temporally regulated ablation of dividing neural progenitors by systemic ganciclovir (GCV) administration. The transgene also harbors an IRES-GFP cassette to mark Nes-ΔTK-expressing cells in the absence of GCV. As determined experimentally, the Nes-ΔTK transgene is expressed in both glial fibrillary acidic protein (GFAP)-positive NSCs and early doublecortin (DCX)-positive neural progenitor cells in the major adult NSC niches: the subventricular zone (SVZ) of the lateral ventricle and the subgranular layer (SGL) of hippocampus(Zhao et al., 2008). To determine that the GCV activated Nes-ΔTK transgene can effectively eliminate endogenous nestin-expressing neural stem/progenitor cells, one-month-old Nes-ΔTK mice were treated with GCV for two weeks via an implanted osmotic minipump. In control mice, the rostral migratory stream (RMS), formed by neural progenitor cells migrating from the SVZ to the olfactory bulb, can be visualized by Nissl staining. In contrast, the RMS was severely diminished in Nes-ΔTK mice after GCV (Figure 4-1B). Consistent with this observation, DCX immunostaining indicated absence of neural progenitor cells in the SVZ and SGZ of GCV-treated Nes-ΔTK animals (Figure 4-1C; bottom panels). Since in the presence of GCV, HSV-thymidine kinase targets only proliferating cells, the GFAP-positive quiescent NSCs were unaffected, although they also expressed the Nes-ΔTK transgene as indicated by GFP co-immunostaining (Figure 4-1C, bottom panels).

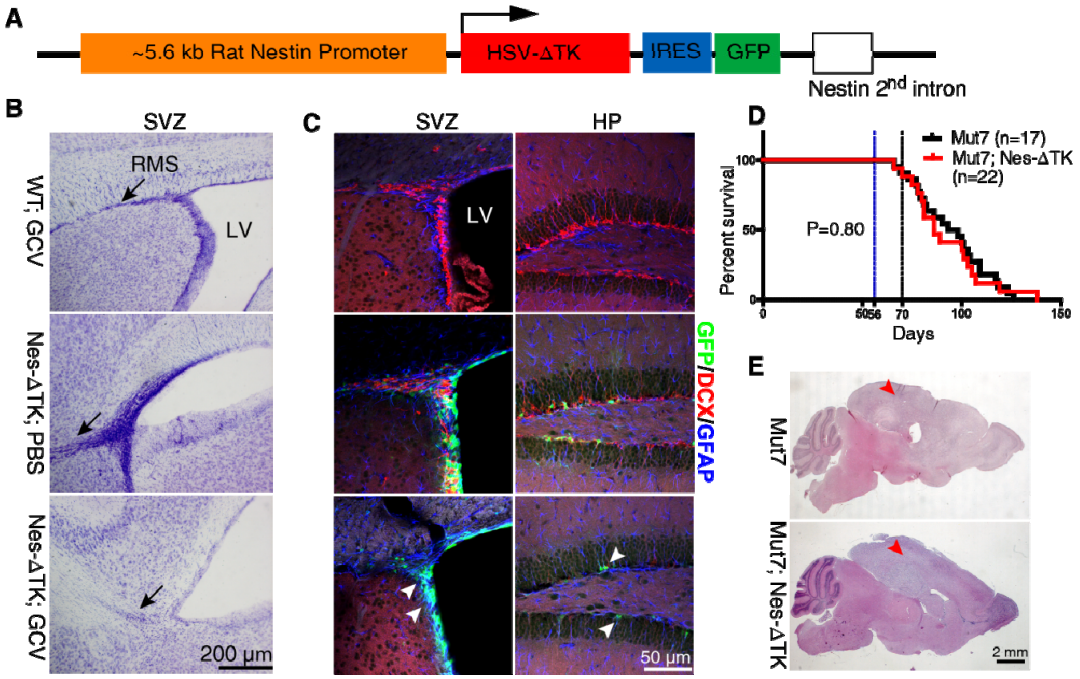

Figure 4-1. Characterization of the Nes-ΔTK-GFP transgene. A) Diagram of the Nes-ΔTK transgene. B,C) GCV administration efficiently ablates NSCs in wild type mice. B) Representative Nissl staining of the subventricular zone (SVZ) region in wild type mice treated with GCV (WT;GCV), Nes-ΔTK transgene mice treated with PBS (Nes-ΔTK;PBS) and Nes-ΔTK transgene mice treated with GCV (Nes-ΔTK;GCV); black arrows indicate the stem cell rostral migratory stream (RMS), which is greatly reduced in the Nes-ΔTK;GCV mice. C) GFP (transgene), GFAP (quiescent neural stem cells) and DCX (committed neural progenitors) immunostaining of the hippocampus (HP) and SVZ stem cell niches. White arrowheads indicate GFP-/GFAP-positive but DCX-negative quiescent neural stem cells (NSCs). D) Kaplan–Meier survival curve of untreated Mut7 and Mut7;Nes-ΔTK animals. No difference in percent survival was observed. E) Representative H&E staining of Mut7 and Mut7;Nes-ΔTK brains without treatment. Infiltrative malignant gliomas are present in the cortex (red arrowhead) of both genotypes.

GFP transgene marks CSCs: In vivo tumor cell hierarchy

To study the function of Nes-ΔTK-positive glioma cells *in vivo*, we utilized a somatic tumor suppressor-based mouse glioma model (hGFAP-Cre;$NF1^{f/+}$;$P53^{f/f}$;$PTEN^{f/+}$*)* developed in our laboratory (Kwon et al., 2008a) (referred to as Mut7). Mut7 mice spontaneously develop malignant glioma by somatic deletion of three of the most frequently mutated tumor suppressors in GBM(Network, 2008). As in wild type mice where the Nes-ΔTK transgene does not affect neurogenesis in the absence of GCV administration (Figure 4-1B&C), introduction of the Nes-ΔTK transgene into the Mut7 genetic background did not impact tumor development or enhance survival (Figure 4-1D). Like Mut7 mice, Mut7;Nes-ΔTK mice developed malignant glioma with 100% penetrance (Figure 4-1E). We observed GFP-positive cells in all tumors and noted that the percentage varied from tumor to tumor (Figure 4-2A). However, the highest content of GFP-positive cells was found at the tumor boundaries (Figure 4-2B). Mut7;Nes-ΔTK tumors exhibited a significant proportion of Ki67-positive/GFP-negative cells and conversely, GFP-positive tumor cells rarely co-stained for Ki67 (Figure 4-2C) indicating that many transgene GFP-positive tumor cells are in a state of relative quiescence.

To determine whether the Nes-ΔTK-GFP-expressing subpopulation in tumors represents CSCs, primary gliomas from Mut7;Nes-ΔTK and Mut7 mice were dissociated and the tumor cells directly injected subcutaneously into nude mice in the presence of continuous GCV or saline treatment (Figure 4-3A). Neither GCV nor saline affected the tumor growth of Mut7-derived cells (Figure 4-3B). In contrast, mice transplanted with Mut7;Nes-ΔTK tumor cells and then treated with GCV developed significantly smaller

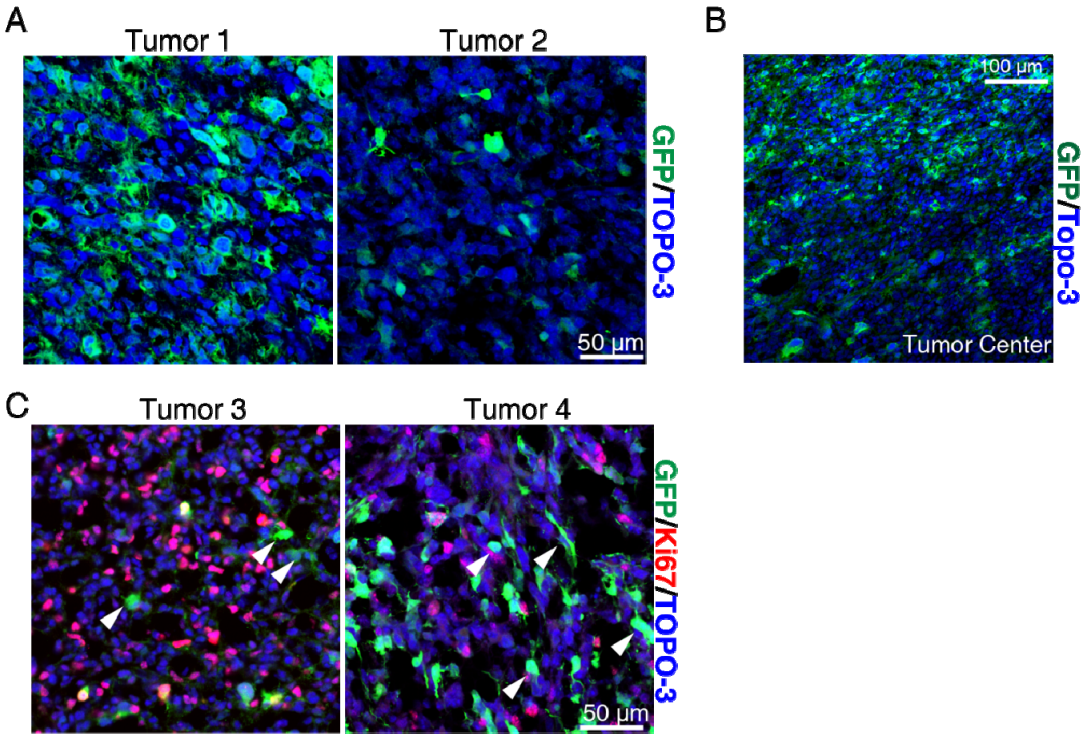

Figure 4-2. Characterization of GFP-positive cells in gliomas from untreated Mut7; Nes-ΔTK animals. A) Representative GFP immunostaining in sections from two untreated gliomas of Mut7;Nes-ΔTK mice. From tumor to tumor, varying numbers of GFP-positive cells were observed. B) GFP staining indicates that Nes-ΔTK-expressing cells tend to localize to the periphery of the tumor bulk. Representative low-magnification GFP staining in a large-sized tumor from untreated Mut7;Nes-ΔTK mice. C) Representative GFP and Ki67 co-immunostaining in two untreated gliomas of Mut7;Nes-ΔTK mice. White arrowheads highlight GFP-positive but Ki67-negative cells, demonstrating that many transgene GFP-positive cells are quiescent.

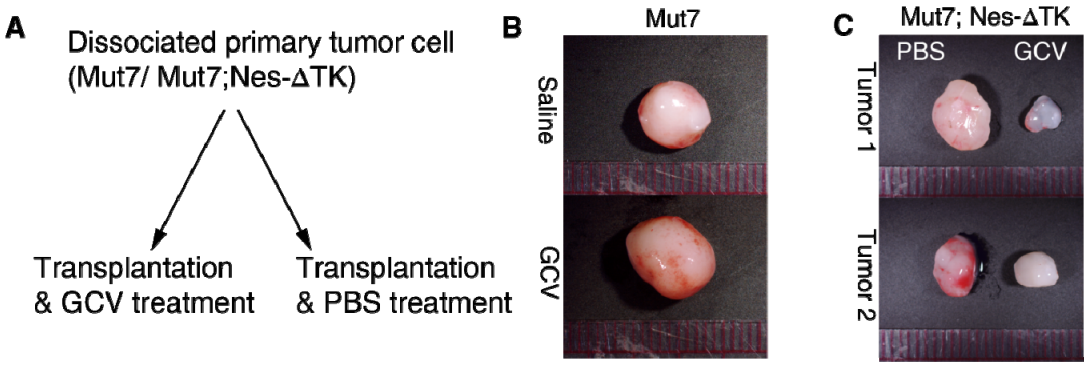

Figure 4-3. Nes-ΔTK-positive cells are enriched for tumor-initiating cells in the transplantation assay. A) Primary tumor transplantation schema. B,C) Representative tumor pictures from transplanted and GCV or PBS-treated Mut7 (B) or Mut7;Nes-ΔTK (C) glioma. Tumors that developed from the GCV-treated host mice implanted with Mut7;Nes-ΔTK tumor cells were much smaller than those from the PBS- or GCV-treated host mice implanted with Mut7 tumor cells or the PBS-treated host mice implanted with Mut7;Nes-ΔTK mice.

tumors that appeared poorly vascularized compared to saline-treated controls (Figure 4-3C). Thus, specific depletion of Nes-ΔTK-GFP-expressing tumor cells severely impairs tumorigenicity following transplantation, identifying the transgene-expressing cells as major drivers of tumor growth in a classic cancer stem cell assay, and supporting the hypothesis that the Mut7;Nes-ΔTK-GFP cells represent endogenous tumor CSCs.

If GFP transgene-positive cells represent CSCs in Mut7;Nes-ΔTK gliomas, lineage tracing of GFP-positive cells should reveal a cellular hierarchy to account for tumor cell heterogeneity (Figure 4-2C). We first "synchronized" the tumors by eradicating pre-existing dividing tumor cells. Temozolomide (TMZ), the primary chemotherapy agent in clinical use to treat GBM patients (Stupp et al., 2005), targets rapidly dividing but not quiescent cells in tumors. In glioma patients, TMZ effectiveness correlates with O-6-methylguanine-DNA methyltransferase (MGMT) promoter methylation status(Hegi et al., 2005). The endogenous MGMT promoter is also methylated in Mut7 gliomas suggesting TMZ would be effective in targeting dividing cells within these tumors (Figure 4-4A). To evaluate TMZ function, ten-week-old Mut7 mice were treated with TMZ for five days, injected with BrdU two hours after the final injection, and sacrificed two hours thereafter (Figure 4-4B). We observed a significant reduction of BrdU-positive cells in both the tumors and NSC niches of TMZ-treated mice (Figure 4-4C&D, data not shown) indicating the effectiveness of TMZ treatment. Thus, synchronization to an approximate "zero basal state" of proliferation was achieved within endogenous tumors prior to initiation of cell lineage pulse/chase labeling experiments.

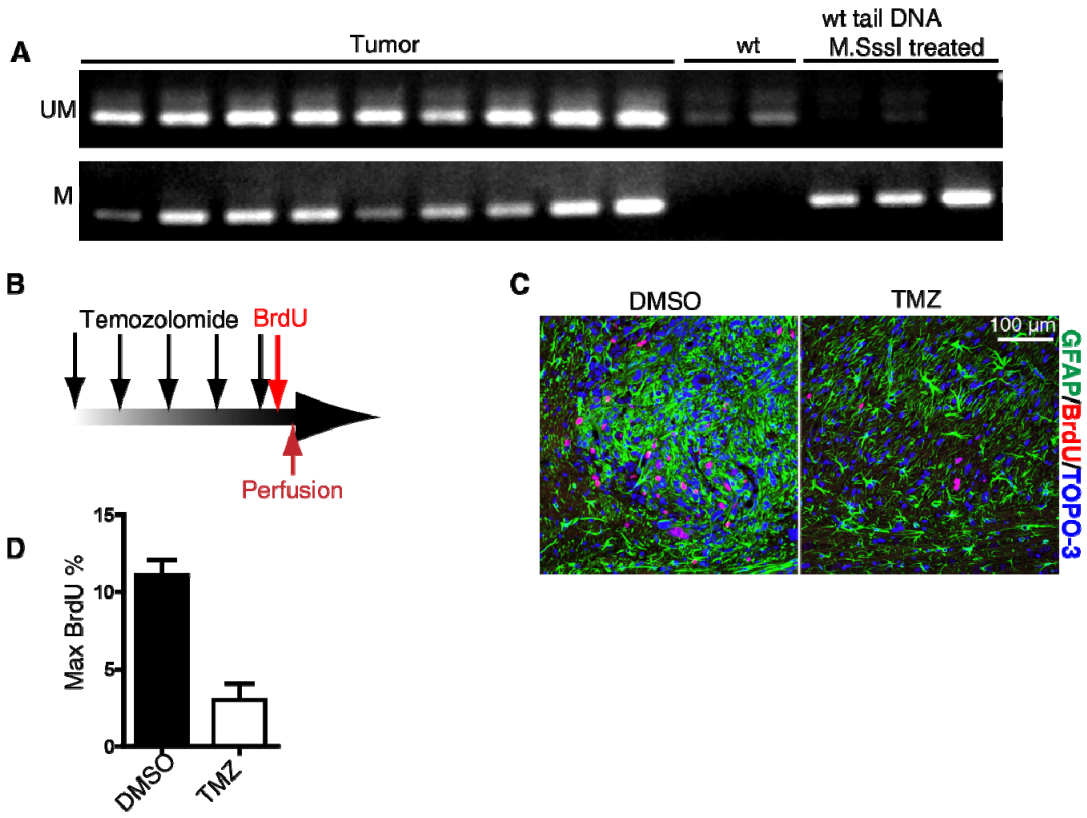

Figure 4-4. Temozolomide (TMZ) kills proliferating mouse glioma cells. A) MGMT methylation status in Mut7 gliomas. Methylation-specific PCR was performed and demonstrated that the MGMT promoter in each Mut7 glioma sample is methylated. No methylation of the MGMT promoter is observed in wild type brain tissue (wt). However. treatment of wild type tail tissue with the methyltransferase M.sssI resulted in methylation-specific amplification of the MGMT promoter. (UM = unmethylated; M = methylated) B) TMZ injection schema. Mut7 mice were treated with TMZ for five days; injected with BrdU two hours after the final TMZ treatment; and sacrificed two hours later for BrdU immunostaining. C) Representative GFAP/BrdU co-staining of DMSO- or TMZ-treated glioma shows a dramatic reduction in the number of BrdU-positive cells. D) Quantification of the percentage of maximal BrdU-positive cells in gliomas from Mut7 mice treated with or without TMZ showed a significant decrease in the TMZ-treated mice. (N=6 for each treatment; $p<0.001$.)

To track the first wave of tumor re-growth after TMZ treatment, the BrdU analogs CldU and IdU were injected into Mut7;Nes-ΔTK mice one day and three days after the final TMZ injection, respectively (Figure 4-5A). Given the variable but relatively low proportion of GFP-transgene positive cells in the tumors (Figure 4-2A-C), if random tumor cells could give rise to proliferating cells after TMZ treatment, then the number of CldU and/or IdU cells that were also GFP positive would be low to insignificant. Instead, examination of tumor sections revealed the large majority of cells incorporating CldU and IdU after relatively short chases also contained GFP expression (Figure 4-5C&D). Moreover, IdU-positive cells retained both GFP and CldU, indicating that following eradication of a majority of pre-existing dividing cells, the emergent population of proliferating cells derived from Nes-ΔTK-GFP-expressing cells and not from random tumor cells (Figure 4-5C&D). When the IdU chase was prolonged to seven days, as anticipated, many long and short pulse analog-labeled cells lost GFP expression, while the high percentage of IdU-labeled cells retaining CldU (85±7%) was consistently maintained (Figure 4-6A-C). Thus, over time, the GFP-expressing CSC population gives rise to cells that progressively lose stem cell properties and concomitantly shut down the Nes-ΔTK-GFP transgene (Figure 4-6D).

Ganciclovir treatment impairs tumor growth.

To examine the effect of Nes-ΔTK-positive cell removal in early endogenous tumor development, we performed GCV treatment on Mut7;Nes-ΔTK mice beginning at eight weeks of age – the earliest time of detectable pre-tumorigenic anomalies in Mut7 mice (Kwon et al., 2008a). To increase the probability of capturing most CSCs in a

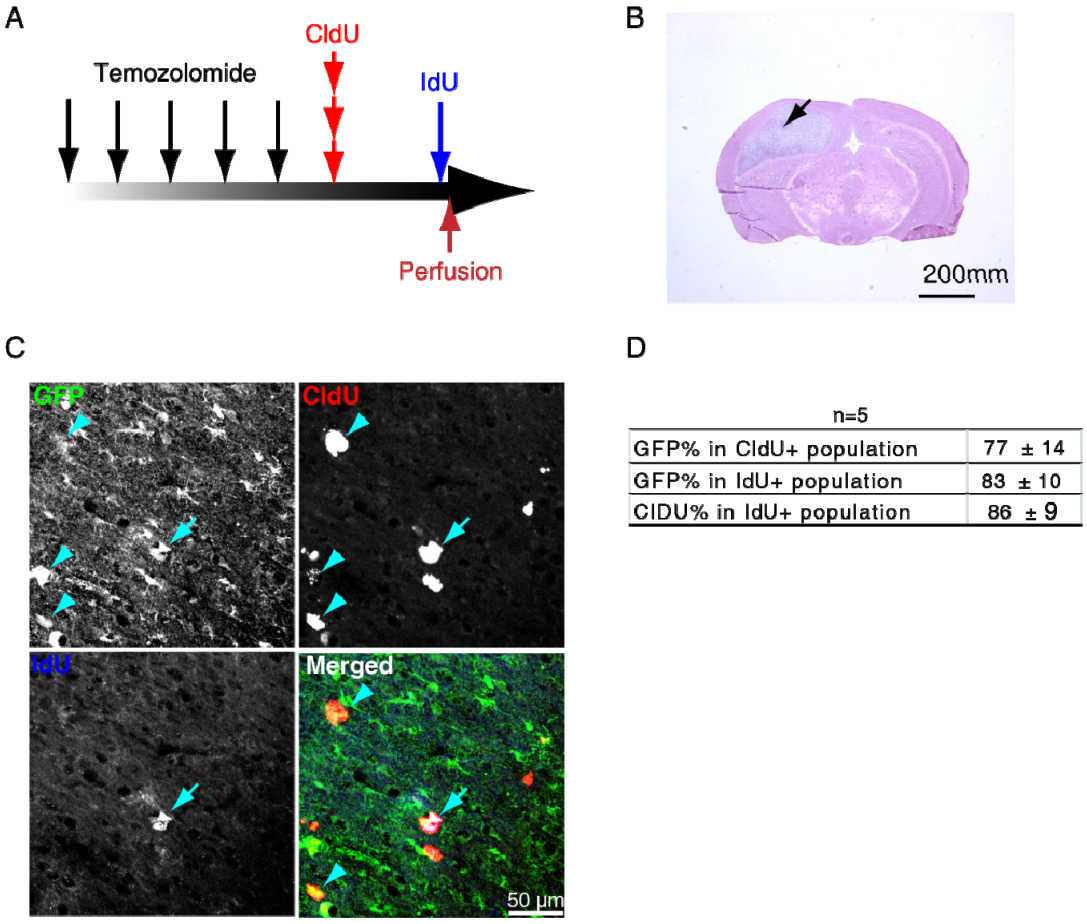

Figure 4-5. Nes-ΔTK-positive cells are resistant to TMZ and produce new tumor cells. A) Schema of TMZ treatment and short-term labeling with BrdU analogs. Mut7;Nes-ΔTK mice were treated with TMZ for 5 days and then injected with the BrdU analog CldU and IdU one and three days after the last TMZ treatment, respectively. B) Representative H&E staining of brain section from Mut7;Nes-ΔTK mice treated with TMZ. Arrow indicates a malignant glioma located on the left side of the cortex. C) Representative tumor section illustrating that repopulating tumor cells after TMZ treatment express the Nes-ΔTK transgene (GFP+); CldU (arrowhead) or IdU (arrow) incorporating cells also express GFP driven by the Nes-ΔTK transgene. D) Quantification of I showing the percentage of GFP-positive cells in CldU- or IdU-positive population. Note that the majority of CldU-positive cells and IdU-positive cells are positive for GFP expression, and also that the majority of IdU-positive cells are CldU-positive, indicating the CldU-positive cells gave rise to the IdU-positive cells.

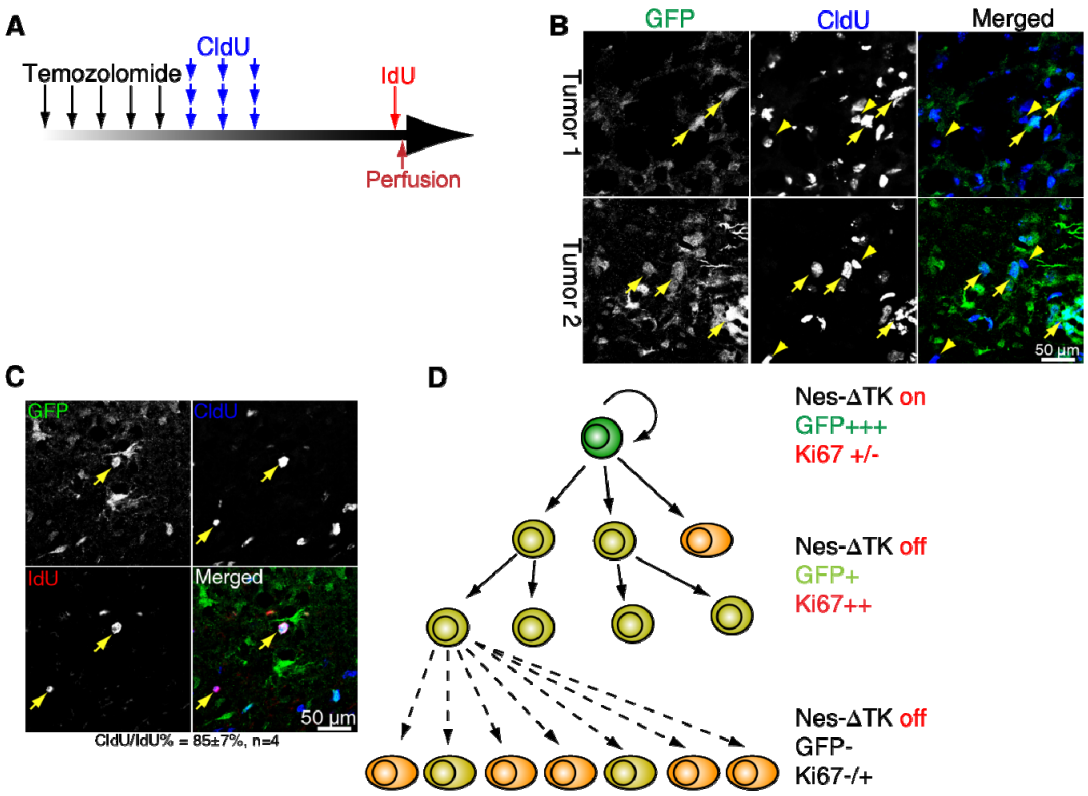

Figure 4-6. *Nes-ΔTK-IRES-GFP*-expressing tumor cells can give rise to both GFP-positive and GFP–negative cells. A) Schema of temozolomide (TMZ) treatment and long-term labeling of BrdU analogs. Mut7;Nes-ΔTK mice were treated with TMZ for 5 days and injected with CldU for three days starting one day after the final TMZ treatment. IdU was injected seven days after the first CldU injection. B) GFP/CldU/IdU immunostaining of Mut7;Nes-ΔTK mice treated with TMZ and labeled with BrdU analogs. GFP-negative and CldU-positive cells are indicated by yellow arrowheads. CldU-positive cells that retain GFP expression are indicated by yellow arrows. C) IdU-incorporating cells (yellow arrows) are mostly derived from CldU-positive cells indicating that the emergent population of proliferating cells arose from Nes-ΔTK-GFP expressing cells. D) Schema of glioma stem cell hierarchy and theoretical status of Nes-ΔTK transgene expression, GFP brightness and proliferative potential. Note that these are not absolute transitions. We hypothesize that this is a gradual process such that some transient amplifying cells may still have the transgene on.

dividing state, GCV treatment lasted for ten weeks, requiring three osmotic minipump placement surgeries that caused technical complications resulting in significant variance of drug delivery as manifested by residual RMS in some of these mice (Figure 4-7A). Accordingly, tumor incidence varied from mouse to mouse with some perishing early with large tumors. However, as a group the GCV-treated cohort showed a clear survival advantage (Figure 4-7B). After ten weeks of treatment, the only surviving mice were those treated with GCV (Figure 4-7C), and analysis of their brains revealed only low-grade lesions (Figure 4-7D). These data indicate that when GCV treatment was effective, survival was substantially prolonged and normal tumor progression was severely impaired. Thus elimination of Nes-ΔTK-positive cells at early/pretumorigenic stages prevents development of high-grade gliomas that are rapidly lethal.

Most ten-week-old Mut7 mice do not show neurological symptoms yet histological examination revealed that all mice harbored malignant astrocytoma of differing grades (63% grade III, 37% grade II) (Figure 4-8). We subjected ten-week-old Mut7;Nes-ΔTK or Mut7 mice to GCV or saline for two months. GCV treatment of Mut7;Nes-ΔTK mice significantly improved survival by approximately thirty days compared to saline control, while neither treatment was effective in improving survival of Mut7 mice (Figure 4-9A). Consistent with this, GFP and nestin double-immunostaining showed that GFP-positive cells were successfully eliminated in gliomas of Mut7;Nes-ΔTK mice following GCV treatment (Figure 4-9B).

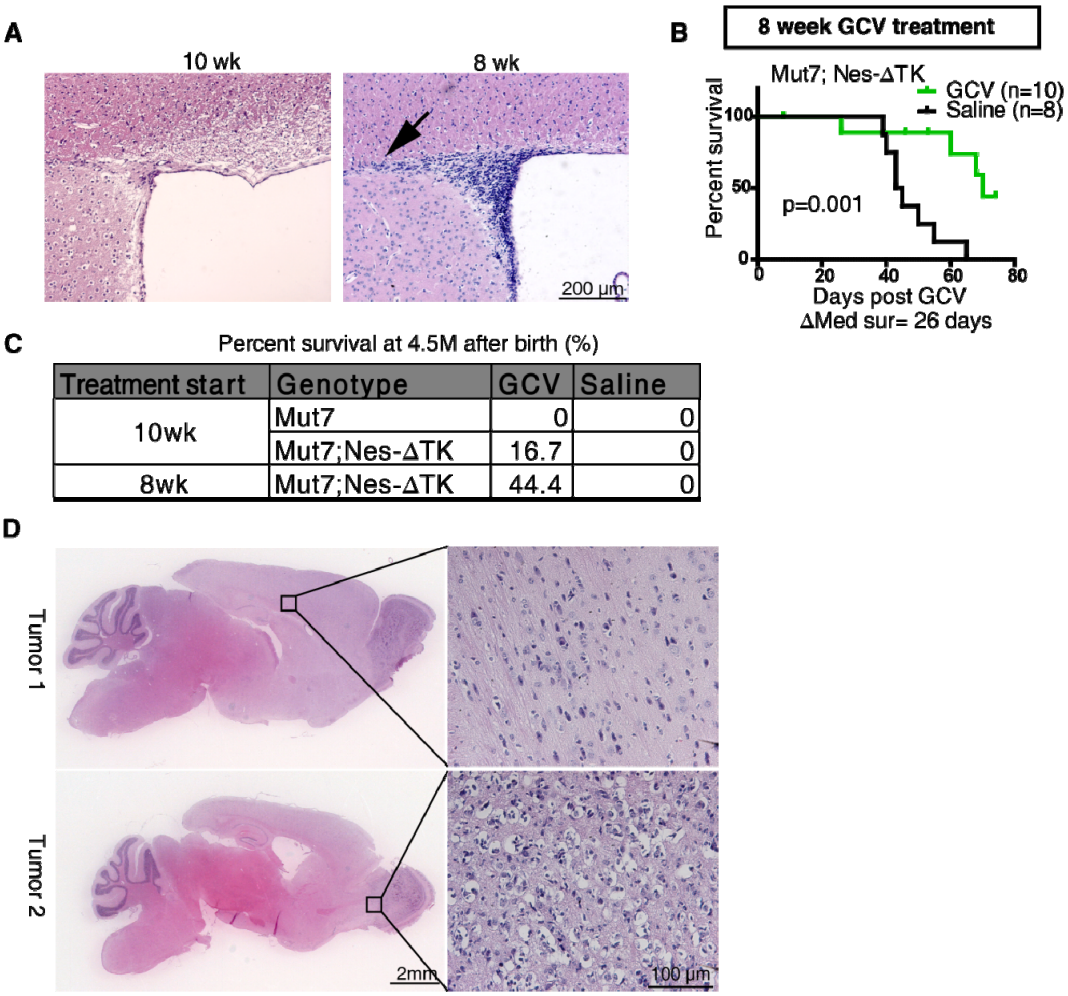

Treatment start	Genotype	GCV	Saline
10wk	Mut7	0	0
	Mut7;Nes-ΔTK	16.7	0
8wk	Mut7;Nes-ΔTK	44.4	0

Figure 4-7 GCV treatment from 8 week of age prolongs survival of Mut7;Nes-ΔTK mice. A) Representative H&E staining of Mut7;Nes-ΔTK SVZ treated with GCV from 10 or 8 weeks of age. Arrow indicates the rostral migratory stream, which was still present in some mice treated with GCV from 8 weeks of age due to inconsistent drug delivery caused by technical problems with the GCV minipump surgeries. B) Kaplan–Meier curve of Mut7;Nes-ΔTK mice treated with Saline or GCV from 8 weeks showed a clear survival advantage for the GCV-treated mice (Log-rank test, n=10 for GCV-treated; n=8 for saline-treated). C) Percentage of mice surviving at 4.5 months after birth following different treatment regimens. GCV-treatment of Mut7;Nes-ΔTK mice beginning at 8 weeks of age increased the 4.5 month survival rate to 44.4% compared to 0% with saline treatment. D) H&E staining of brain sections from two different Mut7;Nes-ΔTK mice treated with GCV from 8 weeks of age showing low grade lesions.

A

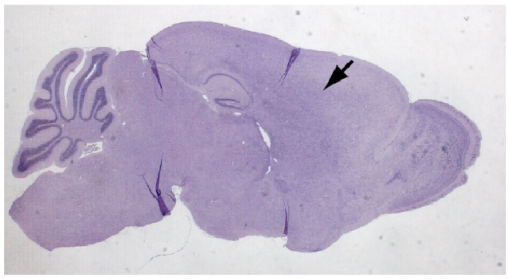

C

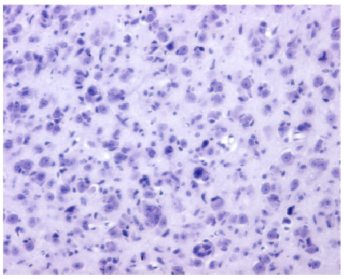

B

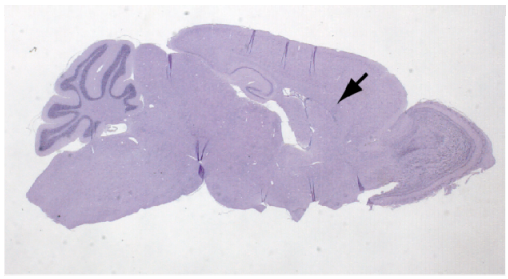

D

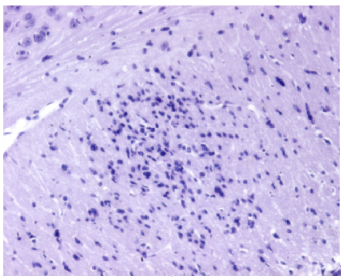

E

Case	Tumor type	Grade	Tumor location	Symptomatic
1	astrocytoma	GIII	corpus callosum	N
2	astrocytoma	GIII	corpus callosum;RMS	N
3	astrocytoma	GIII	cortex, corpus callosum,striatum	N
4	astrocytoma	GII	corpus callosum	N
5	astrocytoma	GIII	cortex	N
6	astrocytoma	GIII	corpus callosum, striatum	N
7	astrocytoma	GIII	cortex, corpus callosum, striatum,extremely infiltrative	Y
8	astrocytoma	GII	corpus callosum	N
9	astrocytoma	GII	striatum, anaplastic	N
10	N/A	N/A	N/A	Dead

Figure 4-8. Analysis of brain sections from 10-week-old untreated Mut7 mice shows 100% incidence of astrocytomas. A-D) low magnification (A,B) and higher magnification (C,D) H&E staining of 10-week-old Mut7 mouse brains with grade III (A,C) or grade II (B,D) glioma. Tumors are indicated by arrows. E) Summary of glioma types, grades and locations in brains of 10-week-old untreated Mut7 mice. 9 out of 9 tumors were astrocytomas.

The residual tumors in the ten-week-old GCV-treated Mut7;Nes-ΔTK mice appeared well-circumscribed with clear boundaries, having lost the classic feature of invasiveness (Figure 4-9C&D). Despite the fact that the Nes-ΔTK transgene is only expressed in a subset of cells in the untreated tumor (Figure 4-2A-C), tumors in GCV-treated Mut7;Nes-ΔTK mice showed a marked reduction of Ki67-positive cells and stem cell markers such as sox2 (Figure 4-9 D-F). One extreme case had almost no Ki67-positive cells (Figure 4-9E, panel 4). These data further support the hypothesis that tumor cells eventually exhaust their proliferative potential in the absence of self-renewing CSCs caused by chronic GCV administration.

TMZ/GCV treatment blocks tumor development.

Despite effective depletion of GFP-expressing CSCs, the residual tumor mass in the GCV-treated mice was significant and life threatening (Figure 4-9C). We therefore attempted a therapeutic strategy that would eliminate both the rapidly proliferating tumor cells and the CSCs (Figure 4-10A). We used a sequential regimen in which tumor-bearing mice were first treated with TMZ for five days followed by treatment with GCV via minipumps two days later (Figure 4-10B). Initially it appeared that this regimen did not prolong the survival of Mut7;Nes-ΔTK mice beyond that of GCV treatment alone (Figure 4-10C). A course of TMZ alone resulted in only slight improvement in survival compared to saline-treated control mice. However, examination of the brains of the sequentially treated mice revealed evidence of only vestigial tumors in the dorsal brain that showed no evidence of transgene-GFP expression, indicating effective depletion of the CSCs by this regimen (Figure 4-10D). We assessed the cellular density of untreated

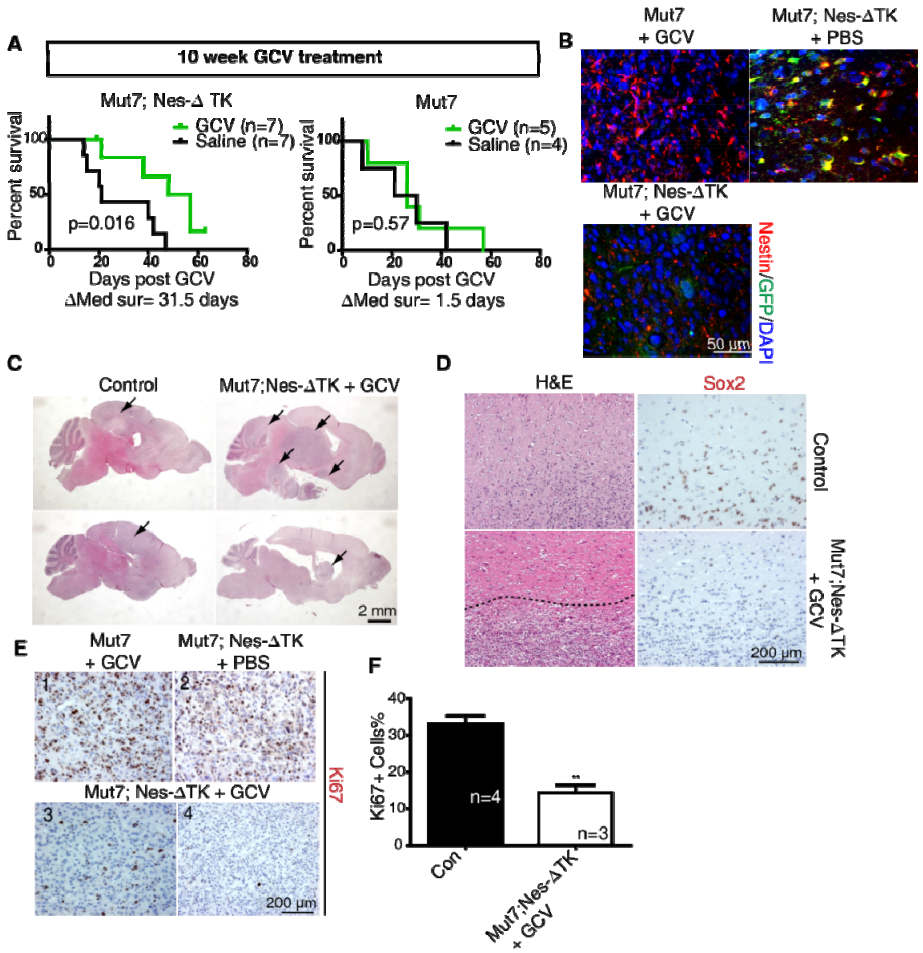

Figure 4-9. GCV treatment prolongs survival of Mut7;Nes-ΔTK mice and reduced overall proliferative index. A) Kaplan–Meier survival curves of Mut7;Nes-ΔTK (left) or Mut7 (right) mice treated with GCV or Saline from 10 weeks. GCV-treatment increased survival of Mut7;Nes-ΔTK mice compared to saline-treated but had no such effect on the Mut7 mice (Log-rank test). B) GFP/Nestin co-immunostaining of gliomas from control (Mut7 mice treated with GCV or Mut7;Nes-ΔTK mice treated with PBS) and GCV-treated Mut7;Nes-ΔTK mice. Elimination of GFP- and nestin double-positive cells in the Mut7;Nes-ΔTK mice treated with GCV from 10 weeks. C) Representative H&E staining of control and GCV-treated Mut7;Nes-ΔTK brains. The tumors in the GCV-treated Mut7;Nes-ΔTK mice are less infiltrative than in control. Tumors are indicated by black arrows. D) Representative H&E and Sox2 staining of tumor edges in control and GCV-treated Mut7;Nes-ΔTK tumor showing the GCV-treated tumor has a defined boundary (dotted line) and lacks infiltrative Sox2+ cells. E, F) GCV treatment decreases proliferation index in Mut7;Nes-ΔTK tumors. E) Representative Ki67 staining of control (panels 1 and 2) or GCV-treated Mut7;Nes-ΔTK tumors (panels 3 and 4) showing the dramatic decrease in proliferation in the GCV-treated Mut7;Nes-ΔTK tumors. G) Quantification of the percentage of Ki67-positive cells in tumor regions with highest number of proliferating cells in cortex. **p<0.01. student-t test.

control tumors at the beginning of the treatment (10 weeks/pre-treatment) or at the end of observation (untreated) and compared to the mice treated with GCV or TMZ/GCV. The cellular density of the residual TMZ/GCV-treated tumors was significantly lower than that of tumors at the beginning of treatment (10 weeks) and dramatically lower than untreated control tumors, which manifested in a spectrum of survival time from 12 to 16 weeks (Figure 4-10E). Thus, the combined treatment had dramatic inhibitory effects on dorsal tumor growth in these mice.

Novel ventral tumors in TMZ/GCV-treated mutant mice.

Although survival was significantly prolonged with TMZ/GCV treatment compared to saline, it was not significantly prolonged beyond the GCV-only treated mice. Examination revealed that despite the dramatic inhibition of original tumor growth with the combination treatment, these mice were not cured of all tumors. The mice with vestigial tumors in the dorsal brain often developed tumors in the ventral region of the brain. Six of seven TMZ/GCV-treated mice showed tumors in the brain stem region, whereas, similar to tumor location in adult human GBM, the majority of gliomas in untreated Mut7 mice and their remnants in the successfully treated mice are located in the dorsal/mid-brain (Figure 4-11A). We examined the TMZ/GCV-resistant hindbrain tumors and found that they exhibited high endogenous nestin protein but were GFP negative (Figure 4-11B). To determine whether the Nes-ΔTK transgene is inactive in these tumor cells, we examined some of the ventral tumors in untreated Mut7;Nes-ΔTK mice and found that these tumors also expressed endogenous nestin but not the Nes-ΔTK transgene (Figure 4-11B).

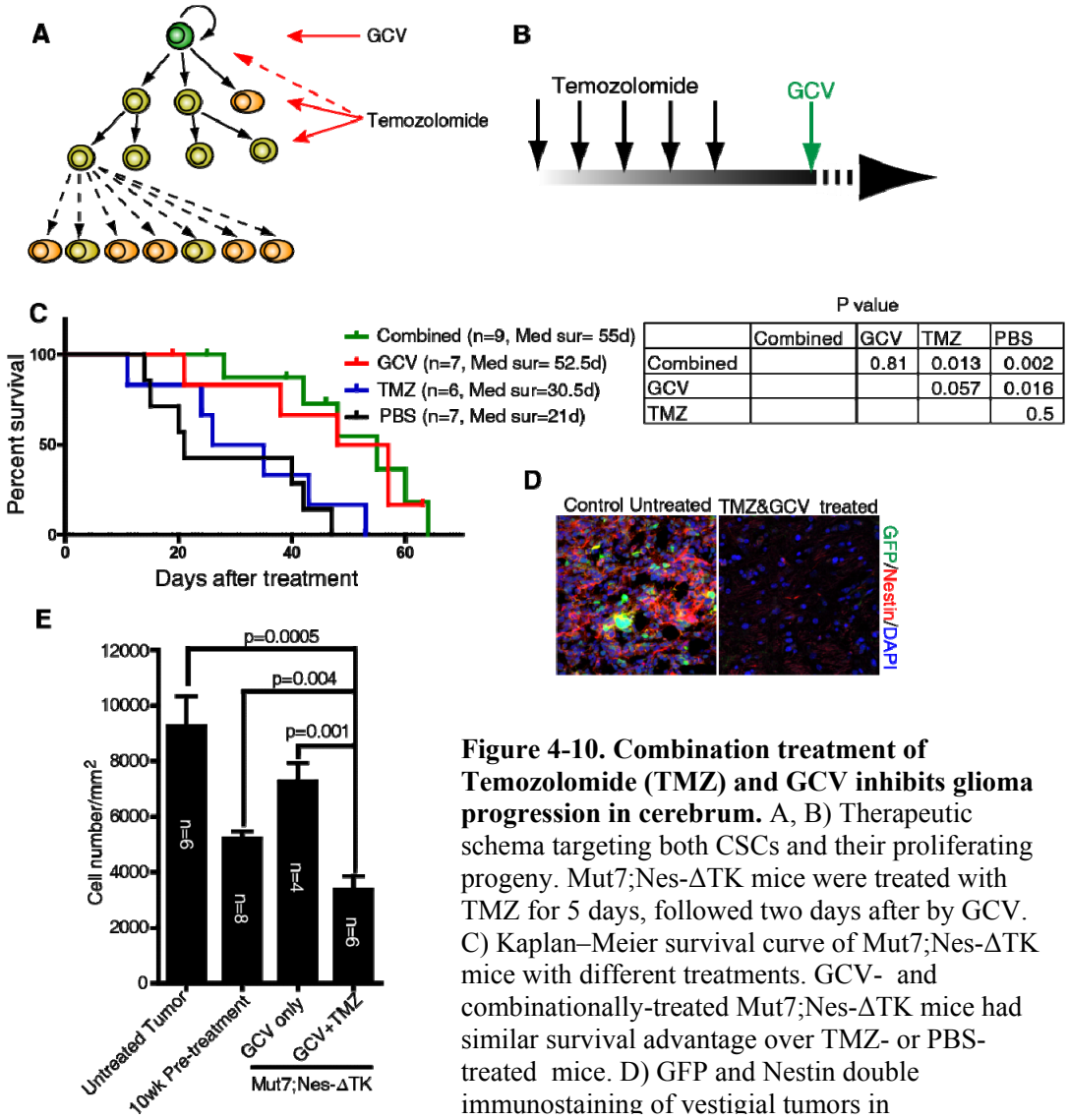

Figure 4-10. Combination treatment of Temozolomide (TMZ) and GCV inhibits glioma progression in cerebrum. A, B) Therapeutic schema targeting both CSCs and their proliferating progeny. Mut7;Nes-ΔTK mice were treated with TMZ for 5 days, followed two days after by GCV. C) Kaplan–Meier survival curve of Mut7;Nes-ΔTK mice with different treatments. GCV- and combinationally-treated Mut7;Nes-ΔTK mice had similar survival advantage over TMZ- or PBS-treated mice. D) GFP and Nestin double immunostaining of vestigial tumors in TMZ/GCV-treated Mut7;Nes-ΔTK mice (right panel) versus tumor in control (left panel) demonstrates depletion of CSCs as evidenced by lack of GFP expression. E) Maximal cell density in cortical tumors with different treatment regimens. Untreated Mut7 were used as control. Tumor density of 10-week-old non-symptomatic Mut7 mice (pre-treatment) was used as a reference starting point. Cell density was significantly lower in the combinationally-treated (TMZ+GCV) Mut7;Nes-ΔTK mice compared to untreated tumor (p=0.0005), compared to tumors in "pre-treatment" mice (p=0.004), and compared to tumors from mice treated with GCV only (p=0.001).

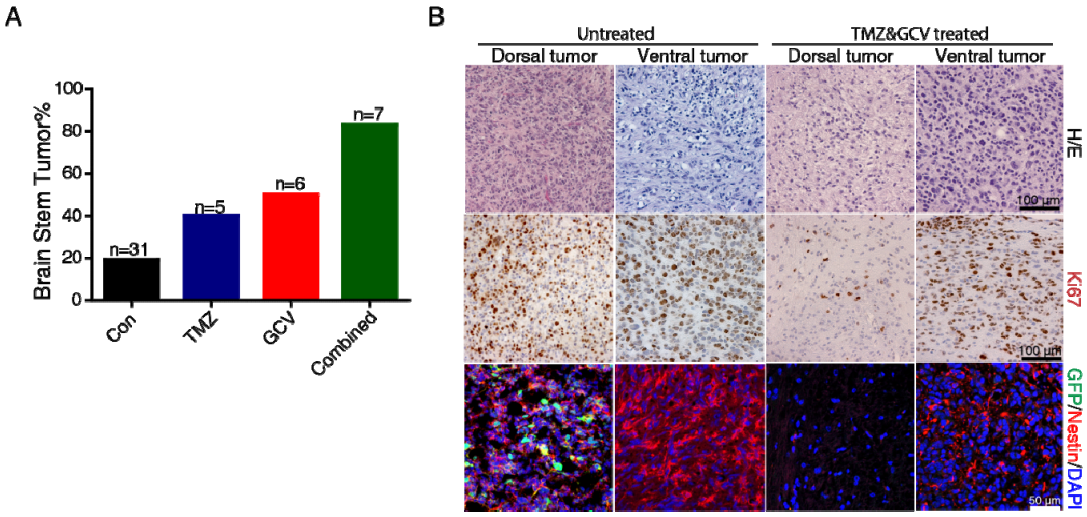

Figure 4-11. Increased incidence of ventrally-located brain tumors where the Nes-ΔTK transgene was silenced. A) Percentage of brains with brain stem tumors in various treated groups. Control group includes treated or untreated Mut7 mice and saline-treated Mut7;Nes-ΔTK mice. A much higher percentage of brain stem tumors was observed in the combinationally-treated Mut7;Nes-ΔTK mice. B) Representative H&E staining (top row), Ki67 immunostaining (middle row), and GFP/Nestin/DAPI staining (bottom row) of dorsal and ventral tumors in control and combinationally-treated Mut7;Nes-ΔTK mice. Ki67 staining indicates high proliferation in ventral tumors compared to the vestigial dorsal tumors. Note that the ventral tumors unmasked in the TMZ/GCV-treated mice are positive for endogenous nestin expression but negative for GFP expression.

To gain further insight into the hindbrain tumors that emerged after TMZ/GCV treatment, we examined the expression of a series of glioma markers (GFAP, Olig2, Ki67, S100B, Sox2). In contrast to typical Mut7 gliomas, all persistent tumors present in the combined TMZ/GCV treatment group showed very low levels of endogenous GFAP and relatively high levels of S100B (Figure 4-12B, Figure 4-13A&B, data not shown). The GFAP expression levels permitted transcriptional profile clustering of two distinct tumor types in the Mut7 strain, one of which is typically located in the ventral brain and rarely observed without the drug-mediated blockade of the more typical dorsal gliomas (Figure 4-13A-D). Furthermore, consistent with the microarray data that GFAP-negative tumors showed higher levels of oligodendrocyte progenitor markers NKX2-2 and GPR17 (Figure 4-13D, Table 4-1), seven out of eleven tumors in the ventral and brain stem region of GCV-treated mice (GCV alone or TMZ&GCV) showed histopathological features of oligodendroglioma (Figure 4-12A-C) including high levels of PDGFRA (Figure 4-12D). This is in contrast to the pure astrocytic tumors typically observed in this mouse model in the absence of TMZ/GCV treatment(Alcantara Llaguno et al., 2009; Kwon et al., 2008a; Zhu et al., 2005a).

To better determine the incidence of GFAP-negative tumors in the Mut7 strain, we examined archived brain sections from untreated Mut7 and Mut7;Nes-ΔTK mice for ventral tumors. We found that six tumor-bearing brain sections out of fifteen samples examined, showed evidence of two distinct foci of brain tumors. In all six cases the cortical foci expressed high levels of GFAP whereas four of six ventral tumor foci were GFAP negative (Figure 4-13C). Thus, the GCV-resistant, Nes-ΔTK-GFP transgene-silent,

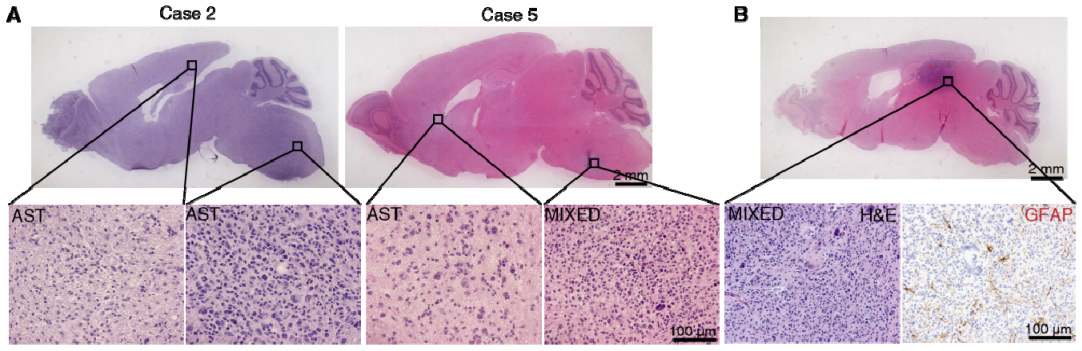

C

cases	Brain stem tumor type	Treatment type
1	*Anaplastic mixed oligodendroglioma*	Temozolomide & GCV from 10 week
2	anaplastic astrocytoma	Temozolomide & GCV from 10 week
3	GBM	Temozolomide & GCV from 10 week
4	*Anaplastic mixed oligodendroglioma*	Temozolomide & GCV from 10 week
5	*Anaplastic mixed oligodendroglioma*	Temozolomide & GCV from 10 week
6	*Anaplastic mixed oligodendroglioma*	Temozolomide & GCV from 10 week
7	*GBM with oligodendroglioma component*	GCV only from 8 week
8	anaplastic astrocytoma	GCV only from 8 week
9	*Anaplastic mixed oligodendroglioma*	GCV only from 10 week
10	anaplastic astrocytoma	GCV only from 10 week
11	*GBM with oligodendroglioma component*	GCV only from 10 week

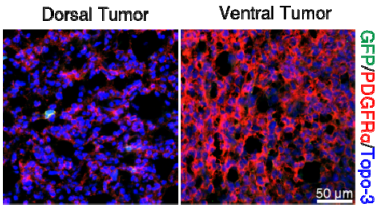

Figure 4-12. Ventral tumors with distinct histology emerge from TMZ/GCV-treated Mut7;Nes-ΔTK mice. A) Representative H&E staining of Mut7;Nes-ΔTK mice treated with temozolomide and GCV from 10 weeks of age. Higher magnification of pure astrocytic (AST, Case 2) and mixed oligodendrocytic (MIXED, Case 5) gliomas in the brain stem region. B) H&E and GFAP staining of the only midbrain tumor to arise in Mut7;Nes-ΔTK mice following combinational TMZ/GCV treatment. This tumor also showed oligodendroglioma features at higher magnification. C) Summary of brain stem tumor histology in treated Mut7;Nes-ΔTK mice. D) Representative GFP and PDGFR-α staining of cortical (dorsal) and brain stem (ventral) tumors. Note the ventral tumor has much higher levels of PDGFR α expression, a marker of oligodendroglioma.

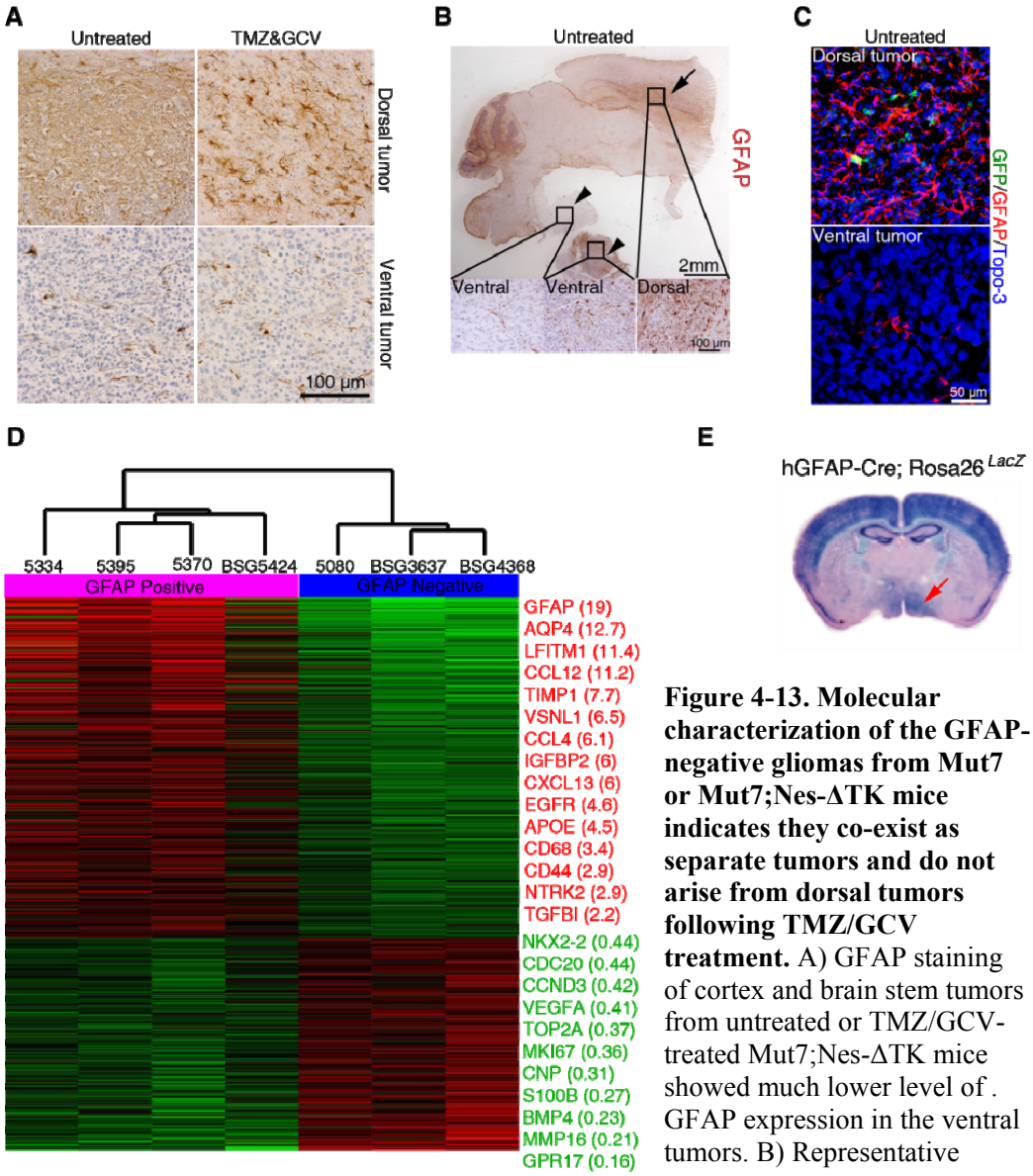

Figure 4-13. Molecular characterization of the GFAP-negative gliomas from Mut7 or Mut7;Nes-ΔTK mice indicates they co-exist as separate tumors and do not arise from dorsal tumors following TMZ/GCV treatment. A) GFAP staining of cortex and brain stem tumors from untreated or TMZ/GCV-treated Mut7;Nes-ΔTK mice showed much lower level of . GFAP expression in the ventral tumors. B) Representative GFAP immunostaining of Mut7 tumor with both cortex (black arrows) and ventral (black arrowheads) tumors. Note the much higher level of GFAP staining in the dorsal tumor. C) GFP and GFAP double immunofluorescence staining of cortex and brain stem tumors from untreated Mut7;Nes-ΔTK mice. Very little GFAP expression and no GFP expression is observed in the ventral tumor. D) Heatmap of gene expression profiles in untreated Mut7 tumor tissues. "BSG" refers to "brain stem gliomas" observed at the time of dissection. Representative differentiated expression genes and fold changes are listed on the right side of the heatmap. E) X-gal staining of adult hGFAP-Cre;Rosa26^{LacZ} brain; Cre activity in the brain stem region is indicated by the red arrow.

GFAP-negative tumors (Figure 4-1B; Figure 4-13C) arise spontaneously and independently in the Mut7 strain but have been previously masked by the presence of the more precocious cortical malignant gliomas that have been the focus of all past and present studies. Once the mortality from the predominantly cortical GFAP-positive gliomas is effectively avoided, the GFAP-negative tumors, located mostly in the hindbrain, have the opportunity to develop and cause morbidity. The similar survival rate observed in the TMZ/GCV-treated and the GCV-alone treated Mut7;Nes-ΔTK mice is likely due to the emergence of these ventral tumors.

Discussion

Here, we address key aspects of the CSC hypothesis in a spontaneous, tumor suppressor-based somatic mouse model of GBM. Through selective genetic tagging of cancer-propagating cells, we are able to observe tumor initiation and progression *in situ* without reliance on surrogate assays to identify or enrich for the cells under study.

In vivo glioma cancer stem cells.

We present evidence that a unique subset of endogenous glioma cells confers tumorigenic potential in the classical cancer stem cell transplantation assay and plays a role in tumor re-growth after chemotherapy. GBMs contain many endogenous nestin-positive cells as evidenced by antibody staining, however the source of these cells is manifold and not exclusive to neural or tumor lineages but also to ependymal cells, endothelial lineage and non-tumorigenic reactive astrocytes that are abundant in this tissue (Abdel-Rahman et al., 2004; Klein et al., 2003). In contrast, our Nes-ΔTK-GFP transgene labels a specific subset of tumor cells that possesses many features proposed for CSCs including relative quiescence and the ability to produce more vigorously-propagating cells that eventually lose their proliferative potential. Elimination of this cell population following GCV treatment resulted in a dramatic reduction in tumor transplantation. The histological features of the endogenous tumors also changed dramatically after GCV treatment in large part due to loss of spontaneous tumor cell infiltration and proliferation. This is consistent with the observation that Nes-ΔTK-GFP-expressing cells preferentially populate the borders of tumor tissue where they likely represent the infiltrative front of the tumor.

In our model system, TMZ, a frontline therapy in the clinical treatment of GBM, efficiently eradicated the transient amplifying population of glioma cells but had no visible effect on the CSC population. Following synchronization of cell proliferation in tumor-bearing mice using TMZ, we found that despite the relatively small proportion of GFP-positive cells present in each tumor, the overriding majority of new CSC-derived cells that incorporated the long and short pulsed BrdU analogs also retained GFP. Thus, over time, the GFP-expressing CSC population gives rise to rapidly proliferating cells that undergo differentiation, losing stem cell properties and turning off the Nes-ΔTK-GFP transgene. The specific effect of TMZ on only the transient amplifying component of tumor cells may explain why in glioma patients treated with this chemotherapeutic agent, gliomas almost always recur.

The observed decrease of overall mitotic index after chronic GCV treatment of Mut7;Nes-ΔTK mice strongly supports the model that, like normal tissue stem cells, CSCs are the only cell type capable of long-term self-renewal and are therefore responsible for maintaining the tumor. However, ablating the CSCs alone did not completely stop tumor growth since the rapidly proliferating CSC-derived (Nes-ΔTK silent) cells were not targeted and could transiently add to the already existent tumor bulk. Therefore additional blockade of the transient proliferating derivatives of CSCs is also required to meaningfully reduce tumor burden.

A tale of two tumors.

An unexpected outcome of this study was the discovery of novel, predominantly ventral tumors that are more latent and became apparent in the context of TMZ/GCV-treated mice when the cortical gliomas under study were cured by CSC ablation. We base our conclusions on the following features of the resistant tumors: 1) They emerge distant from sites of clearly regressing primary dorsal tumors. 2) They do not express GFAP, a common marker of GBM and of all NF1/p53/Pten tumor suppressor-based gliomas studied by us to date (Alcantara Llaguno et al., 2009; Kwon et al., 2008a; Zhu et al., 2005a), but do express high levels of oligodendroglial markers. 3) Their pathological features deviate from that of the classical GBM features of the original tumors (Alcantara Llaguno et al., 2009; Kwon et al., 2008a; Zhu et al., 2005a). In addition, immunohistochemical analysis of archived brain sections from Mut7 and Mut7;Nes-ΔTK mice that did not undergo additional manipulations verified the rare coexistence of GFAP-negative tumors (generally localized in the ventral brains) with the more classic dorsally-localized GBMs (Figure 4-13). Finally, transcriptome analysis of tumor samples reveals a categorically distinct profile for Mut7 GFAP-positive and GFAP-negative tumors consistent with different tumor subtypes. We previously failed to account for the ventral tumors because the mice tend to succumb to the dorsal GBMs before the ventral ones are appreciable.

In light of the above observations, the question then arises: what is the source of these more latent ventral tumors? The hGFAP-cre transgene used to derive Mut7 mice is expressed in embryonic brain including uncharacterized ventral brain regions (Alcantara Llaguno et al., 2009; Kwon et al., 2008a; Zhu et al., 2005a) (Figure 4-13E). Therefore,

the more latent ventral tumors may either also arise in the SVZ and somehow preferentially migrate ventrally, or, alternatively, arise from a more ventral stem/progenitor cell pool(s). This latter possibility would account for the general location and distinct molecular profile, including the lack of expression of the Nes-ΔTK-GFP transgene and endogenous GFAP. A form of ventral brain tumor, brain stem glioma (BSG), occurs in pediatric patients, while adult gliomas are generally found in the cerebrum. BSGs have been generated by over-expression of PDGF-B in the posterior fossa region of neonatal rodents (Becher et al., 2010; Masui et al., 2010), and thought to arise from the fourth ventricle. Additionally, a distinct subclass of GFAP-negative gliomas has been described (Kunz et al., 1986; Marsden et al., 1983; Maruno et al., 1987). Further studies will be required to determine the cell of origin of the BSG-like, GFAP-negative tumors that are unmasked in our TMZ/GCV-treated Mut7;Nes-ΔTK mice.

CHAPTER FIVE

MATERIAL AND METHODS

Mice

All mouse protocols were approved by the Institutional Animal Care and Research Advisory Committee at University of Texas Southwestern Medical Center. All mice were maintained on a mixed 129SvJ/C57BL/6/B6CAB background.

For generating Nestin-CreER^{T2} transgenic mice, a 2.0 kb of CreERT2 and SV40 polyA sequence of pCre-ER^{T2} vector (Feil et al., 1997) were amplified by using a PCR technique that also generated 5' Not 1 and 3' Spe 1 sites of the fragment. After enzymatic digestion, purified fragment was ligated with a 8.9 kb fragment from pNerv (Panchision et al., 2001; Yu et al., 2005) digested with Not 1 and Xba 1. Resulting pNes-CreER^{T2} construct contains a 5.6 kb rat nestin 5' genetic element from pNerv, a 2.0 kb CreER^{T2} and SV40 polyA sequence from pCre-ER^{T2} and a 668 bp of reversed 2nd intron of rat nestin from pNerv (Figure 2-2). After Sal 1 digestion, an 8.3 kb band was purified and microinjected into the pronuclei of fertilized eggs from B6D2F1 mice. Among 28 pups born after two rounds of the transgenic injection six contained the transgene, and four of them transmitted to germline. Rosa26^{lacZ} mice were obtained from Jackson Laboratories (Bar Harbor, ME). All the mice were maintained in mixed genetic background of C57/BL6, Sv129 and B6/CBA. Nestin73-CreER^{T2}; Rosa26^{lacZ} mice were generated by crossing male Nestin-CreER^{T2} mice with female Rosa26^{lacZ} mice. Genotyping of the mice was performed as described previously (Kwon et al., 2006).

To generate Nes-CreER^{T2}; NF1$^{flox/+}$;P53$^{flox/flox}$;Pten$^{flox/+}$ mice, male Nes-CreER^{T2};NF1$^{flox/flox}$;P53$^{flox/flox}$ mice were bred with femal P53$^{flox/flox}$;Pten$^{flox/flox}$. To generate hGFAP-Cre; NF1$^{flox/+}$;P53$^{flox/flox}$;Pten$^{flox/+}$ mice, male hGFAP-Cre; P53$^{flox/flox}$ mice were bred with female NF1$^{flox/flox}$;P53$^{flox/flox}$,Pten$^{flox/flox}$;Nes-Δ TK mice. Tumor prone mice were observed daily after 2 month of age. Mice with sign of neurological abnormality were used for paraformaldehyde (PFA) perfusion or cell culture or tissue collection.

Tamoxifen induction

Tamoxifen (Sigma-aldrich, St. Louis, MO) was dissolved in a sunflower oil (Sigma-aldrich, St. Louis, MO)/ ethanol mixture (9:1) at 6.7 mg/ml. For initial screening of the embryonic induction of the transgenic lines, 150 µl tamoxifen (1mg) or vehicle (sunflower oil/enthanol mixture only) was injected intraperitoneally into pregnant mother mice at embryonic E12.5 (E12.5 hereafter). Embryos were dissected out two days later and subjected to X-gal staining. For in utero induction, 150 µl tamxifen (1mg) or vehicle was injected intraperitoneally into pregnant mothers at E13.5 or E17.5, and pups were analyzed 1 month after birth. For neonatal induction, 12.5 µl tamoxifen (83mg/kg body weight) or vehicle per gram of mouse body weight was injected to lactating mother from P0 or P7, once a day for 5 days. Tamoxifen can be delivered to pups through milk and the pups were analyzed four weeks after the first induction. For induction in adult mice, 12.5 µl tamoxifen (83mg/kg) or vehicle per body weight was injected intraperitoneally into

four or eight week old mice twice a day for 5 consecutive days and analyzed two or four weeks after first induction.

Note: After the paper had been published, we noticed that administration of tamoxifen through gavage caused less harm to the mice especially for pregnant females. Basically, 20 mg tamoxifen was directly dissolved in 1 ml of sunflower oil by rigorous sonication for 30 min or incubation at 37 ℃ overnight. This solution can be safely stored at 4 ℃ for 1 week without exposure to light. 10 mg (0.5 ml) tamoxifen was fed to adult mice through plastic feeding tubes (Instech Solomon) once a day for two continuous days. For pregnant females, one dose of 2.5 – 5 mg tamoxifen was generally effective; fewer doses were given to females at the earliest stages of pregnancy.

Temozolomide, GCV and BrdU injection

Stock ClDU (Sigma) and BrdU (Sigma) were dissolved in PBS at the concentration of 8.5 mg/ml and 10 mg/ml, respectively. 11.5 mg/ml IDU (MP Biomedicals) solution was made fresh each time (Vega and Peterson, 2005). To label dividing cells, 5 ml/kg stock solution was injected intraperitoneally according to the experimental design.

Ganciclovir (GCV) (Cytovene-IV, Roche Pharmaceuticals) treatment was performed as described (Yu et al., 2008). For initial characterization of Nes-ΔTK mice, 1-month-old Nes-ΔTK or control mice were administered GCV (300 mg/kg/d) or PBS via osmotic minipump (Model 2002, 0.5 μl/h, Alzet) for 2 weeks. For treatment starting from 8 week or 10 weeks, 150 mg/kg/d GCV or PBS was delivered through osmotic minipump (Model

2004, 0.25 μl/h, Alzet); pumps were surgically removed and replaced every 4 weeks based on the experimental requirement.

Temozolomide (Sigma) was dissolved in DMSO and injected intraperitoneally at a dose of 82.5 mg/kg/d for five days. For the combinational therapy group, mice were first treated with temozolomide for five days and then osmotic minipumps with GCV were implanted 2 days after the last temozolomide injection.

Temozolomide, BrdU analogs, and pulse chase experiments

To determine TMZ efficiency, 10- to 11-week-old Mut7 mice were first injected intraperitoneally with 82.5 mg/kg/d TMZ for 5 days. 50 mg/kg BrdU was injected 2 hours after the final TMZ administration and mice were perfused 2 hours after BrdU injection. The brain was then paraffin-processed and cut into 5 μm-thick slices. H&E staining was performed every 70 μms to identify tumor location. Adjacent tumor sections were selected for GFAP and BrdU co-immunostaining.

For the short term CldU chase experiments, 10- to 11-week-old Mut7;Nes-ΔTK mice were first treated with TMZ for 5 days. A total of three doses of CldU were injected, with 2-hour intervals, the day after the final TMZ injection. A single dose of IdU was then injected 3 days after the final TMZ injection. For the long term CldU chase experiments, 10- to 11-week-old Mut7;Nes-ΔTK mice were first treated with TMZ for 5 days. CldU was injected 3 times a day, with 2-hour intervals, for 3 days after the final TMZ injection. A single dose of IdU was then injected 7 days after the final TMZ injection. Mice were

perfused 2 hours after the IdU injection and the brains cryoprotected in 30% sucrose, embedded in OCT, and cut into 14 μm-thick frozen sections. GFAP and Ki67 co-immunostaining was performed every 140 μms to locate the tumor area. Adjacent sections were selected for GFP/CldU/IdU triple immuno-fluorescence staining.

Transplantation

Cortex tumors from 10-14 week old Mut7;Nes-Δ TK or Mut7 mice were dissected out. The tumor tissues were dissociated using Accutase (Chemicon) for 10 min, filtered through 70 μm filter (Millipore). Filtered cells were counted and 100,000 cells were transplanted subcutaneously into nude mice with equal volume of matrigel. Osmotic minipumps with GCV or PBS were implanted at the same time on the opposite flank as described above.

Histology and X-gal staining

Mice were dissected and perfused as previously described (Kwon et al., 2006). For whole mount X-gal staining, the embryos or organs were carefully dissected out, washed with phosphate-buffered saline (PBS), and then fixed in 2% (w/v) paraformaldehyde (PFA; in PBS) for 1 hr at 4 °C. Postnatal brains were post fixed in 2% PFA overnight (O/N) at 4 °C, embedded in 2.5% chicken albumin, and then cut into 50-μm thick sections by vibratome (Leica, Nussloch, Germany). X-gal staining of organs and sections were performed as described (Kwon et al., 2006).

For brain tumor histology, mice were perfused with 2% PFA and the brains were post fixed in 4% PFA O/N at 4 °C. 5 μm paraffin sections were collected and H/E staining was performed on every 5th slide (60 μm interval). The slides were initially screened by Jian Chen for the presence and location of tumors and the tumors were then graded by Dr. Dennis K. Burns in the Department of Pathology. For staining using GFP, PDGFRA, and CD31 antibodies, 14 μm cryostat sections were used.

Antibodies and immunostaining

Primary antibodies were used against β-galactosidase (ICN, 1:2000 with biotin amplification), GFAP (DAKO, 1:2000, BDbiosciences, 1:200), doublecortin (Santa Cruz Biotechnology, 1: 200), NeuN (Chemicon, 1:400), Pten (cell signaling, 1:1000), pERK (cell signaling, 1:200), pAKT (Cell signaling, 1:50), Ki67 (Neomarker, 1:200; Novocastra, 1: 2000), TUJ1 (Covance, 1:500), S100β(Sigma, 1:200), Nestin (BDbiosciences, 1:100), AsclI (BDbiosciences, 1:50), APC (Calbiochem, 1:200), Olig2 (Millipore, 1:1000), Sox2 (Millipore, 1:5000), Nestin (BD Biosciences, 1:200), CD44 (BD Biosciences, 1: 75), GFP (Rockland, 1:200, Aves Lab, 1:500), BrdU/IDU (BD Biosciences, 1:100), BrdU/CldU (AbD Serotec,1:500), PDGFRα (Santa Cruz, 1:200). Horseradish peroxidase-based Vectastain ABC Kit (Vector Laboratories) or Cy2/Alexa-488, C3/Alexa555, Cy5-labeled secondary antibodies (Jackson Labs, Invitrogen) were used to visualize the primary antibody staining. Heat-induced antigen retrieval was used on most paraffin sections except for GFP and DCX staining. Images were taken using optical, fluorescence and confocal microscopy (Olympus and Carl Zeiss) and assembled in Adobe Illustrator (Adobe Systems Incorporated).

Tissue collection and microarray analysis

Brains of symptomatic mice were dissected out and sliced into 2 mm-thick sections using a brain matrix (ASI Instruments). Tumor regions were identified by eye under dissection microscope and microdissected out for RNA preparation. The remaining brain tissue after dissection was fixed in 4% PFA at 4℃ overnight and processed for paraffin embedding. Total RNA was extracted using RNeasy Plus Mini Kit (Qiagen) following manufacturer's instructions. RNA samples that passed the quality assessment were processed and hybridized to Mouse-6 V2 BeadChip (Illumina) at the UTSW Genomics and Microarray Core Facility.

Raw expression data was read, quantile normalized, and then exported using BeadStudio (Illumina). Hierarchical clustering and the differentially expressed gene list were generated by R and bioconductor (Gentleman et al., 2004; Smyth, 2005). DEG were calculated using R package "limma" (Smyth, 2004). Probe mapping from mouse to human orthologs was performed using R package "AnnotationTools" (Kuhn et al., 2008). CVE was caculated using R package "Clanc" (Dabney, 2006). Heatmap was generated by Cluster 3.0 (http://bonsai.hgc.jp/~mdehoon/software/cluster/software.htm) and Java TreeView (http://jtreeview.sourceforge.net/). Gene ontology analysis was performed by DAVID Bioinformatics Resources (Dennis et al., 2003; Huang da et al., 2009) and Gene set enrichment analysis (Subramanian et al., 2005).

PCR and QPCR

A primer mixture to assay ΔTK (188bp), GFP (338bp) and βActin (92bp) with a single PCR reaction was used for Nes-ΔTK genotyping. HSV-ΔTK_S: 5’- atgctgcccataaggtatcg-3’; HSV-ΔTK_AS: 5’- gtaatgacaagcgcccagat-3’; GFP_S: 5’- acgtaaacggccacaagttc-3’; GFP_AS: 5’- gtcctccttgaagtcgatgc-3’; βActin_S: 5’- atgaagagttttggcgatgg-3’; βActin_AS: 5’- gagacattgaatggggcagt-3’

Primers for identifying ΔNF1 are 5'- tcagactgattgttgtacctgatggttgtacc -3', 5'- aatgtgaaattggtgtcgagtaaggtaaccac -3', 5'- ttaagagcatctgctgctcttagagggaa -3', the sizes of floxed NF1, wild type NF and ΔNF1 are 640bp, 496bp, 280bp respectively. Primers for identifying ΔPten are 5'- ctcctctactccattcttccc -3', 5'- actcccaccaatgaacaaac -3', 5'- gtactctgagagattattggaaatgag -3', the sizes of floxed Pten, wild type Pten and ΔPten are 335bp, 209bp, 404bp.

Primers used for QPCR to identify glioma subtypes are:

Gene Name	Marker	Sequence (5' - 3')	Tm ℃
OLIG2	PN	cacaggagggactgtgtcct aggaggtgctggaggaagat	60
SOX2	PN	gaacgccttcatggtatggt tctcggtctcggacaaaagt	60
CNTN1	PN	actactgcctggcatccaac ccttcccttccttcaccttc	60
MYT1	PN	agctcagaaagtgatgacaagc	60

		gagtacttgccccgcacat	
NKX2-2	PN	tctacgacagcagcgacaac	60
		ttgtcattgtccggtgactc	
ASCL1	PN	agatgagcaaggtggagacg	60
		gaacccgccatagagttcaa	
PDGFRA	PN	cacaccggatggtacacttg	60
		ggcagagtcatcctcttcca	
DCX	PN	ctcagggagtgcgctacatt	60
		acagaccagttggggttgac	
GPR17	PN	tgctacctgctgatcattcg	60
		tgtggtagggcacaaaacaa	
FLRT1	PN	gctgcttctcaggaacaacc	60
		tctcgctggtgatgtctttg	
CHI3L1	MES	tcctgcgttcttatggcttt	60
		cgctgagcaggagtttctct	
CD44	MES	ggctcatcatcttggcatct	60
		cactgggtttcctgtcttcc	
CEPBB	MES	caagctgagcgacgagtaca	60
		agctgctccaccttcttctg	
TGFBI	MES	tcattggcaccaacaagaaa	60
		tctctcctgggacctttca	
TNFRS1A	MES	cagtctgcagggagtgtgaa	60

		tcagcttggcaaggagagat	
MVP	MES	ggcagaagatcttggaccag	60
		agagccttctccctcaatcc	
PLA2G5	MES	tggcttctacggctgctact	60
		ccgaatggcacagtcttttt	
S100A13	MES	gcagcctgaacatcaatgaa	60
		gccagctctccaatcagtct	
TIMP1	MES	catggaaagcctctgtggat	60
		ctcagagtacgccagggaac	
COL5A1	MES	ggatgttgcctaccgagtct	60
		ctgcctttcttggctttcac	
GAPDH	Reference	catggccttccgtgttccta	60
		cctgcttcaccaccttcttgat	

Primers for methylation-specific PCR (MSPCR) were designed using MSPPrimer (Brandes et al., 2007). Tissue samples were microdissected from paraffin brain tumor or control sections and subjected to genomic DNA extraction. EZ DNA Methylation-Gold Kit (Zymo Research) was used for C-T conversion following manufacturer's protocol. The DNA methyltransferase M.SssI was purchased from Zymo Research. Primers used for MSPCR are:

Primers for methylated promoter (tm= 56 ℃, size= 153bp):

MGMT_M_S: 5’-GGtAGtTtttAGAGttACGtttCGC-3’

MGMT_M_AS: 5'-CAaaCGCGTaCACGaaaTaaaaaCG-3'

Primers for Ummethylated promoter (tm=57 ℃, size=153bp):

MGMT_UM_S: 5'-tttTTTTttGGtAGtTtttAGAGttAtGttttGtG-3'

MGMT_UM_AS: 5'-TACaaaCCaCAaaCaCaTaCACaaaaTaaaaaCa-3'

Nested Primers (tm=51 ℃, size=304bp):

MGMT_Nes_S: 5'- tAtttTTGYGTtAtAtAtTGGGYGTGtTTAtAt-3'

MGMT_Nes_AS: 5'-CAAaTTTTAaaTaCCTaAaCACCAAaATCT-3'

Induction Efficiency Quantification

4 Nestin73-CreER^{T2};Rosa26^{YFP} mice were induced at 4 weeks of age as described above and perfused with 2% PFA at 6 weeks of age. The brains were dissected out, post-fixed in 4% PFA O/N at 4°C, processed and embedded in paraffin blocks. Five-μm thick sagittal sections were cut until the lateral ventricle was gone. H&E staining was performed on every 5th slide to determine comparable sections. Every 10th of comparable sections was subjected to GFP (Aves Labs) and Sox2 (Chemicon) immunofluorescence staining, and 3 random regions of the frontal SVZ of each section were selected for counting. The efficiency was determined by the percentage of GFP (mean 203)/Sox2 (mean 270) double-positive cells out of the total Sox2-positive cells in SVZ.

Quantification of Ki67, cell density and BrdU-percentage in glioma samples

Because of the heterogeneous nature of the tumors, cell density, Ki67-index and BrdU-positive cell percentage were all quantified using the highest staining area (Phillips et al., 2006). Briefly, staining was checked under low-magnification and the highest staining area was identified. The area was viewed at 200X in three continuous 5μm-thick sections and positive cells counted using the measured parameters.

For quantification of GFP/CldU/IdU triple staining, tumor areas with at least one CldU-positive cell were selected, and an 8 μm Z-stack image was scanned and constructed using confocal microscopy (Olympus and Carl Zeiss). A total of ten different areas within each tumor was imaged and subjected to quantification.

APPENDIX A
Top 100 up-regulated genes in mouse tumor samples

ProbeID	logFC	AveExpr	adj.P.Val	Gene_SYMBOL	Gene_Descr
ILMN_1226950	4.54	7.72	1.61E-11	Cdkn2a	cyclin-dependent kinase inhibitor 2A
ILMN_2776047	4.85	8.05	3.41E-11	En1	engrailed 1
ILMN_2614380	3.28	9.99	4.67E-11	Map3k1	mitogen-activated protein kinase kinase kinase 1
ILMN_1228105	3.72	11.17	5.66E-11	Sox10	SRY-box containing gene 10
ILMN_1215908	2.89	8.90	1.68E-10	Chd7	chromodomain helicase DNA binding protein 7
ILMN_2733257	3.91	7.57	1.94E-10	Tcfl5	transcription factor-like 5 (basic helix-loop-helix)
ILMN_1221619	3.77	8.51	2.03E-10	Nkx2-2	NK2 transcription factor related, locus 2 (Drosophila)
ILMN_1233175	2.96	11.65	2.06E-10	Ppp1r14b	protein phosphatase 1, regulatory (inhibitor) subunit 14B
ILMN_1216368	2.88	7.18	2.09E-10	B3gnt5	UDP-GlcNAc:betaGal beta-1,3-N-acetylglucosaminyltransferase 5
ILMN_2915232	2.71	10.64	2.15E-10	Cotl1	coactosin-like 1 (Dictyostelium)
ILMN_2847144	4.89	10.42	2.24E-10	Hist1h2ak	histone cluster 1, H2ak
ILMN_1219574	4.03	11.08	2.24E-10	Hist1h2af	histone cluster 1, H2af
ILMN_1252794	3.75	9.06	2.57E-10	Sall3	sal-like 3 (Drosophila)
ILMN_2795040	5.03	10.21	2.67E-10	Hist1h2ad	histone cluster 1, H2ad
ILMN_2898319	3.79	8.12	2.67E-10	Aldh1l2	aldehyde dehydrogenase 1 family, member L2
ILMN_1238276	3.87	11.10	2.80E-10	Hist1h2ai	histone cluster 1, H2ai
ILMN_2422687	2.53	9.96	2.80E-10	LOC100046895	similar to Quaking protein
ILMN_1259470	2.71	10.59	3.32E-10	Tmem176b	transmembrane protein 176B
ILMN_1218312	3.88	8.08	3.82E-10	2010317E24Rik	RIKEN cDNA 2010317E24 gene
ILMN_2653617	2.25	11.06	4.06E-10	Cd63	CD63 antigen
ILMN_1235932	3.95	10.85	4.06E-10	Pdgfra	platelet derived growth factor receptor, alpha polypeptide
ILMN_1246108	4.99	10.15	4.63E-10	Hist1h2ah	histone cluster 1, H2ah
ILMN_1226839	3.83	12.02	4.68E-10	Hist1h2ac	histone cluster 1, H2ac
ILMN_2740852	3.28	9.63	5.19E-10	F2r	coagulation factor II (thrombin) receptor
ILMN_2741132	2.10	11.51	5.19E-10	Hmgn1	high mobility group nucleosomal binding domain 1
ILMN_2914271	2.36	8.60	5.55E-10	Araf	v-raf murine sarcoma 3611 viral oncogene homolog
ILMN_2773936	4.28	9.04	5.76E-10	S1pr2	sphingosine-1-phosphate receptor 2
ILMN_1248830	3.93	10.87	5.76E-10	Hist1h2an	histone cluster 1, H2an
ILMN_1224003	2.51	9.88	5.76E-10	Ptbp1	polypyrimidine tract binding protein 1
ILMN_2914510	2.12	11.65	5.76E-10	Sept2	septin 2
ILMN_1221568	3.32	8.61	5.80E-10	Cdca7	cell division cycle associated 7
ILMN_2974418	2.30	8.67	5.80E-10	Wdr51b	WD repeat domain 51B
ILMN_2738330	2.19	6.92	5.80E-10	Fabp7	fatty acid binding protein 7, brain
ILMN_1251250	3.58	8.51	5.85E-10	Lhfpl3	lipoma HMGIC fusion partner-like 3
ILMN_2472444	4.65	9.04	5.92E-10	Traf4	TNF receptor associated factor 4
ILMN_1236221	2.95	8.87	5.92E-10	Rev3l	REV3-like, catalytic subunit of DNA polymerase zeta RAD54 like (S. cerevisiae)

ILMN_2834728	2.94	10.10	5.92E-10	Prkd3	protein kinase D3
ILMN_2632034	2.93	7.28	6.27E-10	Cdca7l	cell division cycle associated 7 like
ILMN_2648292	2.18	12.31	7.28E-10	H3f3b	H3 histone, family 3B
ILMN_2732848	4.94	9.69	7.80E-10	Tagln2	transgelin 2
ILMN_2703267	3.92	8.11	8.05E-10	Nes	nestin
ILMN_2624280	2.24	10.99	8.40E-10	Rps27l	ribosomal protein S27-like
ILMN_2705166	1.87	10.13	8.50E-10	St6gal1	beta galactoside alpha 2,6 sialyltransferase 1
ILMN_2717613	2.01	7.27	9.19E-10	Cdk2	cyclin-dependent kinase 2
ILMN_1256012	2.54	8.50	9.37E-10	Zfp521	zinc finger protein 521
ILMN_3157483	2.12	8.37	1.04E-09	Ets1	E26 avian leukemia oncogene 1, 5' domain
ILMN_2631591	2.58	7.56	1.04E-09	E030049G20Rik	RIKEN cDNA E030049G20 gene
ILMN_2760105	2.59	13.17	1.14E-09	Olig1	oligodendrocyte transcription factor 1
ILMN_1254256	2.31	8.62	1.14E-09	Actl6a	actin-like 6A
ILMN_1217309	2.19	9.91	1.18E-09	Tax1bp3	Tax1 (human T-cell leukemia virus type I) binding protein 3
ILMN_2724294	2.50	8.28	1.30E-09	Gpx7	glutathione peroxidase 7
ILMN_2734712	2.44	9.39	1.31E-09	Ptpla	protein tyrosine phosphatase-like (proline instead of catalytic arginine), member a
ILMN_2744380	1.58	9.06	1.31E-09	Npc2	Niemann Pick type C2
ILMN_1232123	2.14	6.52	1.31E-09	Traf3ip2	TRAF3 interacting protein 2
ILMN_3158499	1.99	10.14	1.37E-09	Mdk	midkine
ILMN_1218380	3.13	12.58	1.37E-09	Hist2h2ac	histone cluster 2, H2ac
ILMN_1217454	1.69	11.06	1.54E-09	Lamp2	lysosomal-associated membrane protein 2
ILMN_2717045	2.14	11.10	1.57E-09	Prdx4	peroxiredoxin 4
ILMN_2929896	4.46	7.90	1.57E-09	Pbk	PDZ binding kinase
ILMN_2705935	1.66	11.96	1.57E-09	Nme2	non-metastatic cells 2, protein (NM23B) expressed in
ILMN_1231612	1.91	7.41	1.58E-09	Znhit6	zinc finger, HIT type 6
ILMN_1252831	3.55	10.45	1.72E-09	2310014H01Rik	RIKEN cDNA 2310014H01 gene
ILMN_3119014	2.72	8.38	1.72E-09	Elk3	ELK3, member of ETS oncogene family
ILMN_2738345	2.53	9.72	1.72E-09	Lims2	LIM and senescent cell antigen like domains 2
ILMN_2515784	2.93	9.32	1.73E-09	Tspan6	tetraspanin 6
ILMN_2662214	3.16	8.15	1.75E-09	Cacng4	calcium channel, voltage-dependent, gamma subunit 4
ILMN_2629856	1.60	8.57	1.82E-09	Rrp15	ribosomal RNA processing 15 homolog (S. cerevisiae)
ILMN_2515363	2.18	9.98	1.88E-09	Tpm4	tropomyosin 4
ILMN_2612423	1.45	12.57	1.92E-09	Hnrnpab	heterogeneous nuclear ribonucleoprotein A/B
ILMN_2703748	2.18	7.50	1.94E-09	Luc7l	Luc7 homolog (S. cerevisiae)-like
ILMN_3150724	2.70	7.81	1.96E-09	Ppfibp1	PTPRF interacting protein, binding protein 1 (liprin beta 1)
ILMN_2669793	3.90	9.14	2.06E-09	Ccnd1	cyclin D1
ILMN_1251930	1.87	8.53	2.06E-09	Nasp	nuclear autoantigenic sperm protein (histone-binding)
ILMN_2632257	1.89	7.68	2.10E-09	Lix1l	Lix1-like
ILMN_2993455	2.57	8.02	2.15E-09	Nedd1	neural precursor cell expressed, developmentally down-regulated gene 1

ILMN_2683675	1.45	8.44	2.22E-09	Ehmt1	euchromatic histone methyltransferase 1
ILMN_1222009	3.26	10.48	2.23E-09	Gab1	growth factor receptor bound protein 2-associated protein 1
ILMN_2525605	2.92	12.46	2.23E-09	H2afj	H2A histone family, member J
ILMN_1228535	2.81	9.74	2.23E-09	Pmp22	peripheral myelin protein 22
ILMN_1257485	1.71	8.93	2.23E-09	2610029G23Rik	RIKEN cDNA 2610029G23 gene
ILMN_1219591	2.97	7.78	2.35E-09	1300014I06Rik	RIKEN cDNA 1300014I06 gene
ILMN_2637266	2.08	9.66	2.35E-09	Casp2	caspase 2
ILMN_2592313	3.43	12.48	2.37E-09	Psenen	presenilin enhancer 2 homolog (C. elegans)
ILMN_1257209	2.57	8.75	2.39E-09	Wipf1	WAS/WASL interacting protein family, member 1
ILMN_1243876	2.15	7.25	2.59E-09	Casp8	caspase 8
ILMN_1259946	1.77	11.31	2.64E-09	Cdc42se1	CDC42 small effector 1
ILMN_3131063	3.53	10.23	2.76E-09	Ccnd3	cyclin D3
ILMN_2784078	3.89	9.13	2.81E-09	Mmp15	matrix metallopeptidase 15
ILMN_2734212	1.88	6.74	2.81E-09	Cd1d1	CD1d1 antigen
ILMN_1237371	2.29	9.54	2.86E-09	Smad5	MAD homolog 5 (Drosophila)
ILMN_1220051	2.78	7.58	2.96E-09	Tmpo	thymopoietin
ILMN_3115213	2.93	7.02	3.11E-09	Irx2	Iroquois related homeobox 2 (Drosophila)
ILMN_1250450	1.95	9.84	3.12E-09	Ogfr	opioid growth factor receptor
ILMN_1243329	2.43	8.54	3.13E-09	Dab2	disabled homolog 2 (Drosophila)
ILMN_1227540	1.96	9.91	3.19E-09	Phf10	PHD finger protein 10
ILMN_1237216	2.40	11.08	3.35E-09	Hmgn4	high mobility group nucleosomal binding domain 4
ILMN_2589785	2.46	9.32	3.40E-09	Cnn3	calponin 3, acidic
ILMN_1245858	2.36	11.01	3.40E-09	Epb4.1	erythrocyte protein band 4.1
ILMN_1227128	2.53	9.88	3.47E-09	Sox12	SRY-box containing gene 12
ILMN_3145213	1.66	10.75	3.58E-09	H3f3a	H3 histone, family 3A

APPENDIX B
Top 100 down-regulated genes in mouse glioma samples

Probe ID	logFC	AveExpr	adj.P.Val	Gene_SYMBOL	Gene_Descr
ILMN_2595600	-4.01	7.81	7.07E-12	Rph3a	rabphilin 3A
ILMN_2752431	-4.95	8.37	1.61E-11	Itpka	inositol 1,4,5-trisphosphate 3-kinase A
ILMN_2771433	-3.34	7.51	3.41E-11	Neurod2	neurogenic differentiation 2
ILMN_2822905	-4.17	8.55	5.66E-11	Ngef	neuronal guanine nucleotide exchange factor
ILMN_2702101	-2.23	10.62	8.69E-11	Pld3	phospholipase D family, member 3
ILMN_2632832	-2.43	6.94	8.93E-11	Adap1	ArfGAP with dual PH domains 1
ILMN_2658266	-2.75	7.57	2.06E-10	Gpr22	G protein-coupled receptor 22
ILMN_2760540	-4.57	8.73	2.09E-10	Mpped1	metallophosphoesterase domain containing 1
ILMN_2517171	-3.69	7.81	2.15E-10	Stk16	serine/threonine kinase 16
ILMN_1254178	-2.35	8.04	2.67E-10	Gm88	predicted gene 88
ILMN_2947901	-2.57	7.00	4.06E-10	Aifm3	apoptosis-inducing factor, mitochondrion-associated 3
ILMN_1227403	-3.04	7.54	4.06E-10	Rtn4rl1	reticulon 4 receptor-like 1
ILMN_2756891	-1.98	6.78	5.19E-10	Lpcat4	lysophosphatidylcholine acyltransferase 4
ILMN_2992047	-2.59	7.62	5.70E-10	Rhof	ras homolog gene family, member f
ILMN_2646045	-2.15	6.95	5.92E-10	Fam189a1	family with sequence similarity 189, member A1
ILMN_3145484	-2.22	7.08	5.92E-10	Ppfia3	protein tyrosine phosphatase, receptor type, f polypeptide (PTPRF), interacting protein (liprin), alpha 3
ILMN_2676431	-2.43	6.95	5.92E-10	Fbxw7	F-box and WD-40 domain protein 7
ILMN_2700608	-4.96	10.57	5.92E-10	Stx1a	syntaxin 1A (brain)
ILMN_1223321	-3.18	7.43	5.98E-10	Phyhip	phytanoyl-CoA hydroxylase interacting protein
ILMN_1249790	-2.46	7.01	6.23E-10	Ccdc136	coiled-coil domain containing 136
ILMN_1229379	-3.05	7.44	6.27E-10	Syt13	synaptotagmin XIII
ILMN_2920503	-3.27	7.57	6.27E-10	Tbr1	T-box brain gene 1
ILMN_2713060	-3.34	9.85	6.29E-10	Fam131a	family with sequence similarity 131, member A
ILMN_1220774	-2.27	7.48	6.66E-10	Vwa5b2	von Willebrand factor A domain containing 5B2
ILMN_2538938	-2.08	6.81	7.00E-10	Gm1060	predicted gene 1060
ILMN_2953411	-2.12	11.92	7.28E-10	Ppp3r1	protein phosphatase 3, regulatory subunit B, alpha isoform (calcineurin B, type I)
ILMN_2828265	-3.09	9.22	7.28E-10	5-Sep	septin 5
ILMN_2851735	-2.04	7.13	7.66E-10	Ankrd13d	ankyrin repeat domain 13 family, member D
ILMN_2673064	-2.15	8.56	7.73E-10	Ing2	inhibitor of growth family, member 2
ILMN_1218920	-2.91	7.24	8.08E-10	D130043K22Rik	RIKEN cDNA D130043K22 gene
ILMN_2646949	-2.80	6.87	8.28E-10	Golga7b	golgi autoantigen, golgin subfamily a, 7B
ILMN_1237546	-2.52	6.90	8.34E-10	9130213B05Rik	RIKEN cDNA 9130213B05 gene
ILMN_1257253	-1.78	7.57	8.40E-10	Iqsec2	IQ motif and Sec7 domain 2
ILMN_1216469	-3.28	7.54	8.50E-10	Kcnab1	potassium voltage-gated channel, shaker-related subfamily, beta member 1

ILMN_2653194	-2.83	9.51	9.20E-10	Fbxl16	F-box and leucine-rich repeat protein 16
ILMN_1257751	-2.01	6.98	9.33E-10	Dlgap3	discs, large (Drosophila) homolog-associated protein 3
ILMN_1244081	-4.75	10.57	1.06E-09	Rgs4	regulator of G-protein signaling 4
ILMN_2623591	-2.41	10.71	1.09E-09	Apbb1	amyloid beta (A4) precursor protein-binding, family B, member 1
ILMN_2688560	-2.74	7.16	1.09E-09	Pcnxl2	pecanex-like 2 (Drosophila)
ILMN_2917441	-2.13	7.84	1.14E-09	Rusc1	RUN and SH3 domain containing 1
ILMN_2859960	-2.94	7.98	1.15E-09	Adcy1	adenylate cyclase 1
ILMN_2740628	-1.82	8.93	1.22E-09	Ndrg3	N-myc downstream regulated gene 3
ILMN_1239940	-2.97	7.24	1.31E-09	Gca	grancalcin
ILMN_2963091	-3.25	9.63	1.31E-09	E130012A19Rik	RIKEN cDNA E130012A19 gene
ILMN_2434200	-1.77	6.80	1.35E-09	Adam11	a disintegrin and metallopeptidase domain 11
ILMN_1232514	-1.55	7.79	1.39E-09	St3gal5	ST3 beta-galactoside alpha-2,3-sialyltransferase 5
ILMN_1242415	-2.26	6.78	1.39E-09	Kcnj9	potassium inwardly-rectifying channel, subfamily J, member 9
ILMN_2692938	-1.77	6.47	1.42E-09	Slc30a3	solute carrier family 30 (zinc transporter), member 3
ILMN_2755483	-2.17	8.98	1.46E-09	Kctd1	potassium channel tetramerisation domain containing 1
ILMN_2710151	-1.97	9.41	1.47E-09	Snap47	synaptosomal-associated protein, 47
ILMN_1245352	-3.64	8.30	1.54E-09	Dclk3	doublecortin-like kinase 3
ILMN_2891274	-1.72	6.35	1.55E-09	Rltpr	RGD motif, leucine rich repeats, tropomodulin domain and proline-rich containing
ILMN_2933346	-2.25	8.22	1.55E-09	Actr3b	ARP3 actin-related protein 3 homolog B (yeast)
ILMN_1220834	-2.58	12.30	1.55E-09	Camta2	calmodulin binding transcription activator 2
ILMN_2487421	-2.41	6.96	1.56E-09	Prrt3	proline-rich transmembrane protein 3
ILMN_3082271	-2.33	7.12	1.72E-09	Rims1	regulating synaptic membrane exocytosis 1
ILMN_2733897	-2.17	6.75	1.75E-09	Olfm3	olfactomedin 3
ILMN_1241161	-2.12	12.54	1.77E-09	Camk2n2	calcium/calmodulin-dependent protein kinase II inhibitor 2
ILMN_1246734	-3.68	7.89	1.84E-09	Osbp2	oxysterol binding protein 2
ILMN_2926842	-1.70	6.59	2.04E-09	Flrt2	fibronectin leucine rich transmembrane protein 2
ILMN_2597249	-2.38	7.68	2.07E-09	Abcb9	ATP-binding cassette, sub-family B (MDR/TAP), member 9
ILMN_2710764	-2.72	8.32	2.09E-09	Dlg4	discs, large homolog 4 (Drosophila)
ILMN_2998813	-2.64	7.52	2.11E-09	Sema4f	sema domain, immunoglobulin domain (Ig), TM domain, and short cytoplasmic domain
ILMN_2945940	-3.09	8.78	2.14E-09	Rapgef4	Rap guanine nucleotide exchange factor (GEF) 4
ILMN_1229246	-3.36	7.52	2.14E-09	Spata2L	spermatogenesis associated 2-like
ILMN_1231468	-1.55	6.93	2.23E-09	1700030J22Rik	RIKEN cDNA 1700030J22 gene
ILMN_2728134	-1.85	7.54	2.23E-09	Ism1	isthmin 1 homolog (zebrafish)
ILMN_2853035	-1.96	6.55	2.23E-09	Lin7b	lin-7 homolog B (C. elegans)
ILMN_2684075	-1.68	6.59	2.35E-09	Ar	androgen receptor

ILMN_2625867	-1.90	9.32	2.35E-09	6-Sep	septin 6
ILMN_2750588	-2.32	9.93	2.35E-09	Tmem132a	transmembrane protein 132A
ILMN_2457727	-1.77	7.09	2.45E-09	Adrb1	adrenergic receptor, beta 1
ILMN_1227065	-2.26	7.25	2.47E-09	Rell2	RELT-like 2
ILMN_2484374	-1.89	6.76	2.51E-09	Scn8a	sodium channel, voltage-gated, type VIII, alpha
ILMN_1258190	-2.32	7.52	2.60E-09	2810032G03Rik	RIKEN cDNA 2810032G03 gene
ILMN_2719702	-3.45	7.49	2.61E-09	Rasl10a	RAS-like, family 10, member A
ILMN_1259965	-2.29	6.91	2.73E-09	Npy1r	neuropeptide Y receptor Y1
ILMN_2994995	-3.27	8.89	2.77E-09	Lgi3	leucine-rich repeat LGI family, member 3
ILMN_1237917	-1.81	8.56	2.80E-09	Sparcl1	SPARC-like 1
ILMN_2517100	-2.28	7.10	2.80E-09	Pgm2l1	phosphoglucomutase 2-like 1
ILMN_1225037	-2.63	10.53	2.81E-09	Grit	Rho GTPase-activating protein
ILMN_2980212	-2.11	6.84	2.82E-09	2610034M16Rik	RIKEN cDNA 2610034M16 gene
ILMN_2440634	-2.95	8.72	2.89E-09	Akap5	A kinase (PRKA) anchor protein 5
ILMN_2876325	-1.53	8.37	2.91E-09	Fbxo34	F-box protein 34
ILMN_1219768	-2.22	8.37	2.91E-09	Sgtb	small glutamine-rich tetratricopeptide repeat (TPR)-containing, beta
ILMN_2748222	-2.71	7.55	2.98E-09	Tesc	tescalcin
ILMN_1232800	-1.92	6.83	3.02E-09	Cyfip2	cytoplasmic FMR1 interacting protein 2
ILMN_2619380	-2.20	7.85	3.07E-09	Nckipsd	NCK interacting protein with SH3 domain
ILMN_1254656	-2.09	7.05	3.12E-09	Sprn	shadow of prion protein
ILMN_1216662	-3.24	11.35	3.12E-09	Kif5c	kinesin family member 5C
ILMN_1239133	-2.45	7.31	3.17E-09	Klc2	kinesin light chain 2
ILMN_2604570	-2.55	7.04	3.17E-09	Nptx1	neuronal pentraxin 1
ILMN_1231608	-2.51	7.15	3.21E-09	1700003E16Rik	RIKEN cDNA 1700003E16 gene
ILMN_1257876	-1.82	10.72	3.24E-09	B3gnt1	UDP-GlcNAc:betaGal beta-1,3-N-acetylglucosaminyltransferase 1
ILMN_2740407	-3.02	7.65	3.24E-09	Pde2a	phosphodiesterase 2A, cGMP-stimulated
ILMN_2813547	-4.44	7.94	3.40E-09	Scn4b	sodium channel, type IV, beta
ILMN_2590421	-3.82	7.83	3.63E-09	Spock1	sparc/osteonectin, cwcv and kazal-like domains proteoglycan 1
ILMN_2613414	-1.81	7.20	3.83E-09	Map3k10	mitogen-activated protein kinase kinase kinase 10
ILMN_2915059	-1.84	10.06	4.03E-09	Dgkz	diacylglycerol kinase zeta
ILMN_3002505	-3.15	9.21	4.03E-09	Abhd8	abhydrolase domain containing 8

APPENDIX C
Top 10 functional clusters of up-regulated genes in tumor samples

Annotation Cluster 1 Enrichment Score: 16.66

Category	Term	Count	%	PValue	FDR
GOTERM_CC_FAT	GO:0043228~non-membrane-bounded organelle	255	17.72	1.99E-24	2.85E-21
GOTERM_CC_FAT	GO:0043232~intracellular non-membrane-bounded organelle	255	17.72	1.99E-24	2.85E-21
GOTERM_CC_FAT	GO:0005856~cytoskeleton	107	7.44	2.74E-03	3.85E+00

Annotation Cluster 2 Enrichment Score: 12.89

Category	Term	Count	%	PValue	FDR
GOTERM_BP_FAT	GO:0007049~cell cycle	115	7.99	9.27E-19	1.67E-15
SP_PIR_KEYWORDS	cell cycle	91	6.32	1.98E-18	2.84E-15
GOTERM_BP_FAT	GO:0000278~mitotic cell cycle	60	4.17	3.64E-15	6.61E-12
GOTERM_BP_FAT	GO:0051301~cell division	64	4.45	1.93E-14	3.48E-11
GOTERM_BP_FAT	GO:0022403~cell cycle phase	70	4.86	3.11E-14	5.61E-11
GOTERM_BP_FAT	GO:0022402~cell cycle process	78	5.42	5.30E-14	9.55E-11
SP_PIR_KEYWORDS	cell division	57	3.96	2.16E-13	3.10E-10
SP_PIR_KEYWORDS	mitosis	45	3.13	1.24E-12	1.77E-09
GOTERM_BP_FAT	GO:0000280~nuclear division	46	3.20	1.53E-11	2.76E-08
GOTERM_BP_FAT	GO:0007067~mitosis	46	3.20	1.53E-11	2.76E-08
GOTERM_BP_FAT	GO:0000087~M phase of mitotic cell cycle	46	3.20	3.26E-11	5.87E-08
GOTERM_BP_FAT	GO:0048285~organelle fission	46	3.20	5.64E-11	1.02E-07
GOTERM_BP_FAT	GO:0000279~M phase	57	3.96	1.09E-10	1.96E-07

Annotation Cluster 3 Enrichment Score: 9.27

Category	Term	Count	%	PValue	FDR
SP_PIR_KEYWORDS	dna replication	30	2.08	1.33E-12	1.90E-09
KEGG_PATHWAY	mmu03030:DNA replication	17	1.18	2.42E-09	2.94E-06
GOTERM_BP_FAT	GO:0006259~DNA metabolic process	70	4.86	4.25E-09	7.67E-06
GOTERM_BP_FAT	GO:0006260~DNA replication	36	2.50	6.18E-09	1.11E-05

Annotation Cluster 4 Enrichment Score: 8.18

Category	Term	Count	%	PValue	FDR
GOTERM_CC_FAT	GO:0005694~chromosome	90	6.25	2.99E-24	4.28E-21
GOTERM_CC_FAT	GO:0044427~chromosomal part	79	5.49	1.55E-22	2.22E-19
SP_PIR_KEYWORDS	chromosomal protein	42	2.92	4.20E-15	6.05E-12
GOTERM_CC_FAT	GO:0000785~chromatin	40	2.78	2.84E-11	4.06E-08
KEGG_PATHWAY	mmu05322:Systemic lupus erythematosus	32	2.22	4.03E-11	4.91E-08
SP_PIR_KEYWORDS	nucleosome core	20	1.39	8.68E-11	1.25E-07

INTERPRO	IPR007125:Histone core	19	1.32	1.93E-10	3.27E-07
GOTERM_CC_FAT	GO:0032993~protein-DNA complex	25	1.74	2.54E-10	3.63E-07
GOTERM_CC_FAT	GO:0000786~nucleosome	22	1.53	1.03E-09	1.48E-06
GOTERM_BP_FAT	GO:0051276~chromosome organization	69	4.79	1.80E-09	3.24E-06
GOTERM_BP_FAT	GO:0006323~DNA packaging	29	2.02	2.54E-09	4.59E-06
GOTERM_BP_FAT	GO:0034728~nucleosome organization	23	1.60	5.49E-08	9.89E-05
PIR_SUPERFAMILY	PIRSF002048:histone H2A	10	0.69	6.27E-08	9.39E-05
GOTERM_BP_FAT	GO:0031497~chromatin assembly	22	1.53	2.06E-07	3.71E-04
GOTERM_BP_FAT	GO:0006333~chromatin assembly or disassembly	27	1.88	2.60E-07	4.69E-04
GOTERM_BP_FAT	GO:0065004~protein-DNA complex assembly	22	1.53	2.63E-07	4.75E-04
GOTERM_BP_FAT	GO:0006334~nucleosome assembly	21	1.46	5.88E-07	1.06E-03
INTERPRO	IPR009072:Histone-fold	18	1.25	1.01E-06	1.72E-03
GOTERM_BP_FAT	GO:0006325~chromatin organization	51	3.54	1.58E-06	2.86E-03
INTERPRO	IPR002119:Histone H2A	11	0.76	4.79E-06	8.14E-03
SP_PIR_KEYWORDS	citrullination	9	0.63	7.35E-06	1.05E-02
SMART	SM00414:H2A	11	0.76	1.64E-05	2.21E-02
UP_SEQ_FEATURE	cross-link:Glycyl lysine isopeptide (Lys-Gly) (interchain with G-Cter in ubiquitin)	30	2.08	9.21E-05	1.69E-01
GOTERM_BP_FAT	GO:0043933~macromolecular complex subunit organization	51	3.54	1.08E-04	1.95E-01
GOTERM_BP_FAT	GO:0034621~cellular macromolecular complex subunit organization	37	2.57	2.21E-04	3.98E-01
GOTERM_BP_FAT	GO:0065003~macromolecular complex assembly	44	3.06	1.33E-03	2.38E+00
GOTERM_BP_FAT	GO:0034622~cellular macromolecular complex assembly	30	2.08	3.74E-03	6.53E+00

Annotation Cluster 5 Enrichment Score: 7.07

Category	Term	Count	%	PValue	FDR
GOTERM_CC_FAT	GO:0000775~chromosome, centromeric region	36	2.50	3.24E-14	4.64E-11
GOTERM_CC_FAT	GO:0000793~condensed chromosome	27	1.88	3.13E-08	4.47E-05
SP_PIR_KEYWORDS	kinetochore	19	1.32	2.98E-07	4.28E-04
GOTERM_CC_FAT	GO:0000779~condensed chromosome, centromeric region	18	1.25	7.47E-07	1.07E-03
GOTERM_BP_FAT	GO:0007059~chromosome segregation	19	1.32	1.41E-06	2.54E-03
GOTERM_CC_FAT	GO:0000776~kinetochore	17	1.18	6.06E-06	8.66E-03
GOTERM_CC_FAT	GO:0000777~condensed chromosome kinetochore	15	1.04	1.72E-05	2.46E-02

Annotation Cluster 6 Enrichment Score: 6.44

Category	Term	Count	%	PValue	FDR
SP_PIR_KEYWORDS	ubl conjugation	82	5.70	3.13E-10	4.49E-07
SP_PIR_KEYWORDS	isopeptide bond	45	3.13	1.72E-06	2.46E-03

UP_SEQ_FEATURE	cross-link:Glycyl lysine isopeptide (Lys-Gly) (interchain with G-Cter in ubiquitin)	30	2.08	9.21E-05	1.69E-01

Annotation Cluster 7 Enrichment Score: 6.11

Category	Term	Count	%	PValue	FDR
SP_PIR_KEYWORDS	dna-binding	195	13.55	5.21E-18	7.47E-15
GOTERM_MF_FAT	GO:0003677~DNA binding	229	15.91	7.63E-18	1.19E-14
SP_PIR_KEYWORDS	transcription regulation	175	12.16	2.11E-08	3.03E-05
SP_PIR_KEYWORDS	Transcription	182	12.65	6.86E-06	9.84E-03
GOTERM_BP_FAT	GO:0006350~transcription	177	12.30	6.25E-04	1.12E+00
GOTERM_MF_FAT	GO:0030528~transcription regulator activity	121	8.41	6.68E-04	1.03E+00
GOTERM_MF_FAT	GO:0003700~transcription factor activity	83	5.77	8.98E-04	1.39E+00
GOTERM_BP_FAT	GO:0045449~regulation of transcription	210	14.59	3.28E-03	5.76E+00
GOTERM_BP_FAT	GO:0051252~regulation of RNA metabolic process	132	9.17	9.96E-02	8.49E+01
GOTERM_BP_FAT	GO:0006355~regulation of transcription, DNA-dependent	130	9.03	1.04E-01	8.61E+01

Annotation Cluster 8 Enrichment Score: 6.01

Category	Term	Count	%	PValue	FDR
INTERPRO	IPR000910:High mobility group, HMG1/HMG2	17	1.18	3.55E-07	6.03E-04
UP_SEQ_FEATURE	DNA-binding region:HMG box	15	1.04	1.18E-06	2.17E-03
SMART	SM00398:HMG	17	1.18	2.21E-06	2.98E-03

Annotation Cluster 9 Enrichment Score: 5.99

Category	Term	Count	%	PValue	FDR
GOTERM_CC_FAT	GO:0031981~nuclear lumen	116	8.06	2.66E-10	3.80E-07
GOTERM_CC_FAT	GO:0031974~membrane-enclosed lumen	139	9.66	4.24E-09	6.07E-06
GOTERM_CC_FAT	GO:0070013~intracellular organelle lumen	134	9.31	9.19E-09	1.32E-05
GOTERM_CC_FAT	GO:0043233~organelle lumen	134	9.31	1.08E-08	1.54E-05
GOTERM_CC_FAT	GO:0005730~nucleolus	48	3.34	1.09E-06	1.56E-03
GOTERM_CC_FAT	GO:0005654~nucleoplasm	70	4.86	8.07E-05	1.15E-01
GOTERM_CC_FAT	GO:0044451~nucleoplasm part	57	3.96	1.36E-03	1.93E+00
GOTERM_CC_FAT	GO:0005667~transcription factor complex	24	1.67	8.56E-02	7.22E+01

Annotation Cluster 10 Enrichment Score: 4.70

Category	Term	Count	%	PValue	FDR
GOTERM_CC_FAT	GO:0030529~ribonucleoprotein complex	73	5.07	4.08E-10	5.84E-07
SP_PIR_KEYWORDS	ribonucleoprotein	48	3.34	2.95E-08	4.23E-05
KEGG_PATHWAY	mmu03010:Ribosome	23	1.60	1.33E-06	1.61E-03
GOTERM_MF_FAT	GO:0003735~structural constituent of ribosome	26	1.81	1.41E-04	2.19E-01

GOTERM_CC_FAT	GO:0005840~ribosome	28	1.95	7.01E-04	9.98E-01
SP_PIR_KEYWORDS	ribosomal protein	27	1.88	7.41E-04	1.06E+00
GOTERM_BP_FAT	GO:0006412~translation	43	2.99	7.65E-04	1.37E+00
GOTERM_MF_FAT	GO:0005198~structural molecule activity	46	3.20	2.86E-02	3.63E+01

APPENDIX D
functional clusters of down-regulated genes in tumor samples

Annotation Cluster 1 Enrichment Score: 20.62

Category	Term	Count	%	PValue	FDR
GOTERM_CC_FAT	GO:0045202~synapse	110	7.28	2.13E-41	2.99E-38
GOTERM_CC_FAT	GO:0044456~synapse part	79	5.23	2.65E-32	3.72E-29
SP_PIR_KEYWORDS	synapse	77	5.10	4.07E-31	5.78E-28
SP_PIR_KEYWORDS	cell junction	94	6.23	8.44E-23	1.20E-19
GOTERM_CC_FAT	GO:0030054~cell junction	101	6.69	4.88E-20	6.84E-17
GOTERM_CC_FAT	GO:0044459~plasma membrane part	214	14.17	1.33E-13	1.86E-10
GOTERM_CC_FAT	GO:0045211~postsynaptic membrane	38	2.52	2.07E-12	2.90E-09
SP_PIR_KEYWORDS	postsynaptic cell membrane	33	2.19	4.09E-11	5.81E-08
GOTERM_CC_FAT	GO:0014069~postsynaptic density	18	1.19	2.60E-07	3.64E-04

Annotation Cluster 2 Enrichment Score: 16.19

Category	Term	Count	%	PValue	FDR
GOTERM_BP_FAT	GO:0007267~cell-cell signaling	76	5.03	1.88E-22	3.34E-19
GOTERM_BP_FAT	GO:0019226~transmission of nerve impulse	66	4.37	2.71E-22	4.79E-19
GOTERM_BP_FAT	GO:0007268~synaptic transmission	58	3.84	3.27E-22	5.80E-19
GOTERM_BP_FAT	GO:0050877~neurological system process	95	6.29	9.99E-01	1.00E+02

Annotation Cluster 3 Enrichment Score: 11.63

Category	Term	Count	%	PValue	FDR
GOTERM_MF_FAT	GO:0005516~calmodulin binding	36	2.38	2.02E-13	3.13E-10
UP_SEQ_FEATURE	region of interest:Calmodulin-binding	24	1.59	1.99E-12	3.57E-09
SP_PIR_KEYWORDS	calmodulin-binding	32	2.12	3.12E-11	4.44E-08

Annotation Cluster 4 Enrichment Score: 9.41

Category	Term	Count	%	PValue	FDR
GOTERM_CC_FAT	GO:0008021~synaptic vesicle	32	2.12	1.03E-16	1.55E-13
GOTERM_CC_FAT	GO:0030136~clathrin-coated vesicle	35	2.32	5.39E-13	7.56E-10
GOTERM_CC_FAT	GO:0030135~coated vesicle	37	2.45	5.97E-12	8.37E-09
SP_PIR_KEYWORDS	cytoplasmic vesicle	49	3.25	4.25E-10	6.04E-07
GOTERM_CC_FAT	GO:0031410~cytoplasmic vesicle	81	5.36	4.56E-09	6.40E-06
GOTERM_CC_FAT	GO:0031982~vesicle	81	5.36	1.23E-08	1.72E-05
GOTERM_CC_FAT	GO:0016023~cytoplasmic membrane-bounded vesicle	61	4.04	6.61E-06	9.26E-03
GOTERM_CC_FAT	GO:0031988~membrane-bounded vesicle	61	4.04	1.04E-05	1.46E-02

Annotation Cluster 5 Enrichment Score: 8.35

Category	Term	Count	%	PValue	FDR
GOTERM_BP_FAT	GO:0006836~neurotransmitter transport	28	1.85	8.73E-12	1.55E-08
GOTERM_BP_FAT	GO:0046903~secretion	47	3.11	1.32E-10	2.34E-07
GOTERM_BP_FAT	GO:0032940~secretion by cell	41	2.72	7.72E-10	1.37E-06
GOTERM_BP_FAT	GO:0003001~generation of a signal involved in cell-cell signaling	26	1.72	1.07E-09	1.90E-06
GOTERM_BP_FAT	GO:0007269~neurotransmitter secretion	17	1.13	1.45E-09	2.56E-06
GOTERM_BP_FAT	GO:0001505~regulation of neurotransmitter levels	22	1.46	1.68E-09	2.97E-06
SP_PIR_KEYWORDS	exocytosis	20	1.32	2.61E-09	3.71E-06
GOTERM_BP_FAT	GO:0048489~synaptic vesicle transport	14	0.93	4.53E-08	8.03E-05
GOTERM_BP_FAT	GO:0006887~exocytosis	27	1.79	9.82E-08	1.74E-04
GOTERM_BP_FAT	GO:0016079~synaptic vesicle exocytosis	8	0.53	1.26E-04	2.23E-01

Annotation Cluster 6 Enrichment Score: 8.18

Category	Term	Count	%	PValue	FDR
GOTERM_MF_FAT	GO:0030695~GTPase regulator activity	72	4.77	2.80E-14	4.33E-11
GOTERM_MF_FAT	GO:0060589~nucleoside-triphosphatase regulator activity	72	4.77	6.63E-14	1.03E-10
GOTERM_MF_FAT	GO:0005096~GTPase activator activity	35	2.32	2.05E-06	3.17E-03
GOTERM_MF_FAT	GO:0008047~enzyme activator activity	41	2.72	3.43E-06	5.31E-03
SP_PIR_KEYWORDS	GTPase activation	23	1.52	9.12E-04	1.29E+00

Annotation Cluster 7 Enrichment Score: 8.11

Category	Term	Count	%	PValue	FDR
GOTERM_BP_FAT	GO:0044057~regulation of system process	48	3.18	1.06E-12	1.88E-09
GOTERM_BP_FAT	GO:0048167~regulation of synaptic plasticity	20	1.32	4.69E-10	8.31E-07
GOTERM_BP_FAT	GO:0050804~regulation of synaptic transmission	28	1.85	2.55E-09	4.52E-06
GOTERM_BP_FAT	GO:0051969~regulation of transmission of nerve impulse	29	1.92	2.81E-09	4.97E-06
GOTERM_BP_FAT	GO:0031644~regulation of neurological system process	29	1.92	1.05E-08	1.86E-05
GOTERM_BP_FAT	GO:0048168~regulation of neuronal synaptic plasticity	13	0.86	1.70E-07	3.01E-04
GOTERM_BP_FAT	GO:0048169~regulation of long-term neuronal synaptic plasticity	8	0.53	2.86E-04	5.06E-01

Annotation Cluster 8 Enrichment Score: 7.83

Category	Term	Count	%	PValue	FDR
GOTERM_BP_FAT	GO:0006812~cation transport	95	6.29	2.30E-16	3.89E-13
GOTERM_BP_FAT	GO:0030001~metal ion transport	86	5.70	2.65E-16	3.89E-13
GOTERM_BP_FAT	GO:0006811~ion transport	116	7.68	8.14E-16	1.38E-12

GOTERM_MF_FAT	GO:0022836~gated channel activity	63	4.17	5.34E-15	8.25E-12
GOTERM_MF_FAT	GO:0046873~metal ion transmembrane transporter activity	61	4.04	3.02E-13	4.68E-10
GOTERM_MF_FAT	GO:0015267~channel activity	70	4.64	4.84E-13	7.50E-10
GOTERM_MF_FAT	GO:0022803~passive transmembrane transporter activity	70	4.64	4.84E-13	7.50E-10
GOTERM_MF_FAT	GO:0005261~cation channel activity	55	3.64	5.60E-13	8.67E-10
GOTERM_MF_FAT	GO:0030955~potassium ion binding	36	2.38	6.30E-13	9.76E-10
GOTERM_MF_FAT	GO:0005216~ion channel activity	67	4.44	1.55E-12	2.40E-09
SP_PIR_KEYWORDS	voltage-gated channel	39	2.58	1.91E-12	2.71E-09
SP_PIR_KEYWORDS	potassium	36	2.38	2.70E-12	3.83E-09
GOTERM_MF_FAT	GO:0005244~voltage-gated ion channel activity	44	2.91	4.31E-12	6.68E-09
GOTERM_MF_FAT	GO:0022832~voltage-gated channel activity	44	2.91	4.31E-12	6.68E-09
GOTERM_MF_FAT	GO:0022838~substrate specific channel activity	67	4.44	6.72E-12	1.04E-08
SP_PIR_KEYWORDS	ionic channel	61	4.04	1.43E-11	2.04E-08
SP_PIR_KEYWORDS	potassium transport	33	2.19	1.82E-11	2.58E-08
SP_PIR_KEYWORDS	ion transport	90	5.96	1.90E-11	2.70E-08
GOTERM_BP_FAT	GO:0015672~monovalent inorganic cation transport	58	3.84	5.73E-11	1.02E-07
GOTERM_BP_FAT	GO:0006813~potassium ion transport	39	2.58	9.75E-11	1.73E-07
GOTERM_MF_FAT	GO:0031420~alkali metal ion binding	45	2.98	1.58E-10	2.44E-07
GOTERM_MF_FAT	GO:0022843~voltage-gated cation channel activity	34	2.25	1.86E-10	2.88E-07
GOTERM_MF_FAT	GO:0005267~potassium channel activity	32	2.12	4.23E-09	6.55E-06
SP_PIR_KEYWORDS	potassium channel	23	1.52	9.22E-09	1.31E-05
SP_PIR_KEYWORDS	transport	184	12.19	2.02E-08	2.88E-05
GOTERM_MF_FAT	GO:0005249~voltage-gated potassium channel activity	25	1.66	1.98E-07	3.06E-04
GOTERM_CC_FAT	GO:0034702~ion channel complex	33	2.19	1.05E-06	1.47E-03
INTERPRO	IPR005821:Ion transport	25	1.66	1.84E-06	3.09E-03
INTERPRO	IPR003091:Voltage-dependent potassium channel	13	0.86	9.32E-06	1.56E-02
GOTERM_CC_FAT	GO:0034703~cation channel complex	22	1.46	1.85E-05	2.59E-02
UP_SEQ_FEATURE	short sequence motif:Selectivity filter	15	0.99	1.20E-04	2.15E-01
UP_SEQ_FEATURE	region of interest:Segment H5 (pore-forming)	10	0.66	1.52E-04	2.73E-01
GOTERM_BP_FAT	GO:0055085~transmembrane transport	57	3.77	1.82E-04	3.22E-01
GOTERM_CC_FAT	GO:0034705~potassium channel complex	16	1.06	3.42E-04	4.78E-01
GOTERM_CC_FAT	GO:0008076~voltage-gated potassium channel complex	16	1.06	3.42E-04	4.78E-01
INTERPRO	IPR003968:Potassium channel, voltage dependent, Kv	8	0.53	3.03E-03	4.96E+00
INTERPRO	IPR003131:Potassium channel, voltage dependent, Kv, tetramerisation	11	0.73	4.65E-03	7.52E+00

PIR_SUPERFAMILY	PIRSF002449:potassium voltage-gated channel, alpha subunit, subfamilies A/C/D/F/G/S	6	0.40	9.91E-03	1.37E+01
INTERPRO	IPR000210:BTB/POZ-like	21	1.39	4.89E-02	5.68E+01
INTERPRO	IPR011333:BTB/POZ fold	19	1.26	1.27E-01	8.98E+01
SMART	SM00225:BTB	21	1.39	1.69E-01	9.15E+01
INTERPRO	IPR013089:Kelch related	8	0.53	4.41E-01	1.00E+02
UP_SEQ_FEATURE	domain:BTB	11	0.73	5.20E-01	1.00E+02
INTERPRO	IPR013069:BTB/POZ	10	0.66	6.26E-01	1.00E+02

Annotation Cluster 9 Enrichment Score: 7.65

Category	Term	Count	%	PValue	FDR
GOTERM_BP_FAT	GO:0031175~neuron projection development	49	3.25	6.30E-12	1.12E-08
GOTERM_BP_FAT	GO:0048666~neuron development	57	3.77	3.88E-11	6.87E-08
GOTERM_BP_FAT	GO:0030182~neuron differentiation	69	4.57	8.07E-11	1.43E-07
GOTERM_BP_FAT	GO:0030030~cell projection organization	58	3.84	4.54E-10	8.04E-07
GOTERM_BP_FAT	GO:0048812~neuron projection morphogenesis	39	2.58	1.82E-09	3.23E-06
GOTERM_BP_FAT	GO:0007409~axonogenesis	37	2.45	2.55E-09	4.52E-06
GOTERM_BP_FAT	GO:0048858~cell projection morphogenesis	41	2.72	9.61E-09	1.70E-05
GOTERM_BP_FAT	GO:0048667~cell morphogenesis involved in neuron differentiation	38	2.52	1.66E-08	2.94E-05
GOTERM_BP_FAT	GO:0032990~cell part morphogenesis	41	2.72	3.95E-08	7.00E-05
GOTERM_BP_FAT	GO:0000904~cell morphogenesis involved in differentiation	40	2.65	1.18E-07	2.09E-04
GOTERM_BP_FAT	GO:0000902~cell morphogenesis	50	3.31	3.65E-07	6.47E-04
GOTERM_BP_FAT	GO:0032989~cellular component morphogenesis	53	3.51	1.38E-06	2.44E-03
GOTERM_BP_FAT	GO:0007411~axon guidance	20	1.32	9.83E-05	1.74E-01
GOTERM_BP_FAT	GO:0006928~cell motion	42	2.78	6.06E-03	1.02E+01

Annotation Cluster 10 Enrichment Score: 7.57

Category	Term	Count	%	PValue	FDR
INTERPRO	IPR000008:C2 calcium-dependent membrane targeting	36	2.38	1.43E-11	2.40E-08
INTERPRO	IPR018029:C2 membrane targeting protein	32	2.12	2.04E-11	3.42E-08
SMART	SM00239:C2	36	2.38	1.12E-09	1.49E-06
UP_SEQ_FEATURE	domain:C2 1	19	1.26	7.94E-07	1.43E-03
UP_SEQ_FEATURE	domain:C2 2	19	1.26	7.94E-07	1.43E-03
UP_SEQ_FEATURE	domain:C2	15	0.99	1.80E-03	3.19E+00

BIBLIOGRAPHY

Abdel-Rahman, A., Rao, M. S., and Shetty, A. K. (2004). Nestin expression in hippocampal astrocytes after injury depends on the age of the hippocampus. Glia 47, 299-313.

Aguirre, A., Dupree, J. L., Mangin, J. M., and Gallo, V. (2007). A functional role for EGFR signaling in myelination and remyelination. Nature neuroscience 10, 990-1002.

Aguirre, A. A., Chittajallu, R., Belachew, S., and Gallo, V. (2004). NG2-expressing cells in the subventricular zone are type C-like cells and contribute to interneuron generation in the postnatal hippocampus. The Journal of cell biology 165, 575-589.

Al-Hajj, M., Wicha, M. S., Benito-Hernandez, A., Morrison, S. J., and Clarke, M. F. (2003). Prospective identification of tumorigenic breast cancer cells. Proceedings of the National Academy of Sciences of the United States of America 100, 3983-3988.

Alcantara Llaguno, S., Chen, J., Kwon, C. H., Jackson, E. L., Li, Y., Burns, D. K., Alvarez-Buylla, A., and Parada, L. F. (2009). Malignant astrocytomas originate from neural stem/progenitor cells in a somatic tumor suppressor mouse model. Cancer cell 15, 45-56.

Anderson, K., Lutz, C., van Delft, F. W., Bateman, C. M., Guo, Y., Colman, S. M., Kempski, H., Moorman, A. V., Titley, I., Swansbury, J., et al. (2011). Genetic variegation of clonal architecture and propagating cells in leukaemia. Nature 469, 356-361.

Anido, J., Saez-Borderias, A., Gonzalez-Junca, A., Rodon, L., Folch, G., Carmona, M. A., Prieto-Sanchez, R. M., Barba, I., Martinez-Saez, E., Prudkin, L., et al. (2010). TGF-beta Receptor Inhibitors Target the CD44(high)/Id1(high) Glioma-Initiating Cell Population in Human Glioblastoma. Cancer cell 18, 655-668.

Attolini, C. S., Cheng, Y. K., Beroukhim, R., Getz, G., Abdel-Wahab, O., Levine, R. L., Mellinghoff, I. K., and Michor, F. (2010). A mathematical framework to determine the temporal sequence of somatic genetic events in cancer. Proceedings of the National Academy of Sciences of the United States of America 107, 17604-17609.

Bachoo, R. M., Maher, E. A., Ligon, K. L., Sharpless, N. E., Chan, S. S., You, M. J., Tang, Y., DeFrances, J., Stover, E., Weissleder, R., et al. (2002). Epidermal growth factor receptor and Ink4a/Arf: convergent mechanisms governing terminal differentiation and transformation along the neural stem cell to astrocyte axis. Cancer cell 1, 269-277.

Bajenaru, M. L., Hernandez, M. R., Perry, A., Zhu, Y., Parada, L. F., Garbow, J. R., and Gutmann, D. H. (2003). Optic nerve glioma in mice requires astrocyte Nf1 gene inactivation and Nf1 brain heterozygosity. Cancer Res 63, 8573-8577.

Balordi, F., and Fishell, G. (2007). Mosaic removal of hedgehog signaling in the adult SVZ reveals that the residual wild-type stem cells have a limited capacity for self-renewal. J Neurosci 27, 14248-14259.

Bao, S., Wu, Q., McLendon, R. E., Hao, Y., Shi, Q., Hjelmeland, A. B., Dewhirst, M. W., Bigner, D. D., and Rich, J. N. (2006). Glioma stem cells promote radioresistance by preferential activation of the DNA damage response. Nature 444, 756-760.

Becher, O. J., Hambardzumyan, D., Walker, T. R., Helmy, K., Nazarian, J., Albrecht, S., Hiner, R. L., Gall, S., Huse, J. T., Jabado, N., et al. (2010). Preclinical evaluation of radiation and perifosine in a genetically and histologically accurate model of brainstem glioma. Cancer Res 70, 2548-2557.

Beier, D., Hau, P., Proescholdt, M., Lohmeier, A., Wischhusen, J., Oefner, P. J., Aigner, L., Brawanski, A., Bogdahn, U., and Beier, C. P. (2007). CD133(+) and CD133(-) glioblastoma-derived cancer stem cells show differential growth characteristics and molecular profiles. Cancer Res 67, 4010-4015.

Bleau, A. M., Hambardzumyan, D., Ozawa, T., Fomchenko, E. I., Huse, J. T., Brennan, C. W., and Holland, E. C. (2009). PTEN/PI3K/Akt pathway regulates the side population phenotype and ABCG2 activity in glioma tumor stem-like cells. Cell Stem Cell 4, 226-235.

Boiko, A. D., Razorenova, O. V., van de Rijn, M., Swetter, S. M., Johnson, D. L., Ly, D. P., Butler, P. D., Yang, G. P., Joshua, B., Kaplan, M. J., et al. (2010). Human melanoma-initiating cells express neural crest nerve growth factor receptor CD271. Nature 466, 133-137.

Brandes, J. C., Carraway, H., and Herman, J. G. (2007). Optimal primer design using the novel primer design program: MSPprimer provides accurate methylation analysis of the ATM promoter. Oncogene 26, 6229-6237.

Bruggeman, S. W., Hulsman, D., Tanger, E., Buckle, T., Blom, M., Zevenhoven, J., van Tellingen, O., and van Lohuizen, M. (2007). Bmi1 controls tumor development in an Ink4a/Arf-independent manner in a mouse model for glioma. Cancer cell 12, 328-341.

Burns, K. A., Ayoub, A. E., Breunig, J. J., Adhami, F., Weng, W. L., Colbert, M. C., Rakic, P., and Kuan, C. Y. (2007). Nestin-CreER mice reveal DNA synthesis by nonapoptotic neurons following cerebral ischemia hypoxia. Cereb Cortex 17, 2585-2592.

Calabrese, C., Poppleton, H., Kocak, M., Hogg, T. L., Fuller, C., Hamner, B., Oh, E. Y., Gaber, M. W., Finklestein, D., Allen, M., et al. (2007). A perivascular niche for brain tumor stem cells. Cancer cell 11, 69-82.

Campbell, P. J., Yachida, S., Mudie, L. J., Stephens, P. J., Pleasance, E. D., Stebbings, L. A., Morsberger, L. A., Latimer, C., McLaren, S., Lin, M. L., et al. (2010). The patterns and dynamics of genomic instability in metastatic pancreatic cancer. Nature 467, 1109-1113.

Capela, A., and Temple, S. (2002). LeX/ssea-1 is expressed by adult mouse CNS stem cells, identifying them as nonependymal. Neuron 35, 865-875.

CBTRUS (2009). CBTRUS Statistical Report: Primary Brain and Central Nervous System Tumors Diagnosed in Eighteen States in 2002-2006. . In, (Central Brain Tumor Registry of the United States).

Charrad, R. S., Li, Y., Delpech, B., Balitrand, N., Clay, D., Jasmin, C., Chomienne, C., and Smadja-Joffe, F. (1999). Ligation of the CD44 adhesion molecule reverses

blockage of differentiation in human acute myeloid leukemia. Nature medicine 5, 669-676.

Chen, J., Kwon, C. H., Lin, L., Li, Y., and Parada, L. F. (2009). Inducible site-specific recombination in neural stem/progenitor cells. Genesis 47, 122-131.

Chen, R., Nishimura, M. C., Bumbaca, S. M., Kharbanda, S., Forrest, W. F., Kasman, I. M., Greve, J. M., Soriano, R. H., Gilmour, L. L., Rivers, C. S., et al. (2010). A hierarchy of self-renewing tumor-initiating cell types in glioblastoma. Cancer cell 17, 362-375.

Christensen, K., Schroder, H. D., and Kristensen, B. W. (2008). CD133 identifies perivascular niches in grade II-IV astrocytomas. J Neurooncol 90, 157-170.

Clarke, L., and van der Kooy, D. (2009). Low oxygen enhances primitive and definitive neural stem cell colony formation by inhibiting distinct cell death pathways. Stem cells (Dayton, Ohio) 27, 1879-1886.

Clarke, M. F., Dick, J. E., Dirks, P. B., Eaves, C. J., Jamieson, C. H., Jones, D. L., Visvader, J., Weissman, I. L., and Wahl, G. M. (2006). Cancer stem cells--perspectives on current status and future directions: AACR Workshop on cancer stem cells. Cancer Res 66, 9339-9344.

Collins, A. T., Berry, P. A., Hyde, C., Stower, M. J., and Maitland, N. J. (2005). Prospective identification of tumorigenic prostate cancer stem cells. Cancer Res 65, 10946-10951.

Colman, H., Zhang, L., Sulman, E. P., McDonald, J. M., Shooshtari, N. L., Rivera, A., Popoff, S., Nutt, C. L., Louis, D. N., Cairncross, J. G., et al. (2010). A multigene predictor of outcome in glioblastoma. Neuro Oncol 12, 49-57.

Cooper, L. A. D., Gutman, D. A., Long, Q., Johnson, B. A., Cholleti, S. R., Kurc, T., Saltz, J. H., Brat, D. J., and Moreno, C. S. (2010). The Proneural Molecular Signature Is Enriched in Oligodendrogliomas and Predicts Improved Survival among Diffuse Gliomas. PLoS ONE 5, e12548.

Cozzio, A., Passegue, E., Ayton, P. M., Karsunky, H., Cleary, M. L., and Weissman, I. L. (2003). Similar MLL-associated leukemias arising from self-renewing stem cells and short-lived myeloid progenitors. Genes Dev 17, 3029-3035.

Curtis, S. J., Sinkevicius, K. W., Li, D., Lau, A. N., Roach, R. R., Zamponi, R., Woolfenden, A. E., Kirsch, D. G., Wong, K.-K., and Kim, C. F. (2010). Primary Tumor Genotype Is an Important Determinant in Identification of Lung Cancer Propagating Cells. Cell Stem Cell 7, 127-133.

Dabney, A. R. (2006). ClaNC: point-and-click software for classifying microarrays to nearest centroids. Bioinformatics 22, 122-123.

Dai, C., Celestino, J. C., Okada, Y., Louis, D. N., Fuller, G. N., and Holland, E. C. (2001). PDGF autocrine stimulation dedifferentiates cultured astrocytes and induces oligodendrogliomas and oligoastrocytomas from neural progenitors and astrocytes in vivo. Genes Dev 15, 1913-1925.

Dalerba, P., Dylla, S. J., Park, I. K., Liu, R., Wang, X., Cho, R. W., Hoey, T., Gurney, A., Huang, E. H., Simeone, D. M., et al. (2007). Phenotypic characterization of human colorectal cancer stem cells. Proceedings of the National Academy of Sciences of the United States of America 104, 10158-10163.

Dang, L., White, D. W., Gross, S., Bennett, B. D., Bittinger, M. A., Driggers, E. M., Fantin, V. R., Jang, H. G., Jin, S., Keenan, M. C., et al. (2010). Cancer-associated IDH1 mutations produce 2-hydroxyglutarate. Nature 465, 966.

David N. Louis, W. K. C., H. Ohgaki, Otmar D. Wiestler (2007). WHO classification of tumours of the central nervous system: World Health Organization).

Dawson, M. R., Polito, A., Levine, J. M., and Reynolds, R. (2003). NG2-expressing glial progenitor cells: an abundant and widespread population of cycling cells in the adult rat CNS. Mol Cell Neurosci 24, 476-488.

de Groot, J. F., Fuller, G., Kumar, A. J., Piao, Y., Eterovic, K., Ji, Y., and Conrad, C. A. (2010). Tumor invasion after treatment of glioblastoma with bevacizumab: radiographic and pathologic correlation in humans and mice. Neuro Oncol 12, 233-242.

De La, O. J., Emerson, L. L., Goodman, J. L., Froebe, S. C., Illum, B. E., Curtis, A. B., and Murtaugh, L. C. (2008). Notch and Kras reprogram pancreatic acinar cells to ductal intraepithelial neoplasia. Proceedings of the National Academy of Sciences of the United States of America 105, 18907-18912.

Dennis, G., Jr., Sherman, B. T., Hosack, D. A., Yang, J., Gao, W., Lane, H. C., and Lempicki, R. A. (2003). DAVID: Database for Annotation, Visualization, and Integrated Discovery. Genome Biol 4, P3.

di Tomaso, E., Snuderl, M., Kamoun, W. S., Duda, D. G., Auluck, P. K., Fazlollahi, L., Andronesi, O. C., Frosch, M. P., Wen, P. Y., Plotkin, S. R., et al. (2011). Glioblastoma recurrence after cediranib therapy in patients: lack of "rebound" revascularization as mode of escape. Cancer Res 71, 19-28.

Ding, H., Roncari, L., Shannon, P., Wu, X., Lau, N., Karaskova, J., Gutmann, D. H., Squire, J. A., Nagy, A., and Guha, A. (2001). Astrocyte-specific expression of activated p21-ras results in malignant astrocytoma formation in a transgenic mouse model of human gliomas. Cancer Res 61, 3826-3836.

Ding, H., Shannon, P., Lau, N., Wu, X., Roncari, L., Baldwin, R. L., Takebayashi, H., Nagy, A., Gutmann, D. H., and Guha, A. (2003). Oligodendrogliomas result from the expression of an activated mutant epidermal growth factor receptor in a RAS transgenic mouse astrocytoma model. Cancer Res 63, 1106-1113.

Doetsch, F., Caille, I., Lim, D. A., Garcia-Verdugo, J. M., and Alvarez-Buylla, A. (1999). Subventricular zone astrocytes are neural stem cells in the adult mammalian brain. Cell 97, 703-716.

Doetsch, F., Petreanu, L., Caille, I., Garcia-Verdugo, J.-M., and Alvarez-Buylla, A. (2002). EGF Converts Transit-Amplifying Neurogenic Precursors in the Adult Brain into Multipotent Stem Cells. Neuron 36, 1021-1034.

Dubois, N. C., Hofmann, D., Kaloulis, K., Bishop, J. M., and Trumpp, A. (2006). Nestin-Cre transgenic mouse line Nes-Cre1 mediates highly efficient Cre/loxP mediated recombination in the nervous system, kidney, and somite-derived tissues. Genesis 44, 355-360.

Ebos, J. M., Lee, C. R., Cruz-Munoz, W., Bjarnason, G. A., Christensen, J. G., and Kerbel, R. S. (2009). Accelerated metastasis after short-term treatment with a potent inhibitor of tumor angiogenesis. Cancer cell 15, 232-239.

Feil, R., Wagner, J., Metzger, D., and Chambon, P. (1997). Regulation of Cre recombinase activity by mutated estrogen receptor ligand-binding domains. Biochem Biophys Res Commun 237, 752-757.

Figueroa, M. E., Abdel-Wahab, O., Lu, C., Ward, P. S., Patel, J., Shih, A., Li, Y., Bhagwat, N., Vasanthakumar, A., Fernandez, H. F., et al. (2010). Leukemic IDH1 and IDH2 Mutations Result in a Hypermethylation Phenotype, Disrupt TET2 Function, and Impair Hematopoietic Differentiation. Cancer cell 18, 553-567.

Folkins, C., Shaked, Y., Man, S., Tang, T., Lee, C. R., Zhu, Z., Hoffman, R. M., and Kerbel, R. S. (2009). Glioma tumor stem-like cells promote tumor angiogenesis and vasculogenesis via vascular endothelial growth factor and stromal-derived factor 1. Cancer Res 69, 7243-7251.

Forni, P. E., Scuoppo, C., Imayoshi, I., Taulli, R., Dastru, W., Sala, V., Betz, U. A., Muzzi, P., Martinuzzi, D., Vercelli, A. E., et al. (2006). High levels of Cre expression in neuronal progenitors cause defects in brain development leading to microencephaly and hydrocephaly. J Neurosci 26, 9593-9602.

Freije, W. A., Castro-Vargas, F. E., Fang, Z., Horvath, S., Cloughesy, T., Liau, L. M., Mischel, P. S., and Nelson, S. F. (2004). Gene expression profiling of gliomas strongly predicts survival. Cancer Res 64, 6503-6510.

Frese, K. K., and Tuveson, D. A. (2007). Maximizing mouse cancer models. Nat Rev Cancer 7, 645-658.

Furnari, F. B., Fenton, T., Bachoo, R. M., Mukasa, A., Stommel, J. M., Stegh, A., Hahn, W. C., Ligon, K. L., Louis, D. N., Brennan, C., et al. (2007). Malignant astrocytic glioma: genetics, biology, and paths to treatment. Genes Dev 21, 2683-2710.

Gensert, J. M., and Goldman, J. E. (2001). Heterogeneity of cycling glial progenitors in the adult mammalian cortex and white matter. J Neurobiol 48, 75-86.

Gentleman, R. C., Carey, V. J., Bates, D. M., Bolstad, B., Dettling, M., Dudoit, S., Ellis, B., Gautier, L., Ge, Y., Gentry, J., et al. (2004). Bioconductor: open software development for computational biology and bioinformatics. Genome Biol 5, R80.

Ghashghaei, H. T., Weimer, J. M., Schmid, R. S., Yokota, Y., McCarthy, K. D., Popko, B., and Anton, E. S. (2007). Reinduction of ErbB2 in astrocytes promotes radial glial progenitor identity in adult cerebral cortex. Genes Dev 21, 3258-3271.

Godard, S., Getz, G., Delorenzi, M., Farmer, P., Kobayashi, H., Desbaillets, I., Nozaki, M., Diserens, A. C., Hamou, M. F., Dietrich, P. Y., et al. (2003). Classification of human astrocytic gliomas on the basis of gene expression: a correlated group of genes with angiogenic activity emerges as a strong predictor of subtypes. Cancer Res 63, 6613-6625.

Goh, A. M., Coffill, C. R., and Lane, D. P. (2011). The role of mutant p53 in human cancer. J Pathol 223, 116-126.

Golebiewska, A., Brons, N. H. C., Bjerkvig, R., and Niclou, S. P. (2011). Critical Appraisal of the Side Population Assay in Stem Cell and Cancer Stem Cell Research. Cell Stem Cell 8, 136-147.

Gonzalez-Perez, O., and Alvarez-Buylla, A. (2011). Oligodendrogenesis in the subventricular zone and the role of epidermal growth factor. Brain Res Rev.

Gotz, M., and Barde, Y. A. (2005). Radial glial cells defined and major intermediates between embryonic stem cells and CNS neurons. Neuron 46, 369-372.

Gravendeel, L. A. M., Kouwenhoven, M. C. M., Gevaert, O., de Rooi, J. J., Stubbs, A. P., Duijm, J. E., Daemen, A., Bleeker, F. E., Bralten, L. B. C., Kloosterhof, N. K., et al. (2009). Intrinsic Gene Expression Profiles of Gliomas Are a Better Predictor of Survival than Histology. Cancer research 69, 9065-9072.

Greaves, M. (2010). Cancer stem cells: Back to Darwin? Seminars in Cancer Biology 20, 65-70.

Green, A., and Beer, P. (2010). Somatic mutations of IDH1 and IDH2 in the leukemic transformation of myeloproliferative neoplasms. The New England journal of medicine 362, 369-370.

Gregory, S. G., Sekhon, M., Schein, J., Zhao, S., Osoegawa, K., Scott, C. E., Evans, R. S., Burridge, P. W., Cox, T. V., Fox, C. A., et al. (2002). A physical map of the mouse genome. Nature 418, 743-750.

Grimaldi, P., and Rossi, F. (2006). Lack of neurogenesis in the adult rat cerebellum after Purkinje cell degeneration and growth factor infusion. Eur J Neurosci 23, 2657-2668.

Gross, S., Cairns, R. A., Minden, M. D., Driggers, E. M., Bittinger, M. A., Jang, H. G., Sasaki, M., Jin, S., Schenkein, D. P., Su, S. M., et al. (2010). Cancer-associated metabolite 2-hydroxyglutarate accumulates in acute myelogenous leukemia with isocitrate dehydrogenase 1 and 2 mutations. J Exp Med 207, 339-344.

Gupta, P. B., Chaffer, C. L., and Weinberg, R. A. (2009). Cancer stem cells: mirage or reality? Nature medicine 15, 1010-1012.

Hambardzumyan, D., Parada, L. F., Holland, E. C., and Charest, A. (2011). Genetic modeling of gliomas in mice: New tools to tackle old problems. Glia.

Hegi, M. E., Diserens, A. C., Gorlia, T., Hamou, M. F., de Tribolet, N., Weller, M., Kros, J. M., Hainfellner, J. A., Mason, W., Mariani, L., et al. (2005). MGMT gene silencing and benefit from temozolomide in glioblastoma. The New England journal of medicine 352, 997-1003.

Herrup, K., and Kuemerle, B. (1997). The compartmentalization of the cerebellum. Annual review of neuroscience 20, 61-90.

Holland, E. C., Celestino, J., Dai, C., Schaefer, L., Sawaya, R. E., and Fuller, G. N. (2000). Combined activation of Ras and Akt in neural progenitors induces glioblastoma formation in mice. Nature genetics 25, 55-57.

Holland, E. C., Hively, W. P., DePinho, R. A., and Varmus, H. E. (1998). A constitutively active epidermal growth factor receptor cooperates with disruption of G1 cell-cycle arrest pathways to induce glioma-like lesions in mice. Genes Dev 12, 3675-3685.

Hong, F., and Breitling, R. (2008). A comparison of meta-analysis methods for detecting differentially expressed genes in microarray experiments. Bioinformatics 24, 374-382.

Huang da, W., Sherman, B. T., and Lempicki, R. A. (2009). Systematic and integrative analysis of large gene lists using DAVID bioinformatics resources. Nat Protoc 4, 44-57.

Huang, P. H., Xu, A. M., and White, F. M. (2009). Oncogenic EGFR signaling networks in glioma. Sci Signal 2, re6.

Imayoshi, I., Ohtsuka, T., Metzger, D., Chambon, P., and Kageyama, R. (2006). Temporal regulation of Cre recombinase activity in neural stem cells. Genesis 44, 233-238.

Irizarry, R. A., Warren, D., Spencer, F., Kim, I. F., Biswal, S., Frank, B. C., Gabrielson, E., Garcia, J. G., Geoghegan, J., Germino, G., et al. (2005). Multiple-laboratory comparison of microarray platforms. Nat Methods 2, 345-350.

Ishizawa, K., Rasheed, Z. A., Karisch, R., Wang, Q., Kowalski, J., Susky, E., Pereira, K., Karamboulas, C., Moghal, N., Rajeshkumar, N. V., et al. (2010). Tumor-initiating cells are rare in many human tumors. Cell Stem Cell 7, 279-282.

Jackson, E. L., Garcia-Verdugo, J. M., Gil-Perotin, S., Roy, M., Quinones-Hinojosa, A., VandenBerg, S., and Alvarez-Buylla, A. (2006). PDGFR alpha-positive B cells are neural stem cells in the adult SVZ that form glioma-like growths in response to increased PDGF signaling. Neuron 51, 187-199.

Jacques, T. S., Swales, A., Brzozowski, M. J., Henriquez, N. V., Linehan, J. M., Mirzadeh, Z., C, O. M., Naumann, H., Alvarez-Buylla, A., and Brandner, S. (2010). Combinations of genetic mutations in the adult neural stem cell compartment determine brain tumour phenotypes. The EMBO journal 29, 222-235.

Jaiswal, S., Jamieson, C. H., Pang, W. W., Park, C. Y., Chao, M. P., Majeti, R., Traver, D., van Rooijen, N., and Weissman, I. L. (2009). CD47 is upregulated on circulating hematopoietic stem cells and leukemia cells to avoid phagocytosis. Cell 138, 271-285.

Jamieson, C. H., Ailles, L. E., Dylla, S. J., Muijtjens, M., Jones, C., Zehnder, J. L., Gotlib, J., Li, K., Manz, M. G., Keating, A., et al. (2004). Granulocyte-macrophage progenitors as candidate leukemic stem cells in blast-crisis CML. The New England journal of medicine 351, 657-667.

Jansen, M., Yip, S., and Louis, D. N. (2010). Molecular pathology in adult gliomas: diagnostic, prognostic, and predictive markers. Lancet Neurol 9, 717-726.

Jin, L., Hope, K. J., Zhai, Q., Smadja-Joffe, F., and Dick, J. E. (2006). Targeting of CD44 eradicates human acute myeloid leukemic stem cells. Nature medicine 12, 1167-1174.

Johannessen, C. M., Reczek, E. E., James, M. F., Brems, H., Legius, E., and Cichowski, K. (2005). The NF1 tumor suppressor critically regulates TSC2 and mTOR. Proceedings of the National Academy of Sciences of the United States of America 102, 8573-8578.

Joo, K. M., Kim, S. Y., Jin, X., Song, S. Y., Kong, D. S., Lee, J. I., Jeon, J. W., Kim, M. H., Kang, B. G., Jung, Y., et al. (2008). Clinical and biological implications of CD133-positive and CD133-negative cells in glioblastomas. Lab Invest 88, 808-815.

Jordan, C. T. (2009). Cancer Stem Cells: Controversial or Just Misunderstood? Cell Stem Cell 4, 203-205.

Kamijo, T., Zindy, F., Roussel, M. F., Quelle, D. E., Downing, J. R., Ashmun, R. A., Grosveld, G., and Sherr, C. J. (1997). Tumor suppression at the mouse INK4a locus mediated by the alternative reading frame product p19ARF. Cell 91, 649-659.

Kelly, P. N., Dakic, A., Adams, J. M., Nutt, S. L., and Strasser, A. (2007). Tumor growth need not be driven by rare cancer stem cells. Science (New York, NY 317, 337.

Kemper, K., Sprick, M. R., de Bree, M., Scopelliti, A., Vermeulen, L., Hoek, M., Zeilstra, J., Pals, S. T., Mehmet, H., Stassi, G., and Medema, J. P. (2010). The AC133 epitope, but not the CD133 protein, is lost upon cancer stem cell differentiation. Cancer Res 70, 719-729.

Keunen, O., Johansson, M., Oudin, A., Sanzey, M., Rahim, S. A., Fack, F., Thorsen, F., Taxt, T., Bartos, M., Jirik, R., et al. (2011). Anti-VEGF treatment reduces blood supply and increases tumor cell invasion in glioblastoma. Proceedings of the National Academy of Sciences of the United States of America 108, 3749-3754.

Kim, K., Doi, A., Wen, B., Ng, K., Zhao, R., Cahan, P., Kim, J., Aryee, M. J., Ji, H., Ehrlich, L. I., et al. (2010). Epigenetic memory in induced pluripotent stem cells. Nature 467, 285-290.

Klein, C., Butt, S. J., Machold, R. P., Johnson, J. E., and Fishell, G. (2005). Cerebellum- and forebrain-derived stem cells possess intrinsic regional character. Development (Cambridge, England) 132, 4497-4508.

Klein, T., Ling, Z., Heimberg, H., Madsen, O. D., Heller, R. S., and Serup, P. (2003). Nestin is expressed in vascular endothelial cells in the adult human pancreas. J Histochem Cytochem 51, 697-706.

Knobbe, C. B., Reifenberger, J., and Reifenberger, G. (2004). Mutation analysis of the Ras pathway genes NRAS, HRAS, KRAS and BRAF in glioblastomas. Acta Neuropathol 108, 467-470.

Kokovay, E., Goderie, S., Wang, Y., Lotz, S., Lin, G., Sun, Y., Roysam, B., Shen, Q., and Temple, S. (2010). Adult SVZ lineage cells home to and leave the vascular niche via differential responses to SDF1/CXCR4 signaling. Cell Stem Cell 7, 163-173.

Kouwenhoven, M. C., Gorlia, T., Kros, J. M., Ibdaih, A., Brandes, A. A., Bromberg, J. E., Mokhtari, K., van Duinen, S. G., Teepen, J. L., Wesseling, P., et al. (2009). Molecular analysis of anaplastic oligodendroglial tumors in a prospective randomized study: A report from EORTC study 26951. Neuro Oncol 11, 737-746.

Kouwenhoven, M. C., Kros, J. M., French, P. J., Biemond-ter Stege, E. M., Graveland, W. J., Taphoorn, M. J., Brandes, A. A., and van den Bent, M. J. (2006). 1p/19q loss within oligodendroglioma is predictive for response to first line temozolomide but not to salvage treatment. Eur J Cancer 42, 2499-2503.

Kranendijk, M., Struys, E. A., van Schaftingen, E., Gibson, K. M., Kanhai, W. A., van der Knaap, M. S., Amiel, J., Buist, N. R., Das, A. M., de Klerk, J. B., et al. (2010). IDH2 mutations in patients with D-2-hydroxyglutaric aciduria. Science (New York, NY 330, 336.

Krivtsov, A. V., Twomey, D., Feng, Z., Stubbs, M. C., Wang, Y., Faber, J., Levine, J. E., Wang, J., Hahn, W. C., Gilliland, D. G., et al. (2006). Transformation from

committed progenitor to leukaemia stem cell initiated by MLL-AF9. Nature 442, 818-822.

Kuhn, A., Luthi-Carter, R., and Delorenzi, M. (2008). Cross-species and cross-platform gene expression studies with the Bioconductor-compliant R package 'annotationTools'. BMC Bioinformatics 9, 26.

Kunz, J., Gottschalk, J., Janisch, W., and Schulz, W. (1986). [Cell proliferation and glial fibrillary acidic protein in brain tumors]. Acta Histochem 80, 53-61.

Kuo, C. T., Mirzadeh, Z., Soriano-Navarro, M., Rasin, M., Wang, D., Shen, J., Sestan, N., Garcia-Verdugo, J., Alvarez-Buylla, A., Jan, L. Y., and Jan, Y. N. (2006). Postnatal deletion of Numb/Numblike reveals repair and remodeling capacity in the subventricular neurogenic niche. Cell 127, 1253-1264.

Kwon, C. H., Zhao, D., Chen, J., Alcantara, S., Li, Y., Burns, D. K., Mason, R. P., Lee, E. Y., Wu, H., and Parada, L. F. (2008a). Pten haploinsufficiency accelerates formation of high-grade astrocytomas. Cancer Res 68, 3286-3294.

Kwon, C. H., Zhou, J., Li, Y., Kim, K. W., Hensley, L. L., Baker, S. J., and Parada, L. F. (2006). Neuron-specific enolase-cre mouse line with cre activity in specific neuronal populations. Genesis 44, 130-135.

Kyritsis, A. P., Bondy, M. L., Rao, J. S., and Sioka, C. (2010). Inherited predisposition to glioma. Neuro Oncol 12, 104-113.

Lagace, D. C., Whitman, M. C., Noonan, M. A., Ables, J. L., DeCarolis, N. A., Arguello, A. A., Donovan, M. H., Fischer, S. J., Farnbauch, L. A., Beech, R. D., et al. (2007). Dynamic contribution of nestin-expressing stem cells to adult neurogenesis. J Neurosci 27, 12623-12629.

Lathia, J. D., Gallagher, J., Heddleston, J. M., Wang, J., Eyler, C. E., Macswords, J., Wu, Q., Vasanji, A., McLendon, R. E., Hjelmeland, A. B., and Rich, J. N. (2010). Integrin alpha 6 regulates glioblastoma stem cells. Cell Stem Cell 6, 421-432.

Latini, A., Scussiato, K., Rosa, R. B., Llesuy, S., Bello-Klein, A., Dutra-Filho, C. S., and Wajner, M. (2003). D-2-hydroxyglutaric acid induces oxidative stress in cerebral cortex of young rats. Eur J Neurosci 17, 2017-2022.

Laywell, E. D., Rakic, P., Kukekov, V. G., Holland, E. C., and Steindler, D. A. (2000). Identification of a multipotent astrocytic stem cell in the immature and adult mouse brain. Proceedings of the National Academy of Sciences of the United States of America 97, 13883-13888.

Lee, A., Kessler, J. D., Read, T. A., Kaiser, C., Corbeil, D., Huttner, W. B., Johnson, J. E., and Wechsler-Reya, R. J. (2005). Isolation of neural stem cells from the postnatal cerebellum. Nature neuroscience 8, 723-729.

Lee, J., Kotliarova, S., Kotliarov, Y., Li, A., Su, Q., Donin, N. M., Pastorino, S., Purow, B. W., Christopher, N., Zhang, W., et al. (2006). Tumor stem cells derived from glioblastomas cultured in bFGF and EGF more closely mirror the phenotype and genotype of primary tumors than do serum-cultured cell lines. Cancer cell 9, 391-403.

Lee, J., Son, M. J., Woolard, K., Donin, N. M., Li, A., Cheng, C. H., Kotliarova, S., Kotliarov, Y., Walling, J., Ahn, S., et al. (2008). Epigenetic-mediated dysfunction of the bone morphogenetic protein pathway inhibits differentiation of glioblastoma-initiating cells. Cancer cell 13, 69-80.

Lendahl, U., Zimmerman, L. B., and McKay, R. D. (1990). CNS stem cells express a new class of intermediate filament protein. Cell 60, 585-595.

Li, A., Walling, J., Ahn, S., Kotliarov, Y., Su, Q., Quezado, M., Oberholtzer, J. C., Park, J., Zenklusen, J. C., and Fine, H. A. (2009a). Unsupervised analysis of transcriptomic profiles reveals six glioma subtypes. Cancer Res 69, 2091-2099.

Li, C., Heidt, D. G., Dalerba, P., Burant, C. F., Zhang, L., Adsay, V., Wicha, M., Clarke, M. F., and Simeone, D. M. (2007). Identification of pancreatic cancer stem cells. Cancer Res 67, 1030-1037.

Li, H., Collado, M., Villasante, A., Strati, K., Ortega, S., Canamero, M., Blasco, M. A., and Serrano, M. (2009b). The Ink4/Arf locus is a barrier for iPS cell reprogramming. Nature 460, 1136-1139.

Li, L., Dutra, A., Pak, E., Labrie, J. E., 3rd, Gerstein, R. M., Pandolfi, P. P., Recht, L. D., and Ross, A. H. (2009c). EGFRvIII expression and PTEN loss synergistically induce chromosomal instability and glial tumors. Neuro Oncol 11, 9-21.

Li, Z., Bao, S., Wu, Q., Wang, H., Eyler, C., Sathornsumetee, S., Shi, Q., Cao, Y., Lathia, J., McLendon, R. E., et al. (2009d). Hypoxia-inducible factors regulate tumorigenic capacity of glioma stem cells. Cancer cell 15, 501-513.

Ligon, K. L., Huillard, E., Mehta, S., Kesari, S., Liu, H., Alberta, J. A., Bachoo, R. M., Kane, M., Louis, D. N., Depinho, R. A., et al. (2007). Olig2-regulated lineage-restricted pathway controls replication competence in neural stem cells and malignant glioma. Neuron 53, 503-517.

Lim, D. A., Tramontin, A. D., Trevejo, J. M., Herrera, D. G., Garcia-Verdugo, J. M., and Alvarez-Buylla, A. (2000). Noggin antagonizes BMP signaling to create a niche for adult neurogenesis. Neuron 28, 713-726.

Lim, E., Vaillant, F., Wu, D., Forrest, N. C., Pal, B., Hart, A. H., Asselin-Labat, M. L., Gyorki, D. E., Ward, T., Partanen, A., et al. (2009). Aberrant luminal progenitors as the candidate target population for basal tumor development in BRCA1 mutation carriers. Nature medicine 15, 907-913.

Louis, D. N., Ohgaki, H., Wiestler, O. D., Cavenee, W. K., Burger, P. C., Jouvet, A., Scheithauer, B. W., and Kleihues, P. (2007). The 2007 WHO classification of tumours of the central nervous system. Acta Neuropathol 114, 97-109.

Lu, Y., Huggins, P., and Bar-Joseph, Z. (2009). Cross species analysis of microarray expression data. Bioinformatics 25, 1476-1483.

Maher, E. A., Brennan, C., Wen, P. Y., Durso, L., Ligon, K. L., Richardson, A., Khatry, D., Feng, B., Sinha, R., Louis, D. N., et al. (2006). Marked genomic differences characterize primary and secondary glioblastoma subtypes and identify two distinct molecular and clinical secondary glioblastoma entities. Cancer Res 66, 11502-11513.

Majeti, R., Chao, M. P., Alizadeh, A. A., Pang, W. W., Jaiswal, S., Gibbs, K. D., Jr., van Rooijen, N., and Weissman, I. L. (2009). CD47 is an adverse prognostic factor and therapeutic antibody target on human acute myeloid leukemia stem cells. Cell 138, 286-299.

Mani, S. A., Guo, W., Liao, M. J., Eaton, E. N., Ayyanan, A., Zhou, A. Y., Brooks, M., Reinhard, F., Zhang, C. C., Shipitsin, M., et al. (2008). The epithelial-

mesenchymal transition generates cells with properties of stem cells. Cell 133, 704-715.

Marsden, H. B., Kumar, S., Kahn, J., and Anderton, B. J. (1983). A study of glial fibrillary acidic protein (GFAP) in childhood brain tumours. Int J Cancer 31, 439-445.

Marumoto, T., Tashiro, A., Friedmann-Morvinski, D., Scadeng, M., Soda, Y., Gage, F. H., and Verma, I. M. (2009). Development of a novel mouse glioma model using lentiviral vectors. Nature medicine 15, 110-116.

Maruno, M., Yoshimine, T., Ushio, Y., Hayakawa, T., Jamshidi, J., Arita, N., Bitoh, S., and Mogami, H. (1987). [Immunohistochemical study of human brain tumors with vimentin and astroprotein (GFAP)]. No To Shinkei 39, 579-585.

Masui, K., Suzuki, S. O., Torisu, R., Goldman, J. E., Canoll, P., and Iwaki, T. (2010). Glial progenitors in the brainstem give rise to malignant gliomas by platelet-derived growth factor stimulation. Glia 58, 1050-1065.

Mazumdar, J., O'Brien, W. T., Johnson, R. S., LaManna, J. C., Chavez, J. C., Klein, P. S., and Simon, M. C. (2010). O2 regulates stem cells through Wnt/beta-catenin signalling. Nat Cell Biol 12, 1007-1013.

Mellinghoff, I. K., Wang, M. Y., Vivanco, I., Haas-Kogan, D. A., Zhu, S., Dia, E. Q., Lu, K. V., Yoshimoto, K., Huang, J. H., Chute, D. J., et al. (2005). Molecular determinants of the response of glioblastomas to EGFR kinase inhibitors. The New England journal of medicine 353, 2012-2024.

Mendelsohn, J., and Baselga, J. (2000). The EGF receptor family as targets for cancer therapy. Oncogene 19, 6550-6565.

Menn, B., Garcia-Verdugo, J. M., Yaschine, C., Gonzalez-Perez, O., Rowitch, D., and Alvarez-Buylla, A. (2006). Origin of oligodendrocytes in the subventricular zone of the adult brain. J Neurosci 26, 7907-7918.

Merkle, F. T., Tramontin, A. D., Garcia-Verdugo, J. M., and Alvarez-Buylla, A. (2004). Radial glia give rise to adult neural stem cells in the subventricular zone. Proceedings of the National Academy of Sciences of the United States of America 101, 17528-17532.

Mignone, J. L., Kukekov, V., Chiang, A. S., Steindler, D., and Enikolopov, G. (2004). Neural stem and progenitor cells in nestin-GFP transgenic mice. The Journal of comparative neurology 469, 311-324.

Ming, G. L., and Song, H. (2005). Adult neurogenesis in the mammalian central nervous system. Annual review of neuroscience 28, 223-250.

Molofsky, A. V., Slutsky, S. G., Joseph, N. M., He, S., Pardal, R., Krishnamurthy, J., Sharpless, N. E., and Morrison, S. J. (2006). Increasing p16INK4a expression decreases forebrain progenitors and neurogenesis during ageing. Nature 443, 448-452.

Network, T. C. G. A. R. (2008). Comprehensive genomic characterization defines human glioblastoma genes and core pathways. Nature 455, 1061-1068.

Nickerson, M. L., Warren, M. B., Toro, J. R., Matrosova, V., Glenn, G., Turner, M. L., Duray, P., Merino, M., Choyke, P., Pavlovich, C. P., et al. (2002). Mutations in a novel gene lead to kidney tumors, lung wall defects, and benign tumors of the

hair follicle in patients with the Birt-Hogg-Dube syndrome. Cancer cell 2, 157-164.

Notta, F., Mullighan, C. G., Wang, J. C. Y., Poeppl, A., Doulatov, S., Phillips, L. A., Ma, J., Minden, M. D., Downing, J. R., and Dick, J. E. (2011). Evolution of human BCR-ABL1 lymphoblastic leukaemia-initiating cells. Nature 469, 362-367.

Noushmehr, H., Weisenberger, D. J., Diefes, K., Phillips, H. S., Pujara, K., Berman, B. P., Pan, F., Pelloski, C. E., Sulman, E. P., Bhat, K. P., et al. (2010). Identification of a CpG island methylator phenotype that defines a distinct subgroup of glioma. Cancer cell 17, 510-522.

Ohgaki, H., and Kleihues, P. (2007). Genetic pathways to primary and secondary glioblastoma. Am J Pathol 170, 1445-1453.

Paez-Ribes, M., Allen, E., Hudock, J., Takeda, T., Okuyama, H., Vinals, F., Inoue, M., Bergers, G., Hanahan, D., and Casanovas, O. (2009). Antiangiogenic therapy elicits malignant progression of tumors to increased local invasion and distant metastasis. Cancer cell 15, 220-231.

Panchision, D. M., Pickel, J. M., Studer, L., Lee, S. H., Turner, P. A., Hazel, T. G., and McKay, R. D. (2001). Sequential actions of BMP receptors control neural precursor cell production and fate. Genes Dev 15, 2094-2110.

Parsons, D. W., Jones, S., Zhang, X., Lin, J. C., Leary, R. J., Angenendt, P., Mankoo, P., Carter, H., Siu, I. M., Gallia, G. L., et al. (2008). An integrated genomic analysis of human glioblastoma multiforme. Science (New York, NY 321, 1807-1812.

Patrawala, L., Calhoun, T., Schneider-Broussard, R., Zhou, J., Claypool, K., and Tang, D. G. (2005). Side Population Is Enriched in Tumorigenic, Stem-Like Cancer Cells, whereas ABCG2+ and ABCG2? Cancer Cells Are Similarly Tumorigenic. Cancer research 65, 6207-6219.

Pekcec, A., Loscher, W., and Potschka, H. (2006). Neurogenesis in the adult rat piriform cortex. Neuroreport 17, 571-574.

Persson, A. I., Petritsch, C., Swartling, F. J., Itsara, M., Sim, F. J., Auvergne, R., Goldenberg, D. D., Vandenberg, S. R., Nguyen, K. N., Yakovenko, S., et al. (2010). Non-Stem Cell Origin for Oligodendroglioma. Cancer cell 18, 669-682.

Phillips, H. S., Kharbanda, S., Chen, R., Forrest, W. F., Soriano, R. H., Wu, T. D., Misra, A., Nigro, J. M., Colman, H., Soroceanu, L., et al. (2006). Molecular subclasses of high-grade glioma predict prognosis, delineate a pattern of disease progression, and resemble stages in neurogenesis. Cancer cell 9, 157-173.

Piccirillo, S. G., Reynolds, B. A., Zanetti, N., Lamorte, G., Binda, E., Broggi, G., Brem, H., Olivi, A., Dimeco, F., and Vescovi, A. L. (2006). Bone morphogenetic proteins inhibit the tumorigenic potential of human brain tumour-initiating cells. Nature 444, 761-765.

Piccirillo, S. G. M., Combi, R., Cajola, L., Patrizi, A., Redaelli, S., Bentivegna, A., Baronchelli, S., Maira, G., Pollo, B., Mangiola, A., et al. (2009). Distinct pools of cancer stem-like cells coexist within human glioblastomas and display different tumorigenicity and independent genomic evolution. Oncogene 28, 1807-1811.

Po, A., Ferretti, E., Miele, E., De Smaele, E., Paganelli, A., Canettieri, G., Coni, S., Di Marcotullio, L., Biffoni, M., Massimi, L., et al. (2010). Hedgehog controls neural

stem cells through p53-independent regulation of Nanog. The EMBO journal 29, 2646-2658.

Polo, J. M., Liu, S., Figueroa, M. E., Kulalert, W., Eminli, S., Tan, K. Y., Apostolou, E., Stadtfeld, M., Li, Y., Shioda, T., et al. (2010). Cell type of origin influences the molecular and functional properties of mouse induced pluripotent stem cells. Nat Biotechnol 28, 848-855.

Prestegarden, L., Svendsen, A., Wang, J., Sleire, L., Skaftnesmo, K. O., Bjerkvig, R., Yan, T., Askland, L., Persson, A., Sakariassen, P. O., and Enger, P. O. (2010). Glioma cell populations grouped by different cell type markers drive brain tumor growth. Cancer Res 70, 4274-4279.

Quintana, E., Shackleton, M., Sabel, M. S., Fullen, D. R., Johnson, T. M., and Morrison, S. J. (2008). Efficient tumour formation by single human melanoma cells. Nature 456, 593-598.

Ramirez-Castillejo, C., Sanchez-Sanchez, F., Andreu-Agullo, C., Ferron, S. R., Aroca-Aguilar, J. D., Sanchez, P., Mira, H., Escribano, J., and Farinas, I. (2006). Pigment epithelium-derived factor is a niche signal for neural stem cell renewal. Nature neuroscience 9, 331-339.

Read, T. A., Fogarty, M. P., Markant, S. L., McLendon, R. E., Wei, Z., Ellison, D. W., Febbo, P. G., and Wechsler-Reya, R. J. (2009). Identification of CD15 as a marker for tumor-propagating cells in a mouse model of medulloblastoma. Cancer cell 15, 135-147.

Reilly, K. M., and Jacks, T. (2001). Genetically engineered mouse models of astrocytoma: GEMs in the rough? Semin Cancer Biol 11, 177-191.

Reilly, K. M., Loisel, D. A., Bronson, R. T., McLaughlin, M. E., and Jacks, T. (2000). Nf1;Trp53 mutant mice develop glioblastoma with evidence of strain-specific effects. Nature genetics 26, 109-113.

Reitman, Z. J., Parsons, D. W., and Yan, H. (2010). IDH1 and IDH2: not your typical oncogenes. Cancer cell 17, 215-216.

Ricci-Vitiani, L., Pallini, R., Biffoni, M., Todaro, M., Invernici, G., Cenci, T., Maira, G., Parati, E. A., Stassi, G., Larocca, L. M., and De Maria, R. (2010). Tumour vascularization via endothelial differentiation of glioblastoma stem-like cells. Nature 468, 824-828.

Rivers, L. E., Young, K. M., Rizzi, M., Jamen, F., Psachoulia, K., Wade, A., Kessaris, N., and Richardson, W. D. (2008). PDGFRA/NG2 glia generate myelinating oligodendrocytes and piriform projection neurons in adult mice. Nature neuroscience 11, 1392-1401.

Robanus-Maandag, E., Dekker, M., van der Valk, M., Carrozza, M. L., Jeanny, J. C., Dannenberg, J. H., Berns, A., and te Riele, H. (1998). p107 is a suppressor of retinoblastoma development in pRb-deficient mice. Genes Dev 12, 1599-1609.

Roesch, A., Fukunaga-Kalabis, M., Schmidt, E. C., Zabierowski, S. E., Brafford, P. A., Vultur, A., Basu, D., Gimotty, P., Vogt, T., and Herlyn, M. (2010). A temporarily distinct subpopulation of slow-cycling melanoma cells is required for continuous tumor growth. Cell 141, 583-594.

Saito, Y., Uchida, N., Tanaka, S., Suzuki, N., Tomizawa-Murasawa, M., Sone, A., Najima, Y., Takagi, S., Aoki, Y., Wake, A., et al. (2010). Induction of cell cycle

entry eliminates human leukemia stem cells in a mouse model of AML. Nat Biotechnol 28, 275-280.

Sakariassen, P. O., Prestegarden, L., Wang, J., Skaftnesmo, K. O., Mahesparan, R., Molthoff, C., Sminia, P., Sundlisaeter, E., Misra, A., Tysnes, B. B., et al. (2006). Angiogenesis-independent tumor growth mediated by stem-like cancer cells. Proceedings of the National Academy of Sciences of the United States of America 103, 16466-16471.

Semenza, G. L. (2010). Defining the role of hypoxia-inducible factor 1 in cancer biology and therapeutics. Oncogene 29, 625-634.

Shai, R., Shi, T., Kremen, T. J., Horvath, S., Liau, L. M., Cloughesy, T. F., Mischel, P. S., and Nelson, S. F. (2003). Gene expression profiling identifies molecular subtypes of gliomas. Oncogene 22, 4918-4923.

Sharif, A., Legendre, P., Prevot, V., Allet, C., Romao, L., Studler, J. M., Chneiweiss, H., and Junier, M. P. (2007). Transforming growth factor alpha promotes sequential conversion of mature astrocytes into neural progenitors and stem cells. Oncogene 26, 2695-2706.

Shen, Q., Goderie, S. K., Jin, L., Karanth, N., Sun, Y., Abramova, N., Vincent, P., Pumiglia, K., and Temple, S. (2004). Endothelial cells stimulate self-renewal and expand neurogenesis of neural stem cells. Science (New York, NY 304, 1338-1340.

Singh, S. K., Hawkins, C., Clarke, I. D., Squire, J. A., Bayani, J., Hide, T., Henkelman, R. M., Cusimano, M. D., and Dirks, P. B. (2004). Identification of human brain tumour initiating cells. Nature 432, 396-401.

Smith, J. S., Alderete, B., Minn, Y., Borell, T. J., Perry, A., Mohapatra, G., Hosek, S. M., Kimmel, D., O'Fallon, J., Yates, A., et al. (1999). Localization of common deletion regions on 1p and 19q in human gliomas and their association with histological subtype. Oncogene 18, 4144-4152.

Smith, J. S., Perry, A., Borell, T. J., Lee, H. K., O'Fallon, J., Hosek, S. M., Kimmel, D., Yates, A., Burger, P. C., Scheithauer, B. W., and Jenkins, R. B. (2000). Alterations of chromosome arms 1p and 19q as predictors of survival in oligodendrogliomas, astrocytomas, and mixed oligoastrocytomas. J Clin Oncol 18, 636-645.

Smyth, G. K. (2004). Linear models and empirical bayes methods for assessing differential expression in microarray experiments. Stat Appl Genet Mol Biol 3, Article3.

Smyth, G. K. (2005). Limma: linear models for microarray data. In Bioinformatics and Computational Biology Solutions using R and Bioconductor, W.H. R. Gentleman and V. Carey and S. Dudoit and R. Irizarry, ed. (New York: Springer), pp. 397--420.

So, C. W., Karsunky, H., Passegue, E., Cozzio, A., Weissman, I. L., and Cleary, M. L. (2003). MLL-GAS7 transforms multipotent hematopoietic progenitors and induces mixed lineage leukemias in mice. Cancer cell 3, 161-171.

Soda, Y., Marumoto, T., Friedmann-Morvinski, D., Soda, M., Liu, F., Michiue, H., Pastorino, S., Yang, M., Hoffman, R. M., Kesari, S., and Verma, I. M.

Transdifferentiation of glioblastoma cells into vascular endothelial cells. Proceedings of the National Academy of Sciences.

Son, M. J., Woolard, K., Nam, D. H., Lee, J., and Fine, H. A. (2009). SSEA-1 is an enrichment marker for tumor-initiating cells in human glioblastoma. Cell Stem Cell 4, 440-452.

Sottile, V., Li, M., and Scotting, P. J. (2006). Stem cell marker expression in the Bergmann glia population of the adult mouse brain. Brain research 1099, 8-17.

Spassky, N., Merkle, F. T., Flames, N., Tramontin, A. D., Garcia-Verdugo, J. M., and Alvarez-Buylla, A. (2005). Adult ependymal cells are postmitotic and are derived from radial glial cells during embryogenesis. J Neurosci 25, 10-18.

Squatrito, M., Brennan, C. W., Helmy, K., Huse, J. T., Petrini, J. H., and Holland, E. C. (2010). Loss of ATM/Chk2/p53 Pathway Components Accelerates Tumor Development and Contributes to Radiation Resistance in Gliomas. Cancer cell 18, 619-629.

Stiles, C. D., and Rowitch, D. H. (2008). Glioma stem cells: a midterm exam. Neuron 58, 832-846.

Stommel, J. M., Kimmelman, A. C., Ying, H., Nabioullin, R., Ponugoti, A. H., Wiedemeyer, R., Stegh, A. H., Bradner, J. E., Ligon, K. L., Brennan, C., et al. (2007). Coactivation of receptor tyrosine kinases affects the response of tumor cells to targeted therapies. Science (New York, NY 318, 287-290.

Struys, E. A. (2006). D-2-Hydroxyglutaric aciduria: unravelling the biochemical pathway and the genetic defect. J Inherit Metab Dis 29, 21-29.

Stupp, R., Mason, W. P., van den Bent, M. J., Weller, M., Fisher, B., Taphoorn, M. J., Belanger, K., Brandes, A. A., Marosi, C., Bogdahn, U., et al. (2005). Radiotherapy plus concomitant and adjuvant temozolomide for glioblastoma. The New England journal of medicine 352, 987-996.

Subramanian, A., Tamayo, P., Mootha, V. K., Mukherjee, S., Ebert, B. L., Gillette, M. A., Paulovich, A., Pomeroy, S. L., Golub, T. R., Lander, E. S., and Mesirov, J. P. (2005). Gene set enrichment analysis: a knowledge-based approach for interpreting genome-wide expression profiles. Proceedings of the National Academy of Sciences of the United States of America 102, 15545-15550.

Sun, L., Hui, A. M., Su, Q., Vortmeyer, A., Kotliarov, Y., Pastorino, S., Passaniti, A., Menon, J., Walling, J., Bailey, R., et al. (2006). Neuronal and glioma-derived stem cell factor induces angiogenesis within the brain. Cancer cell 9, 287-300.

Sun, X. Z., Takahashi, S., Cui, C., Zhang, R., Sakata-Haga, H., Sawada, K., and Fukui, Y. (2002). Normal and abnormal neuronal migration in the developing cerebral cortex. J Med Invest 49, 97-110.

Sweet-Cordero, A., Mukherjee, S., Subramanian, A., You, H., Roix, J. J., Ladd-Acosta, C., Mesirov, J., Golub, T. R., and Jacks, T. (2005). An oncogenic KRAS2 expression signature identified by cross-species gene-expression analysis. Nature genetics 37, 48-55.

T. F. Cloughesy, M. D. P., P. Y. Wen, T. Mikkelsen, L. E. Abrey, D. Schiff, W. K. Yung, Z. Maoxia, I. Dimery, H. S. Friedman (2008 (May 20 suppl; abstr 2010b)). A phase II, randomized, non-comparative clinical trial of the effect of bevacizumab (BV) alone or in combination with irinotecan (CPT) on 6-month progression free

survival (PFS6) in recurrent, treatment-refractory glioblastoma (GBM). J Clin Oncol 26.

Takahashi, K., and Yamanaka, S. (2006). Induction of pluripotent stem cells from mouse embryonic and adult fibroblast cultures by defined factors. Cell 126, 663-676.

Tso, C. L., Freije, W. A., Day, A., Chen, Z., Merriman, B., Perlina, A., Lee, Y., Dia, E. Q., Yoshimoto, K., Mischel, P. S., et al. (2006). Distinct transcription profiles of primary and secondary glioblastoma subgroups. Cancer Res 66, 159-167.

Uhrbom, L., Dai, C., Celestino, J. C., Rosenblum, M. K., Fuller, G. N., and Holland, E. C. (2002). Ink4a-Arf loss cooperates with KRas activation in astrocytes and neural progenitors to generate glioblastomas of various morphologies depending on activated Akt. Cancer Res 62, 5551-5558.

Uhrbom, L., Hesselager, G., Nister, M., and Westermark, B. (1998). Induction of brain tumors in mice using a recombinant platelet-derived growth factor B-chain retrovirus. Cancer Res 58, 5275-5279.

Uhrbom, L., Kastemar, M., Johansson, F. K., Westermark, B., and Holland, E. C. (2005). Cell type-specific tumor suppression by Ink4a and Arf in Kras-induced mouse gliomagenesis. Cancer Res 65, 2065-2069.

Utikal, J., Polo, J. M., Stadtfeld, M., Maherali, N., Kulalert, W., Walsh, R. M., Khalil, A., Rheinwald, J. G., and Hochedlinger, K. (2009). Immortalization eliminates a roadblock during cellular reprogramming into iPS cells. Nature 460, 1145-1148.

Vega, C. J., and Peterson, D. A. (2005). Stem cell proliferative history in tissue revealed by temporal halogenated thymidine analog discrimination. Nat Methods 2, 167-169.

Verhaak, R. G., Hoadley, K. A., Purdom, E., Wang, V., Qi, Y., Wilkerson, M. D., Miller, C. R., Ding, L., Golub, T., Mesirov, J. P., et al. (2010). Integrated genomic analysis identifies clinically relevant subtypes of glioblastoma characterized by abnormalities in PDGFRA, IDH1, EGFR, and NF1. Cancer cell 17, 98-110.

Visvader, J. E. (2011). Cells of origin in cancer. Nature 469, 314-322.

Vitucci, M., Hayes, D. N., and Miller, C. R. (2010). Gene expression profiling of gliomas: merging genomic and histopathological classification for personalised therapy. Br J Cancer.

Wang, R., Chadalavada, K., Wilshire, J., Kowalik, U., Hovinga, K. E., Geber, A., Fligelman, B., Leversha, M., Brennan, C., and Tabar, V. (2010). Glioblastoma stem-like cells give rise to tumour endothelium. Nature 468, 829-833.

Wang, Y., Yang, J., Zheng, H., Tomasek, G. J., Zhang, P., McKeever, P. E., Lee, E. Y., and Zhu, Y. (2009). Expression of mutant p53 proteins implicates a lineage relationship between neural stem cells and malignant astrocytic glioma in a murine model. Cancer cell 15, 514-526.

Ward, P. S., Patel, J., Wise, D. R., Abdel-Wahab, O., Bennett, B. D., Coller, H. A., Cross, J. R., Fantin, V. R., Hedvat, C. V., Perl, A. E., et al. (2010). The common feature of leukemia-associated IDH1 and IDH2 mutations is a neomorphic enzyme activity converting alpha-ketoglutarate to 2-hydroxyglutarate. Cancer cell 17, 225-234.

Wei, Q., Clarke, L., Scheidenhelm, D. K., Qian, B., Tong, A., Sabha, N., Karim, Z., Bock, N. A., Reti, R., Swoboda, R., et al. (2006). High-grade glioma formation results

from postnatal pten loss or mutant epidermal growth factor receptor expression in a transgenic mouse glioma model. Cancer Res 66, 7429-7437.

Weiss, W. A., Burns, M. J., Hackett, C., Aldape, K., Hill, J. R., Kuriyama, H., Kuriyama, N., Milshteyn, N., Roberts, T., Wendland, M. F., et al. (2003). Genetic determinants of malignancy in a mouse model for oligodendroglioma. Cancer Res 63, 1589-1595.

Xiao, A., Wu, H., Pandolfi, P. P., Louis, D. N., and Van Dyke, T. (2002). Astrocyte inactivation of the pRb pathway predisposes mice to malignant astrocytoma development that is accelerated by PTEN mutation. Cancer cell 1, 157-168.

Xiao, A., Yin, C. Y., Yang, C. Y., Di Cristofano, A., Pandolfi, P. P., and Van Dyke, T. (2005). Somatic induction of Pten loss in a preclinical astrocytoma model reveals major roles in disease progression and avenues for target discovery and validation. Cancer research 65, 5172-5180.

Xu, W., Yang, H., Liu, Y., Yang, Y., Wang, P., Kim, S. H., Ito, S., Yang, C., Xiao, M. T., Liu, L. X., et al. (2011). Oncometabolite 2-Hydroxyglutarate Is a Competitive Inhibitor of alpha-Ketoglutarate-Dependent Dioxygenases. Cancer cell 19, 17-30.

Yachida, S., Jones, S., Bozic, I., Antal, T., Leary, R., Fu, B., Kamiyama, M., Hruban, R. H., Eshleman, J. R., Nowak, M. A., et al. (2010). Distant metastasis occurs late during the genetic evolution of pancreatic cancer. Nature 467, 1114-1117.

Yan, H., Parsons, D. W., Jin, G., McLendon, R., Rasheed, B. A., Yuan, W., Kos, I., Batinic-Haberle, I., Jones, S., Riggins, G. J., et al. (2009). IDH1 and IDH2 mutations in gliomas. The New England journal of medicine 360, 765-773.

Yen, K. E., Bittinger, M. A., Su, S. M., and Fantin, V. R. (2010). Cancer-associated IDH mutations: biomarker and therapeutic opportunities. Oncogene 29, 6409-6417.

Yu, T. S., Dandekar, M., Monteggia, L. M., Parada, L. F., and Kernie, S. G. (2005). Temporally regulated expression of Cre recombinase in neural stem cells. Genesis 41, 147-153.

Yu, T. S., Zhang, G., Liebl, D. J., and Kernie, S. G. (2008). Traumatic brain injury-induced hippocampal neurogenesis requires activation of early nestin-expressing progenitors. J Neurosci 28, 12901-12912.

Zbinden, M., Duquet, A., Lorente-Trigos, A., Ngwabyt, S.-N., Borges, I., and Ruiz i Altaba, A. (2010). NANOG regulates glioma stem cells and is essential in vivo acting in a cross-functional network with GLI1 and p53. The EMBO journal 29, 2659-2674.

Zhang, C. L., Zou, Y., He, W., Gage, F. H., and Evans, R. M. (2008). A role for adult TLX-positive neural stem cells in learning and behaviour. Nature.

Zhao, C., Deng, W., and Gage, F. H. (2008). Mechanisms and functional implications of adult neurogenesis. Cell 132, 645-660.

Zhao, S., Lin, Y., Xu, W., Jiang, W., Zha, Z., Wang, P., Yu, W., Li, Z., Gong, L., Peng, Y., et al. (2009). Glioma-derived mutations in IDH1 dominantly inhibit IDH1 catalytic activity and induce HIF-1alpha. Science (New York, NY 324, 261-265.

Zheng, H., Ying, H., Wiedemeyer, R., Yan, H., Quayle, S. N., Ivanova, E. V., Paik, J. H., Zhang, H., Xiao, Y., Perry, S. R., et al. (2010). PLAGL2 regulates Wnt signaling to impede differentiation in neural stem cells and gliomas. Cancer cell 17, 497-

509.

Zheng, H., Ying, H., Yan, H., Kimmelman, A. C., Hiller, D. J., Chen, A. J., Perry, S. R., Tonon, G., Chu, G. C., Ding, Z., et al. (2008). p53 and Pten control neural and glioma stem/progenitor cell renewal and differentiation. Nature 455, 1129-1133.

Zhou, B.-B. S., Zhang, H., Damelin, M., Geles, K. G., Grindley, J. C., and Dirks, P. B. (2009). Tumour-initiating cells: challenges and opportunities for anticancer drug discovery. Nat Rev Drug Discov 8, 806-823.

Zhou, B. B., and Sausville, E. A. (2003). Drug discovery targeting Chk1 and Chk2 kinases. Prog Cell Cycle Res 5, 413-421.

Zhu, H., Acquaviva, J., Ramachandran, P., Boskovitz, A., Woolfenden, S., Pfannl, R., Bronson, R. T., Chen, J. W., Weissleder, R., Housman, D. E., and Charest, A. (2009). Oncogenic EGFR signaling cooperates with loss of tumor suppressor gene functions in gliomagenesis. Proceedings of the National Academy of Sciences of the United States of America 106, 2712-2716.

Zhu, X., Bergles, D. E., and Nishiyama, A. (2008). NG2 cells generate both oligodendrocytes and gray matter astrocytes. Development (Cambridge, England) 135, 145-157.

Zhu, Y., Guignard, F., Zhao, D., Liu, L., Burns, D. K., Mason, R. P., Messing, A., and Parada, L. F. (2005a). Early inactivation of p53 tumor suppressor gene cooperating with NF1 loss induces malignant astrocytoma. Cancer cell 8, 119-130.

Zhu, Y., Harada, T., Liu, L., Lush, M. E., Guignard, F., Harada, C., Burns, D. K., Bajenaru, M. L., Gutmann, D. H., and Parada, L. F. (2005b). Inactivation of NF1 in CNS causes increased glial progenitor proliferation and optic glioma formation. Development (Cambridge, England) 132, 5577-5588.

Zhuo, L., Theis, M., Alvarez-Maya, I., Brenner, M., Willecke, K., and Messing, A. (2001). hGFAP-cre transgenic mice for manipulation of glial and neuronal function in vivo. Genesis 31, 85-94.

Zimmerman, L., Parr, B., Lendahl, U., Cunningham, M., McKay, R., Gavin, B., Mann, J., Vassileva, G., and McMahon, A. (1994). Independent regulatory elements in the nestin gene direct transgene expression to neural stem cells or muscle precursors. Neuron 12, 11-24.